
CONSTRAINED AND VANISHING EXPRESSIVITY OF QUANTUM FOURIER MODELS

Hela Mhiri^{1,2}, Léo Monbroussou^{1,3}, Mario Herrero-González^{1,4}, Slimane Thabet^{1,5}, Elham Kashefi^{1,4}, and Jonas Landman^{4,6}

¹Laboratoire d'Informatique de Paris 6, CNRS, Sorbonne Université, 4 Place Jussieu, 75005 Paris, France

²ENSTA Paris, Institut Polytechnique de Paris, France

³CEMIS, Direction Technique, Naval Group, 83190 Ollioules, France

⁴School of Informatics, University of Edinburgh, United Kingdom

⁵PASQAL SAS, 7 avenue Léonard de Vinci, 91300 Massy, France

⁶QC Ware, Palo Alto, USA and Paris, France

In this work, we highlight an unforeseen behavior of the expressivity of Parameterized Quantum Circuits (PQC) for machine learning. A large class of these models, seen as Fourier Series which frequencies are derived from the encoding gates, were thought to have their Fourier coefficients mostly determined by the trainable gates. Here, we demonstrate a new correlation between the Fourier coefficients of the quantum model and its encoding gates. In addition, we display a phenomenon of vanishing expressivity in certain settings, where some Fourier coefficients vanish exponentially when the number of qubits grows. These two behaviors imply novel forms of constraints which limit the expressivity of PQCs, and therefore imply a new inductive bias for Quantum models. The key concept in this work is the notion of a frequency redundancy in the Fourier series spectrum, which determines its importance. Those theoretical behaviours are observed in numerical simulations.

1 Introduction

Quantum Machine Learning (QML) is an important field of study as an application of quantum computing [1]. While many fault tolerant algorithms propose significant advantage over their classical counterparts, many technological milestones must be reached for implementation. Variational quantum algorithms [2] are promising candidates for near term QML methods. Indeed, a popular approach consists in training Parametrized Quantum Circuits (PQCs) as neural networks. To do so, the classical data must be encoded in a quantum state through encoding gates, whereas trainable gates that depend on internal parameters will be optimized during the hybrid training procedure.

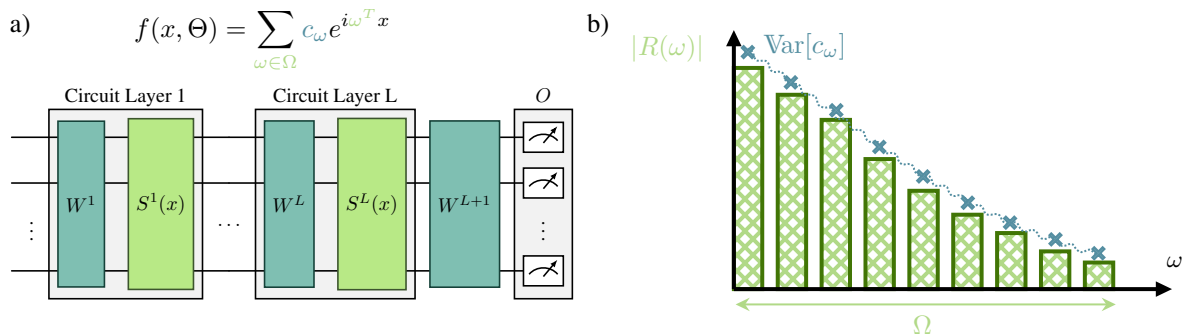


Figure 1: Parameterized quantum models, a) can be seen as Fourier series with frequencies $\omega \in \Omega$. b) illustrates the relation between the frequencies redundancies $|R(\omega)|$, i.e. the number of times a frequency appears in the spectrum, and their Fourier coefficients variance $\text{Var}[c_{\omega}]$. This connection constrains the expressivity of quantum Fourier models.

Many studies have been conducted to understand the potential and limitations of Quantum models. Multiple works focus on the trainability of such models and highlight the exponential concentration and vanishing gradient phenomena [3, 4, 5, 6].

On the other hand, another fundamental question concerns the expressivity of these models, namely which hypothesis class the quantum model is exploring. From the seminal paper [7], we know that if one considers an encoding scheme where the classical input is encoded as the time evolution of some Hamiltonian, the quantum model generated by the PQC can be described as a Fourier series in the classical input. The spectrum is determined by the encoding layers while the Fourier coefficients are mainly controlled by the trainable layers (See Section 2 for more details).

In this work we highlight a new connection between the Fourier coefficients and the encoding gates as illustrated in Fig. 1. This connection is made through the new concept of frequency *redundancy*, which captures the number of times a frequency appears in the spectrum (see Definition 1 for details).

The concept of frequency redundancy emerged from previous works [8, 9] attempting to find a classical approximation to any Quantum Fourier model. Indeed, one could use the same frequencies in the spectrum, or a sample from them, to train a classical Fourier series that is guaranteed to have same or better performance than the quantum model on generic machine learning tasks. If this question remains open in general [10, 11], it was observed in [8] that some frequencies were more important to include in the Fourier series, as their Fourier coefficients had always a greater contribution.

In this paper, we formally establish that some Fourier coefficients have more freedom than others depending on the choice of the encoding Hamiltonians. Using the notion of redundancy, we show that the encoding strategy implies an *inductive bias* in the quantum model, as the Fourier coefficients with high redundancies will have a greater impact. To prove the connection between the frequency redundancies and their importance in the Fourier model, we namely prove that the variance of any Fourier coefficient is roughly proportional to the redundancy of its frequency. We further use this result to establish the *vanishing expressivity* phenomenon: some or all Fourier coefficients can suffer from exponentially vanishing variance as the number of qubits increases while the global quantum model does not exhibit an exponentially vanishing variance. Moreover, we establish another constraint on the 2-norm of the Fourier coefficient vector that holds for any Quantum Fourier Model.

The manuscript is structured as follows. In Section 2, we introduce the framework we consider in the study of quantum models from PQCs. We also define relevant mathematical tools and concepts required for our study. In Section 3, we present our main results that show the inductive bias in the quantum model that arises from some spectrum properties. In Section 4, we discuss in more details the impact of the proven Fourier model constraints on the model behavior. Finally, we present numerical simulations in Section 5 proving our theoretical results and we conclude in Section 6.

Related Work

In [7], it has been shown that a large class of parameterized quantum models with classical data encoding can be expressed as Fourier series. Moreover, by considering reuploading schemes, the spectrum size can be efficiently increased leading to quantum models that serve as universal function approximators [12, 7]. Hence, this framework arises as a powerful tool to further assess the performance and potential of such quantum models. Specifically, much focus has been accorded to the study of the quantum spectrum and its characteristics [7, 13, 14] by exploring different choices of the encoding Hamiltonians. Besides, in [15], the author proposed to learn the frequencies of the quantum model that fit best the learning task at hand. On the other hand, a variety of works used this Fourier representation to propose dequantization schemes of the quantum model. In [8], an efficient construction of a classical model based solely on the circuit description was proposed where the classical model is expected to have similar or better performance than the quantum model in various machine learning tasks. However, it has been pointed out in [10, 11] that the quantum model may not necessarily converge to the same solution as the classical model, leading to different generalization performances. This statement has been further examined in [16] where the authors show that under complexity-theoretic assumptions, there exists quantum models that cannot be dequantized by any efficient method. Thus, it is now highly important to understand the inductive bias of quantum Fourier models that differentiate them from their classical *dequantizers*.

In this work, we focus on studying the bias in the quantum model Fourier coefficients and how it is linked to the structure of the quantum circuit (i.e. encoding strategy, observable, etc.). In this line of work, [13] related the phenomenon of benign overfitting in quantum interpolating Fourier models to the frequency distribution and state preparation showing that the encoding strategy provides an inductive bias that impacts directly the generalization performance. Moreover, [17] provided encoding dependent generalization bounds for such models. Nonetheless, these works provide generic results about quantum Fourier models performance without taking into account the parameterized Fourier coefficients structure in finer details. In a more recent work [18], the authors explored encoding dependent concentration of the Fourier coefficients in the quantum reuploading scheme under the Haar measure assumption proving a phenomenon of vanishing expressivity for high frequencies. In addition, [19] explored exponential concentration sources in quantum Reservoir computing by using the Fourier representation. In this work, we further explore the degree

to which the Fourier coefficients concentrate around their mean under different assumptions about the parameterized part of the circuit and show that the encoding strategy constraints the Fourier coefficients variance for arbitrary PQC's, limiting their theoretical expressivity and giving insights about their generalization performance.

2 Framework

In this Section, we present the framework we consider throughout this work. We first describe the considered circuit structure, and recall how to define the Fourier representation of the associated quantum model in Section 2.1. In particular, we introduce the notion of frequency redundancy and how it could be tuned through the choice of the encoding strategy. Finally, we provide in Section 2.2 some figure of merits for characterizing the expressivity of Quantum models.

2.1 Quantum Fourier Model

We consider a standard supervised learning task, where a parameterized function f , called *model*, must be optimized to match targets in a finite dataset. We define *Quantum models* on n qubits as the family of parameterized functions $f : \mathcal{X} \times \Theta \rightarrow \mathbb{R}$ obtained by measuring the expectation value of some hermitian observable O , such that:

$$f(x, \theta) = \langle 0 | U(x, \theta)^\dagger O U(x, \theta) | 0 \rangle \quad (1)$$

where $U(x, \theta)$ is a 2^n -dimensional unitary, $\theta \in \Theta$ is the vector of trainable parameters and $x = (x_1, \dots, x_D) \in \mathcal{X} \subset \mathbb{R}^D$ is the classical data vector.

We consider a circuit unitary composed of alternating *encoding* and *trainable* layers as depicted in Figure 1 of the form:

$$U(x, \theta) = W^{L+1}(\theta) \left[\prod_{l=1}^L S^l(x) W^l(\theta) \right] \quad (2)$$

where L is the total number of circuit layers (i.e. a circuit layer is made of an encoding layer and a trainable layer), $W^l(\theta)$ s are formed by trainable gates depending on the parameter vector θ , which is optimized during training whereas $S^l(x)$ s only depend on input data values.

In the remainder of this work, we adopt the *Hamiltonian encoding* strategy where the classical input components are encoded as the time evolution of some Hamiltonians $S^l(x) = \prod_{k=1}^D e^{-ix_k H_l^{(k)}}$. From the seminal work [7], we know that if one considers the Hamiltonian encoding strategy, then the quantum model generated by the circuit described in Eq.(2) can be written as a Fourier Series where its spectrum Ω depends on the eigenvalues of the encoding Hamiltonians and the associated Fourier coefficients depend mainly on the parameterized unitaries. Under these assumptions, we call the obtained model a Quantum Fourier Model (QFM), which is defined as follows:

$$f(x, \theta) = \sum_{\omega \in \Omega} c_\omega(\theta) e^{i\omega^T x} \quad (3)$$

The above equation tends to imply that $c_\omega(\theta)$ is solely determined by the parameterized unitaries $W^l(\theta)$ s. However, in this work, we show that the dependence of the Fourier coefficients on the encoding gates is more subtle. To highlight the relation between the frequencies and the encoding Hamiltonian's eigenvalues, we expand Eq.(1) in the case of one-dimensional input vectors ($D = 1$) and provide a generalization to the higher dimensional setting in Appendix A.1. We denote by $d = 2^n$ the dimension of the Hilbert space (with n the number of qubits) and we assume without loss of generality¹ that $S^l(x) = \text{diag}(\lambda_1^l, \dots, \lambda_d^l)$. We also drop the explicit dependence on θ in $W^l(\theta)$ for simplicity and obtain:

$$f(x, \theta) = \sum_{J, J' \in \llbracket 1, d \rrbracket^L} \sum_{k, k'=1}^d W_{j'_1, 0}^{1*} \dots W_{j'_L, k'}^{L+1*} \cdot W_{j_1, 0}^1 \dots W_{j_L, k}^{L+1} \cdot O_{k, k'} \cdot e^{-ix(\sum_{l=1}^L (\lambda_{j_l}^l - \lambda_{j'_l}^l))} \quad (4)$$

We note that $J = (j_1, \dots, j_L)$ is a multi-index where each component j_l refers to the choice of the j^{th} eigenvalue of the Hamiltonian H_l (J maps to a path in the tree from Fig.2).

¹One can simply consider that $S^l(x) = PDP^{-1}$ and inject P in the expression of W^l and P^{-1} in W^{l+1} .

From Eq.(4), we see that the spectrum Ω can be constructed from the eigenvalues of the encoding Hamiltonians in each layer as follows:

$$\Omega = \left\{ \sum_{j_l \in J} \lambda_{j_l}^l - \sum_{j'_l \in J'} \lambda_{j'_l}^l \mid (J, J') \in \llbracket 1, d \rrbracket^L \right\} \quad (5)$$

We note here that the spectrum Ω contains redundant frequencies by construction but in the remainder of this work we consider that Ω denotes the set of distinct frequencies.

As shown in Fig.2, the choice of two *paths* (J, J') in the quantum spectrum tree leads to the generation of a frequency ω by computing the difference of the sum of eigenvalues over each path. One can easily notice that several pairs of paths could lead to the generation of the same frequency. This can happen if an eigenvalue is degenerate, or if several paths of the tree end at the same leaf value (sum of eigenvalues over a path), or eventually if several pairs have the same difference value. The number of those paths evolve with the choice of the different encoding Hamiltonians, the degeneracy of their eigenvalues, and the number L of circuit layers.

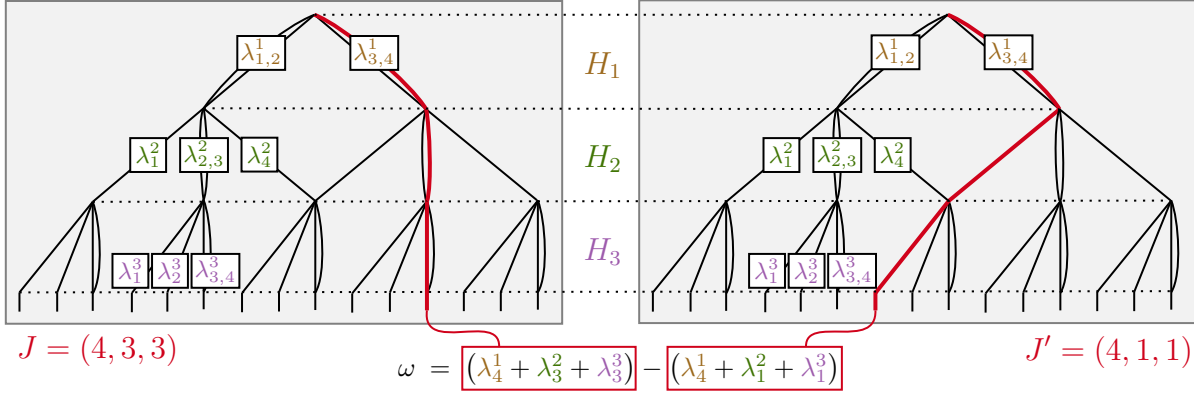


Figure 2: Quantum Spectrum Tree. The frequencies of a Quantum Fourier model are derived from the eigenvalues of the encoding Hamiltonians. Each path in the quantum spectrum tree represents a different choice of eigenvalues $\lambda_{j_l}^l$ from Hamiltonians H_ℓ s. Some edges are duplicated, expressing that the some eigenvalue are degenerate for some Hamiltonians (not at scale). Each frequency ω in the model comes from the difference of two paths in the tree, as shown in the example in red. For a Quantum model acting on $n = 2$ qubits with $L = 3$ circuit layers and encoding hamiltonians H_1, H_2 and H_3 , we give in red a pair of paths in the tree $J = (4, 3, 3), J' = (4, 1, 1)$ generating the frequency $\omega = (\lambda_4^1 + \lambda_3^2 + \lambda_3^3) - (\lambda_4^1 + \lambda_1^2 + \lambda_1^3)$.

By grouping paths (J, J') in Eq.(4) leading to a certain frequency, we formally define the *Frequency Generator* $R(\omega)$ as the set of all paths leading to the generation of the frequency ω and denote the cardinality of this set by the frequency *redundancy* $|R(\omega)|$. As we will demonstrate in Section 3, the redundancy of a frequency will have a crucial role in characterizing the expressivity of QFMs.

Definition 1 (Frequency Generator). *Consider an L -layer Quantum Fourier model as described in Eq.(1-5). For a given frequency ω , we define its generator $R(\omega)$ as the set of eigenvalue indices leading to the generation of ω .*

$$R(\omega) = \left\{ (J, J') \in \llbracket 1, d \rrbracket^L \times \llbracket 1, d \rrbracket^L \mid \sum_{j_l \in J} \lambda_{j_l}^l - \sum_{j'_l \in J'} \lambda_{j'_l}^l = \omega \right\} \quad (6)$$

We call the **redundancy** of a frequency ω the size of its Generator: $|R(\omega)|$.

Since $\sum_{\omega \in \Omega} |R(\omega)| = 2^{2n \times L} = d^{2L}$ by construction, the normalized redundancies $\left\{ \frac{|R(\omega)|}{d^{2L}} \right\}_{\omega \in \Omega}$ define a natural weighted probability distribution over the spectrum Ω . Therefore, by considering different encoding Hamiltonians, one can obtain different probability distributions over the spectrum that will impact the behavior of the associated Quantum model.

For example, Let's consider the standard case of Pauli encoding [7], where single qubit rotation gates are used to encode the classical input $x \in \mathbb{R}$ as the rotation angle. In this case, the encoding Hamiltonian in each layer is a Pauli string. If the Pauli strings do not contain the identity, then the obtained spectrum is simply $\Omega = \llbracket -nL, nL \rrbracket$. Moreover, one can easily show that the spectrum distribution defined by the redundancies follows a standard Gaussian

distribution. Hence, this encoding strategy gives rise to a linear size spectrum (linear in n and L) and concentrates the redundancies in the lower values as detailed in Appendix A.2.

On the contrary, the exponential encoding strategy introduced in [14], which uses scaled Pauli rotations for encoding (See Appendix A.2), leads to an exponential size spectrum of consecutive integer frequencies. Specifically, the obtained spectrum is $\Omega = \left[-\frac{3^{nL}-1}{2}, \frac{3^{nL}-1}{2} \right]$ and some frequencies (not necessarily high frequencies) have redundancies that do not scale exponentially in n and L . However, if one wants to obtain a fully non-degenerate spectrum (except for the null frequency), then a single circuit layer made of a non-local encoding Hamiltonian must be used as mentioned in [14] and explained in Appendix A.2. This is the case for the *Golomb* encoding introduced in [13] where the size of the spectrum is exponentially large ($|\Omega| = 2^{\binom{d}{2}} + 1$) and all non zero coefficients have a redundancy of one.

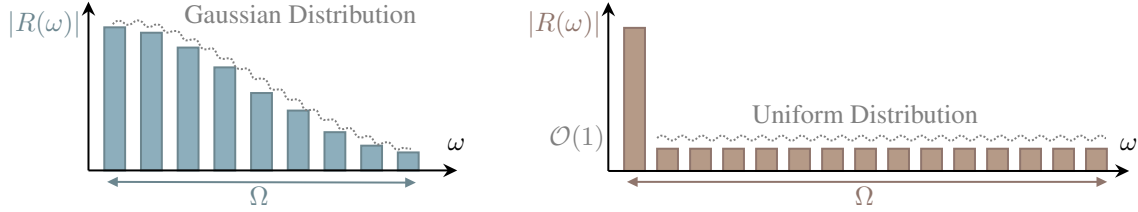


Figure 3: Comparison of two Hamiltonian encoding strategies leading to very different spectrums (x-axis) and distributions (normalized height of the bars). On the left we present an illustration a highly degenerate spectrum (e.g. Pauli encoding spectrum distribution), and on the right an illustration of a weakly degenerate spectrum (e.g. Golomb encoding spectrum distribution).

As illustrated in Fig.3, one could choose a particular set of Hamiltonians to design a quantum model with a specific spectrum distribution. In this work, we will show that this choice does not only impact the spectrum of the quantum Fourier model, but also the Fourier coefficients concentration. In addition, previous work [8] showed the possibility of classically approximating such PQCs for Machine Learning tasks. While having an exponential size spectrum may be a leeway to avoid this classical approximation, we will show in Section 3 that models with a large spectrum tend to have more constrained Fourier coefficients, hence limiting their expressivity and making their classical approximation potentially more efficient.

2.2 Expressivity measures of Quantum models

In this Section, we discuss the different metrics of expressivity that are relevant for our study. A common expressivity measure of a PQC that has been extensively used in the literature [20, 21] is how uniformly the ensemble of the generated unitaries explore the unitary group. In the context of learning a function generated by a PQC, it is usually sufficient to characterize the distance to the Haar measure up to the second moment. Hence, we define a PQC that forms a 2-design as follows :

Definition 2 (2-design). *A PQC $U(\Theta)$ is said to form a 2-design if the set of unitaries it generates $\{U(\theta)\}_{\theta \in \Theta}$ is sufficiently Haar distributed over the unitary space to match the uniform distribution of unitaries up to the second moment. We define the 2nd moment superoperator of the distribution generated by $U(\Theta)$ as:*

$$M_{U(\Theta)}^{(2)} = \int_{\Theta} dU(\theta) U(\theta)^{\otimes 2} \otimes (U(\theta)^*)^{\otimes 2} \quad (7)$$

We denote U_H the set of Haar uniformly distributed unitaries. We then also define the superoperator:

$$\mathcal{A}_{U(\Theta)}^{(2)} = M_{U(\Theta)}^{(2)} - M_{U_H}^{(2)} \quad (8)$$

such that $U(\Theta)$ forms an exact 2-design if $\mathcal{A}_{U(\Theta)}^{(2)} = 0$.

To characterize the landscape of a Quantum Model, we usually compute its variance with respect to the trainable parameters distribution (PQC distribution) and use the Chebyshev inequality to quantify its *concentration* around its average value. In this context, the mathematical concept of a 2-design allows to ease the calculation of the 2nd moment super-operator $M_{U(\Theta)}^{(2)}$ [22]. However, such an assumption on the parameterized circuit leads the Quantum *model exponential concentration* phenomena where the variance of the model vanishes with the dimension of the considered exponential-size Hilbert space [3, 5, 20]. Hence, we formally define the model exponential concentration as follows.

Definition 3 (Model Exponential Concentration). *Consider a quantum model $f(x, \theta)$ such as define in Eq. (1). The model is said to exhibit a concentration phenomenon with respect to the set of trainable parameters θ when:*

$$\text{Var}_\theta[f(x, \theta)] = \mathcal{O}\left(\frac{1}{b^n}\right) \quad (9)$$

for some constant $b > 1$.

To further characterize the landscape of Quantum Models generated by arbitrary PQCs, one can compute the model's variance as a function of the ε -distance to a 2-design. Indeed, it has been shown in [20], that the closer the PQC is to a 2-design, the flatter the cost landscape is, leading to a trade-off between expressivity (according to this definition) and trainability. We note that previous works [4, 20] have considered ε to be the infinite norm or diamond norm of the superoperator $\mathcal{A}_{U(\Theta)}^{(2)}$. For convenience, we quantify the non-uniformity using the *monomial* definition of the distance to a 2-design [23]:

Definition 4. [Monomial definition of ε -approximate 2-design] *An ansatz $U(\Theta)$ forms a monomial ε -approximate 2-design if:*

$$\max_{p,q,r,s \in [d]} |(\mathcal{A}_{U(\Theta)}^{(2)})_{p,q,r,s}| \leq \frac{\varepsilon}{d^2} \quad (10)$$

where $(\mathcal{A}_{U(\Theta)}^{(2)})_{p,q,r,s}$ is a coefficient of the d^4 -dimensional matrix $\mathcal{A}_{U(\Theta)}^{(2)}$.

Along with the expressivity characterization of the parameterized part in a Quantum model by its ε -distance to a 2-design, the expressivity of a QFM should be also examined through its Fourier representation, i.e. the signature of the specific Hamiltonian encoding strategy. In a recent work [19], authors have proposed to define the *Fourier expressivity* as the smallest set of functions such that the quantum model defined in Eq. (1) could be expressed as a linear combination of those functions. According to this definition and the Fourier decomposition of the quantum model (see Eq. (3)), the Fourier expressivity is bounded by the spectrum size $|\Omega|$.

In this work, we similarly choose to focus on characterizing the expressivity of a Quantum model through Fourier lens. Indeed, we show how individual Fourier coefficients may suffer from exponential concentration depending on the spectrum distribution. Therefore, we say that a QFM suffers from *vanishing expressivity* if some or all Fourier coefficients are exponentially concentrated around their mean.

Definition 5 (Vanishing Expressivity). *Consider a quantum Fourier model such as defined in Eq. (3) with spectrum Ω . The Fourier model is said to suffer from vanishing expressivity when some Fourier coefficient have an exponentially vanishing variance in the number of qubits n :*

$$\exists \Omega_{\text{vanish}} \subset \Omega \quad | \quad \forall \omega \in \Omega_{\text{vanish}} \quad \text{Var}_\theta[c_\omega(\theta)] = \mathcal{O}\left(\frac{1}{b^n}\right) \quad (11)$$

for some constant $b > 1$.

3 Main Results

In this section, we present our main theorems and corollaries on expressivity constraints in Quantum Fourier models. Specifically, we study the concentration of Fourier coefficients by computing their variance under different assumptions about the parameterized unitaries distribution. We then show that the variance is always constrained by the frequency redundancy and that some Fourier coefficients may exhibit an exponential concentration phenomena, leading to *vanishing expressivity*.

To do so, we start by considering the global 2-design hypothesis on the parameterized unitaries and provide an exact expression of the variance in Theorem 1 and 2 for a reuploading model. Secondly, we relax the global 2-design assumption and provide an upper bound on the variance under the ε -approximate 2-design hypothesis in Theorem 3. Finally, we consider the brick-wise circuit architecture with local 2-design blocks and give an upper bound on the variance in this setting. This circuit architecture falls within the ε -approximate 2-design assumption, but with more structure allowing us to take into account the locality of the observable.

3.1 Trainable layers as global 2-design

As described in Section 2.2, in the unitary space, the expressivity of a PQC is often characterized by how uniformly the parameterized unitaries explore the unitary group and an ansatz is said to be maximally expressive if its unitary

distribution approximates the Haar measure (i.e. in case of the absence of prior knowledge about the optimal unitary). However, it has been shown in [3, 5], that the quantum model and its gradient exhibit an exponential concentration phenomena under the 2-design assumption, resulting in an unexpressive ansatz in practice.

Here, we explore the implications of considering a maximally expressive ansatz (i.e. each of the parameterized layers forms an exact 2-design) in the post measurement space through the assessment of the Fourier coefficients variance. We further comment on the exponential concentration in Fourier space.

First, we provide an exact expression of the Fourier coefficient variance for a QFM with a single circuit layer ($L = 1$) in Theorem 1. We then extend the result to a reuploading model with $L \geq 1$ in Theorem 2.

Theorem 1. *Consider a single layered Quantum Fourier model with Fourier coefficients $c_\omega(\theta)$ in the form of Eq. (3) with spectrum Ω and redundancies $|R(\omega)|$. We assume that each of the two parameterized layers form independently a 2-design (under the uniform distribution over their parameters). The expectation and variance of each Fourier coefficient in the spectrum Ω is given by:*

$$\begin{aligned}\mathbb{E}_\theta[c_\omega(\theta)] &= \frac{\text{Tr}(O)}{d}\delta_\omega^0 \\ \text{Var}_\theta[c_\omega(\theta)] &= \left(\frac{d\|O\|_2^2 - \text{Tr}(O)^2}{d(d^2 - 1)}\right) \frac{|R(\omega)|}{d(d+1)} + \frac{\text{Tr}(O)^2 - d\|O\|_2^2}{d^2(d^2 - 1)}\delta_\omega^0\end{aligned}\quad (12)$$

This result establishes that the variance of a Fourier coefficient is linear in its frequency redundancy. Consequently, under the 2-design assumption, the distribution of the Fourier coefficients is determined by the frequency distribution and hence by the encoding Hamiltonians. We present in Section 5 two distinct scenarios to illustrate this phenomena for a spiked and a flat frequency distribution.

Theorem 2. *Consider an L -layered Quantum Fourier model with Fourier coefficients $c_\omega(\theta)$ in Eq. (3) with spectrum Ω and redundancies $|R(\omega)|$. We assume that each of the parameterized layers form independently a 2-design (under the uniform distribution over their parameters). The expectation and variance of each Fourier coefficient in the spectrum Ω is given by:*

$$\begin{aligned}\mathbb{E}_\theta[c_\omega(\theta)] &= \frac{\text{Tr}(O)}{d}\delta_\omega^0 \\ \text{Var}_\theta[c_\omega(\theta)] &\simeq \frac{d\|O\|_2^2 - \text{Tr}(O)^2}{d(d^2 - 1)} \left[\frac{|R_1^L(\omega)| - |R_2^L(\omega)|}{d(d+1)(d^2 - 1)^{L-1}} + \sum_{j=3}^L \frac{|R_j^L(\omega)|}{d(d^2 - 1)^{L-j+2}} \right] + \frac{\text{Tr}(O)^2 - d\|O\|_2^2}{d^2(d^2 - 1)}\delta_\omega^0\end{aligned}\quad (13)$$

Here $R_j^L(\omega)$ denotes the partial spectrum formed from the j^{th} up to the L^{th} encoding layers as defined in Definition (6).

Theorem 2 provides a generalization of Theorem 1 for a reuploading model and is obtained by exploiting the recursive relation between the partial spectrums as detailed in Appendix B.1, proving both theorems.

As in the previous case of a single layered circuit, we find that the variance of a Fourier coefficients is linear in its frequency redundancy but also in the partial redundancies. This implies that, under the 2-design assumption, the distribution of the Fourier coefficients is determined by the frequency distribution in the partial spectra, showing again that the Fourier coefficient distribution is dictated by the encoding Hamiltonians.

Another behavior that one can deduce from Theorem 2, is the scaling of the Fourier coefficients variance as the Hilbert space dimension d grows exponentially in the number of qubits, which we explicit in the following Corollary.

Corollary 1. *Consider the same settings of Theorem 2.*

For any choice of the encoding Hamiltonians, we get

$$\text{Var}_\theta[c_\omega(\theta)] = \mathcal{O}\left(\frac{\|O\|_2^2}{d^2} \left[1 + \frac{L-2}{d^3}\right]\right)$$

From Corollary 1, we see that, for observables verifying $\|O\|_2^2 \leq d$ (i.e. holds for Pauli strings and projectors), each coefficient is exponentially vanishing in the number of qubits irrespective of the encoding strategy. Indeed, this bound is simply obtained by using the fact that all the redundancies of a partial spectrum sum up to d^{2l} where l is the number of layers defining the partial spectrum. This result can be viewed as an exponential concentration statement of each Fourier coefficient in a reuploading model, aligning with results in [3] about the exponential concentration of the model under the 2-design assumption.

While useful to show the connection between the Fourier coefficients and the spectrum redundancies, considering global 2-design is a strong assumption leading to exponential concentration. In practice, it is very unlikely that one will use trainable layers forming 2-design for learning purposes, thus we propose in the following to relax this hypothesis by first considering trainable layers as approximate 2-design and then as made of local 2-design blocks.

3.2 Trainable layers as global ε -approximate 2-design

Let us now consider the broader setting of ε -approximate 2-design according to Definition 4. By moving away from highly expressive ansatz, one might question if it is feasible to break free from the constraining redundancy dependence of the Fourier coefficients variance established in Theorem 2, or if such dependency is an intrinsic inductive bias of the quantum model.

We further build on results from [20] about the model concentration and explore encoding dependent concentration for single Fourier components, giving a finer interpretation of the model expressivity through Fourier lens.

In the following theorem, we provide an upper bound on the Fourier coefficients variance for a single layered circuit formed by arbitrary trainable layers.

Theorem 3. *Consider a single layered Quantum Fourier model with spectrum Ω , Fourier coefficients $c_\omega(\theta)$ and redundancies $|R(\omega)|$. We assume that each of the two parameterized layers forms an ε -approximate 2-design according to the monomial definition introduced in Definition (4). The variance of the model's Fourier coefficients obeys the following bound:*

$$\text{Var}_\theta[c_\omega(\theta)] \leq \text{Var}_{\text{Haar}}[c_\omega(\theta)] + \left(\frac{C_1\varepsilon}{d^2} + \frac{C_2\varepsilon}{d(d+1)} \right) |R(\omega)| + C_2 \frac{\varepsilon^2}{d^2} |R(\omega)|^2 \quad (14)$$

where $C_1 = \frac{d\|O\|^2 - \text{Tr}(O)^2}{d(d^2-1)}$, $C_2 = \sum_{l,k} \frac{|O_{l,k}^{\otimes 2}|}{d^2}$ and $\text{Var}_{\text{Haar}}[c_\omega]$ is the variance of a Fourier coefficient under the 2-design assumption given in Theorem 1.

Theorem 3 shows that the variance of a Fourier coefficient in the approximate 2-design scenario is constrained by the combined action of the redundancy and the ε -distance of the parameterized unitaries to a 2-design. Consequently, for a fixed choice of the parameterized unitaries distribution and thus for a fixed ε value, the degree to which each Fourier coefficient concentrates around its mean is dictated by its corresponding frequency redundancy. Therefore, we prove that the connection between the Fourier coefficients concentration and their respective redundancies still hold beyond the 2-design assumption. We provide the proof of Theorem 3 in Appendix B.2 and show in Section 5.3 the bound simulation for different encoding strategies with different spectrum distributions.

To better understand what this bound can tell us about the expressivity of the Quantum model in the Fourier space, we provide in the following Corollary a similar bound for the quantum model variance. Ultimately, we are interested in finding scenarios where the model's variance is not vanishing whereas all or some of its Fourier coefficients suffer from exponential concentration.

Corollary 2. *Consider a single layered Quantum Fourier model $f(x, \theta)$. We assume that each of the two parameterized layers forms an ε -approximate 2-design according to the monomial definition introduced in Definition 4. For a fixed $x \in \mathcal{X}$, the variance of the model $f(x, \theta)$ obeys the following bound:*

$$\text{Var}_\theta[f(x, \theta)] \leq \text{Var}_{\text{Haar}}[f(x, \theta)] + \left(\frac{C_1\varepsilon}{d^2} + \frac{C_2\varepsilon}{d(d+1)} \right) d^2 + C_2\varepsilon^2 d^2 \quad (15)$$

where $\text{Var}_{\text{Haar}}[f(x, \theta)]$ is the variance under the 2-design assumption detailed in Appendix B.3 and the constants C_1 and C_2 have the same definition as in Theorem 3.

Corollary 2 establishes a bound on the global model similar to the one given in Theorem 3 for each Fourier coefficient but instead of having the dependence on $|R(\omega)|$, we have a d^2 term instead. The proof of this Corollary is detailed in Appendix B.3.

By combining Theorem 3 and Corollary 2, we can actually capture scenarios where relatively low redundant frequencies are vanishing whereas there is a leeway for the global cost to not be. We further discuss these scenarios with regards to different encoding schemes and hypothesis on the problem variables in Section 3.2.

However, this upper bound is relatively tight for global observables and much looser for local observables. This observation does not come as a surprise since the obtained bound as a function of the *global* ε expressivity measure of the circuit does not capture the observable-circuit interaction in finer details. Specifically, the interaction between an

m -local observable and the remainder of circuit is captured by the backward light cone of the observable, which is the sub-circuit containing all blocks with at least one qubit causally connected to the local observable input qubits. In the next section, we explore the Fourier coefficients variance by taking into account the locality of the observable.

3.3 Trainable layers as local 2-design blocks

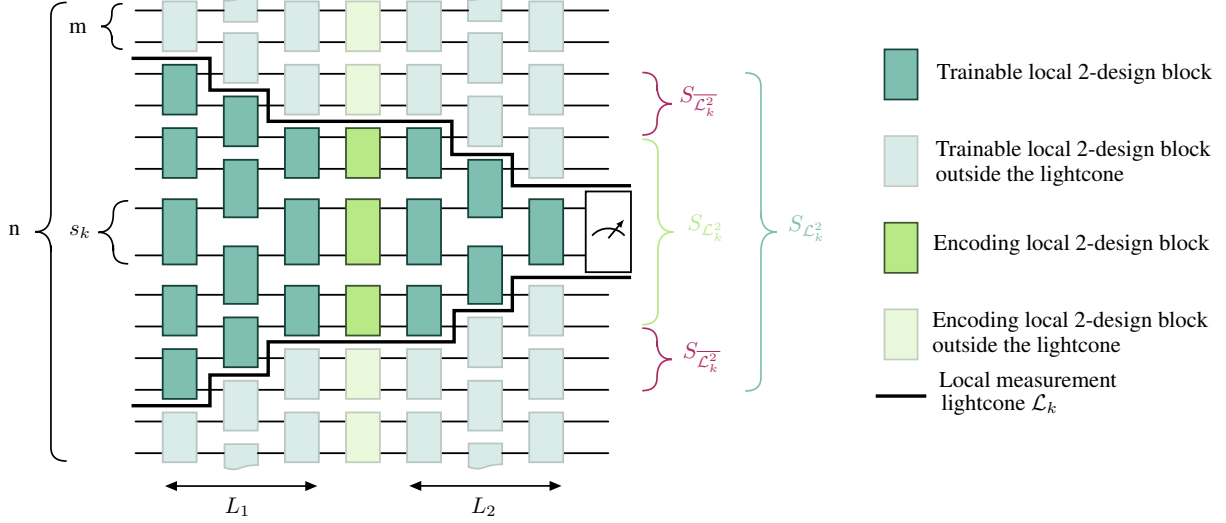


Figure 4: Brickwise circuit architecture made of local blocks acting on neighboring qubits. As shown, L_1 is the depth of the pre-encoding variational block and L_2 is the depth of the post-encoding one. We consider an m -local observable acting non trivially on subspace s_k and we denote its backward light cone by the subcircuit \mathcal{L}_k . We denote by $S_{\mathcal{L}_k}$ the subspace on which the backward light cone acts non trivially and S_{E_k} the subspace on which the encoding layer (made of the green blocks) acts non trivially inside the light cone. we also define $S_{\overline{E_k}}$ as the compliment of S_{E_k} in $S_{\mathcal{L}_k}$.

In this section, we consider a brickwise circuit architecture formed by parameterized local 2-design blocks and encoding blocks, which has been previously studied in [24]. As depicted in Fig.4, the n -qubit circuit is made of layers of m -qubit unitaries (parameterized and encoding unitaries) acting on alternating groups of m neighboring qubits. We consider that each of the parameterized blocks forms an exact 2-design on the m -qubit subsystem on which it acts non trivially. This setting is a special case of the *global* ε -approximate 2-design [25]. However, it will give us more accurate results when one considers local observables acting non trivially on a subsystem s_k of the form $O = \hat{O}_{s_k} \otimes \mathbb{1}_{\overline{s_k}}$. Indeed, by considering this circuit architecture, the backward *causal light cone* of such local observables is well defined and one can easily notice that the effective model spectrum will be reduced. In this setting, we derive the expression of the Fourier coefficients variance in Appendix B.4.3. However, since the obtained expression requires cumbersome calculations, we give in the following theorem an upper bound on the Fourier coefficients variance for two different assumptions on the local observable.

Theorem 4. Consider a single layered Quantum Fourier model with Fourier coefficients $c_\omega(\theta)$ in the form of Eq. (3) using a brick wise circuit architecture with spectrum Ω , redundancies $|R(\omega)|$ and observable $O = \hat{O}_{s_k} \otimes \mathbb{1}_{\overline{s_k}}$. Assume that each variational block forms a 2-design on the corresponding m -qubit subsystem.

1. If $\|\hat{O}_{s_k}\|_2^2 \leq 2^m$, then:

$$\text{Var}[c_\omega] \leq \left(\frac{2^{m+1}}{2^{2m} - 1} \right)^{2L_2} |R_{E_k}(\omega)|^2 \quad (16)$$

2. If \hat{O}_{s_k} is a projector of rank r , then:

$$\text{Var}[c_\omega] \leq \left(\frac{2^{m+1}}{2^{2m} - 1} \right)^{2L_2} \left(\frac{r}{2^m} \right)^2 |R_{E_k}(\omega)|^2 \quad (17)$$

where $R_{E_k}(\omega)$ is the frequency generator obtained from the encoding blocks inside the observable backward light cone \mathcal{L}_k (acting non trivially on S_{E_k}) and L_2 is the depth of the post-encoding parameterized block $W^{(2)}$.

Theorem 4 gives us an upper bound on the variance of the Fourier coefficients while considering a circuits made of local 2-design blocks. Once again, we observe that this quantity is constrained by the spectrum redundancy. In addition, this result indicates that the vanishing Fourier coefficient phenomenon could depend on the circuit depth while considering a local observable. The proof of this Theorem is given in Appendix B.4.

4 Discussing the Quantum Fourier model constraints

In this work, we established a connection between the spectrum redundancies and the statistical behaviour of Fourier coefficients for arbitrary PQCs. Namely, we showed an *inductive bias* of the Fourier model where the variance of a Fourier coefficient is upper bounded by a polynome in its redundancy. we further introduced the concept of *vanishing expressivity* where the variance of some Fourier coefficient is exponentially vanishing in the number of qubits. In this section, we further discuss these phenomena and study their implications on PQC design guidelines in 4.1. In addition, we briefly discuss controllability-related constraints on the Fourier coefficients and provide a generic bound on the 2-norm of the Fourier coefficients vector in 4.2. Finally, we discuss the limitations of the framework and the assumptions we considered and thus the limitations of the obtained results in 4.3.

4.1 Vanishing Fourier Coefficients and Vanishing Cost Functions

In this Section, we discuss the *vanishing expressivity* phenomenon that we established in our main results (See Section 3). Mainly we emphasize the fact that this phenomenon is highly dependent on the chosen encoding strategy by providing concrete examples and comparing the model exponential concentration (*global* concentration) and Fourier coefficients exponential concentration (*local* concentration) phenomena.

Theorem 1 and Theorem 2 highlight an exact link between the variance of the Fourier coefficients and the spectrum redundancies under the hypothesis that each trainable layer forms a 2-design. In addition to showing a previously unknown link between the encoding part and the Fourier coefficients (correlated through the redundancies), one can notice that under the 2-design hypothesis, each Fourier coefficient has a vanishing variance for a reasonable assumption on the observable norm (i.e. $\|O\|_2^2 \leq d$) as detailed in Corollary 1. This result does not come as a surprise since we already know from [3, 5] that under the 2-design hypothesis, the quantum model suffers from *global* concentration. Consequently, the fact that all Fourier coefficients in this setting exhibit vanishing variances independently of the encoding strategy can be seen as a restatement of the *global* exponential concentration by a *local* exponential concentration phenomenon in the Fourier space.

With Theorem 3, we propose a study of the Fourier coefficients variance beyond the global two design hypothesis for a circuit with a single encoding layer. To unpack what insights can be gained from this result, we first consider the observable O to be a Pauli string, then a non trivial projector with rank r . By computing the constants C_1 and C_2 defined in Theorem 3 in each case, we get the following bounds for the Pauli string observable (Eq.(18)) and the rank r projector (Eq.(19)) respectively:

$$\text{Var}[c_\omega] \leq \left(\frac{1}{d} + \frac{|R(\omega)|\varepsilon}{d} + \frac{|R(\omega)|^2\varepsilon^2}{d^2} \right) \quad (18)$$

$$\text{Var}[c_\omega] \leq \left(\left(\frac{dr^2}{d^3(d^2-1)} + \frac{r^2}{d^3(d+1)} \right) |R(\omega)|\varepsilon + \frac{\varepsilon^2|R(\omega)|^2r^2}{d^4} \right) \quad (19)$$

We can conclude that according to the scaling of the distance of the trainable layer to a 2-design and depending on the spectrum redundancies, the Fourier coefficients can be exponentially vanishing. According to the fact that $|R(\omega)| \leq d^{2L}$ (with $d = 2^n$ and $L = 1$ here), one can notice that the variance of all or a part of the Fourier coefficients can vanish independently of the quantum model concentration, leading to the *vanishing expressivity* phenomenon.

An interesting scenario is to consider an encoding strategy where the size of the spectrum is exponential in the number of qubits and hence less prone to classical dequantization. This implies that the spectrum is weakly degenerate with many frequencies ω such that $|R(\omega)| = \mathcal{O}(1)$. This is the case for exponential encoding but also for Golomb encoding. In the latter setup, we have that $|R(\omega)| = 1 \quad \forall \omega \in \Omega^*$. Thus,

$$\forall \omega \in \Omega^*, \quad \text{Var}[c_\omega] \leq \left(\left(\frac{dr^2}{d^3(d^2-1)} + \frac{r^2}{d^3(d+1)} \right) \varepsilon + \frac{\varepsilon^2r^2}{d^4} \right) \quad (20)$$

And according to Corollary 2, we have:

$$\text{Var}[f] \leq \left(\left(\frac{r^2}{d^2-1} + \frac{r^2}{d(d+1)} \right) \varepsilon + \varepsilon^2r^2 \right) \quad (21)$$

When considering $r = \mathcal{O}(\text{poly}(n))$, one can distinguish the different regimes of ε where the variance of the model as well as of the Fourier coefficients are guaranteed to vanish. We notice that while there is a leeway for the global model to be non vanishing, all the Fourier coefficients suffer from exponential concentration for a reasonably wide ε range as depicted in Fig.5.

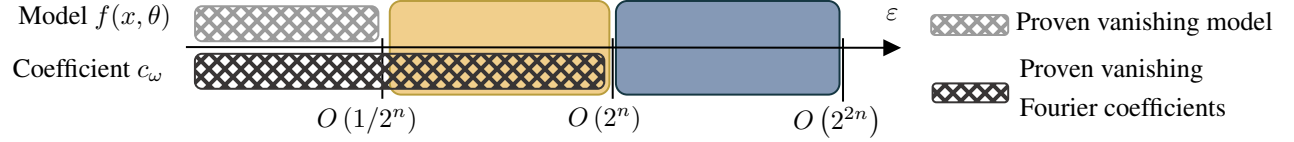


Figure 5: Illustration of the vanishing model and vanishing Fourier coefficient phenomena according to the ε distance to a 2-design, considering coefficients c_ω with redundancies $|R(\omega)| = \mathcal{O}(1)$ and a projector of rank $r = \mathcal{O}(\text{poly}(n))$. In this setup, one can notice that the vanishing expressivity phenomenon can happen independently of the model concentration for ε in the yellow part. Specifically, the dashed grey part corresponds to ε range where the quantum model f is proven to be vanishing while the black one corresponds to the vanishing Fourier coefficients regime. The yellow part indicated the regime where the Fourier coefficients are vanishing but not necessarily the case for the corresponding model. Finally, the behaviour of the model and its coefficients is unknown in the blue part.

Consequently, although the quantum model has theoretically access to an exponential number of frequencies, the contribution of each frequency is vanishing.

When considering general encoding strategies, Theorem 3 implies that frequencies with low redundancies are more likely to suffer from exponential concentration, limiting the expressivity of the quantum model. Specifically, for fixed variational ansatz and thus fixed ε , the upper bound on the Fourier coefficient variance allows high redundant frequencies to possibly escape exponential concentration while the low redundant ones will exhibit vanishing variance, leading to a *vanishing expressivity* phenomenon.

Finally, we propose to study the case where the trainable layers consist of local 2-design blocks. This framework has been used in the seminal paper [24] to link the model gradient vanishing phenomenon to the use of global measurement and to the depth of the quantum circuit. Our motivation is to avoid using the global 2-design hypothesis that can be seen as too restrictive, leading to exponential concentration and thus to vanishing Fourier coefficients. Theorem 4 illustrates once again the link between the spectrum redundancies and the variance of the Fourier coefficients. Let us recall the main result from this Theorem from Eq. (16):

$$\text{Var}[c_\omega] \leq \left(\frac{2^{m+1}}{2^{2m} - 1} \right)^{2L_2} |R_{E_k}(\omega)|^2$$

with L_2 the number of the post-encoding layer $W^{(2)}$ as depicted in Fig.(4) and $R_{E_k}(\omega)$ is the frequency generator obtained from the encoding gates inside the m -local observable backward light cone. We can notice that if the redundancy of a frequency is relatively low ($|R_{E_k}(\omega)| = \mathcal{O}(1)$), then the variance of its corresponding Fourier coefficient will vanish for a depth L_2 linear in n .

4.2 Fourier Norm Bound and Controllability constraints

In this work, we focused on studying variances by considering a uniform distribution over the parameter vector θ . This assumption is often considered while studying the characteristics of PQC for machine learning tasks since the most popular initialization strategy of the parameters is the uniform initialization and since this choice is reasonable to give generic results about the quantum model landscape [4, 6, 20]. In this setting, we showed that constraints on the Fourier model arises from the choice of the encoding strategy.

By considering the expanded expression of the Quantum Fourier model given in Eq.(4), one could notice that the choice of the Fourier spectrum and its redundancies affects the *controllability* of the Fourier model. Indeed, an important property of PQCs should be evoked, which is the controllability of the trainable unitaries. As discussed in [4], the controllability of an ansatz, usually characterized by the Dynamical Lie Algebra defined from the circuit generators, is a measure of how large the set of unitaries that can be expressed by the considered ansatz is compared to the whole unitary group. It can also be rephrased as the degree of freedom we have on the unitary coefficients, which has been further explored in [26]. Hence, this controllability notion will be key in characterizing the controllability of Fourier coefficients.

Namely, by looking more closely at the Fourier coefficient expression given again in Fig.6, one can simply observe that a pair of paths $(J, J') \in R(\omega)$ from the frequency generator defined in Definition 1 allocates coefficients of the

trainable unitary matrices to its frequency. In addition, some unitary coefficients are shared among different Fourier coefficients as a consequence of some branches in the generating tree (see Fig.2) being shared between different frequencies. Consequently, this can potentially create correlations between the Fourier coefficients. Therefore, if the trainable layers have a low controllability as defined in [4], it could lead to the impossibility of controlling independently a large number of Fourier coefficients. This is particularly important according to the fact that increasing the number of parameters seems to increase the control and decrease the distance to a 2-design (see for example the evolution of the distance to a 2-design in the case of Periodic Ansatz through the Theorem 1 in [4]).

In this context, we establish a generic constraint on the quantum model Fourier coefficients that holds for any Hamiltonian encoding scheme and that is independent of the PQC distribution in the following theorem.

Theorem 5 (Fourier Norm Bound). *Consider an L -layered Quantum Fourier model $f(x, \theta)$ with spectrum Ω and observable O as defined in Eq.(3). Then,*

$$\forall x \in \mathbb{R}^d, \forall \theta \in \Theta, |f(x, \theta)|^2 \leq \|O\|_\infty^2 \quad (22)$$

$$\forall \theta \in \Theta, \sum_{\omega \in \Omega} |c_\omega(\theta)|^2 \leq \|O\|_\infty^2 \quad (23)$$

The first part of Theorem 5 is a trivial constraint that holds for any Quantum model of the form in Eq.(1) even outside of the Fourier framework. This constraint has been mentioned in [11] to highlight the fact the a Quantum Fourier model can not achieve any linear function in the Fourier basis given by its spectrum. The second part of the theorem is more subtle. It shows that the 2-norm of the Fourier coefficient vector is upper bounded by the observable largest eigenvalue, introducing another *inductive bias* in quantum Fourier models. Indeed, this result goes in line with the trivial correlation seen between different Fourier coefficients through their expression (See Eq.(4)) and if combined with the information about the spectrum distribution, it can give us preliminary insights about why classical approximation methods based on Random Fourier Features [8] may fail to *dequantize* efficiently Quantum Fourier models, which we leave for future work. We provide the proof of Theorem 5 in Appendix B.5.

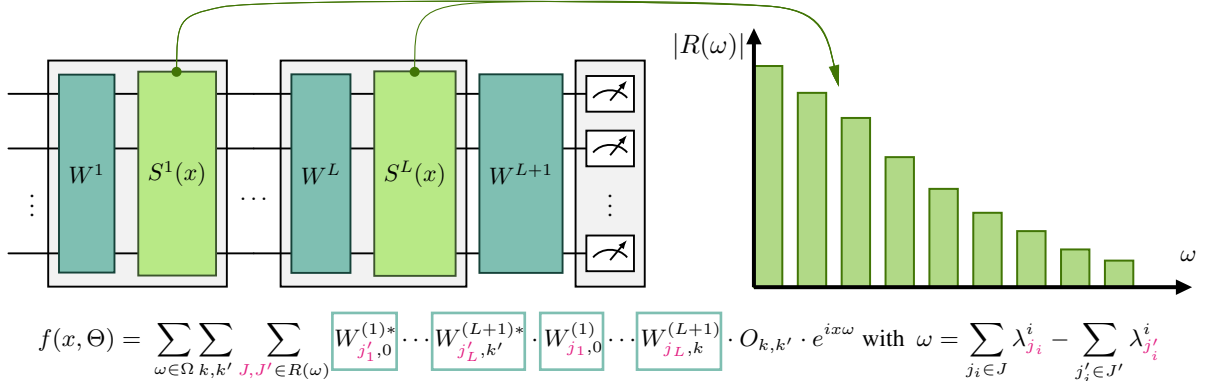


Figure 6: Illustration of the Eq.(4), showing that the encoding layer not only define the Fourier spectrum but also the redundancies, allocating coefficients from the trainable layers to different Fourier coefficients.

4.3 Limitation of the Framework

In this Section, we propose to discuss the limitations of our framework and the mathematical hypothesis used in our main results presented in Section 3.

We first proposed to consider the trainable layers as global 2-designs in Theorem 2. It is well known [5] that this hypothesis leads to exponential concentration, and one could intuitively expect that exponential concentration will also lead to vanishing Fourier coefficients (see Eq.(3)). This was confirmed in our results as the Fourier coefficients were proven to be always exponentially vanishing in this setup. Then, we considered the trainable layers as approximate 2-designs in Theorem 3 to cover arbitrary PQCs. However, we were only able to propose an upper-bound on the variance of the Fourier coefficients while considering a single encoding layer ($L = 1$). This results allowed us to highlight a vanishing expressivity phenomenon where Fourier coefficients can vanish even when the global model is not vanishing, limiting the expressivity of the quantum Fourier model. We propose in Section C.2 to numerically study the case of approximate 2-design trainable layers with a reuploading circuit, and we observe that the behaviour of the Fourier coefficients described in Theorem 3 seems to hold for $L > 1$.

Nonetheless, it is hard to discuss the scaling of the monomial distance ε in the number of qubits or to compute it numerically. Thanks to Corollary 2 and Theorem 3, we can state that an exponentially small ε causes the model exponential concentration and an exponential ε (in the number of qubits) causes Fourier coefficients, corresponding to frequencies with constant redundancies, exponential concentration. However the evolution of the ε -distance to a 2-design for an arbitrary PQC is still an open question.

In Theorem 4, we considered trainable layers made of local 2-design. This hypothesis was used in [24] to show that using global measurements in PQCs leads to Barren Plateaus and show a direct connection between the depth of the circuit and the presence of Barren plateau in the case of local measurements. In an analog way, our study shows that the variance of the Fourier coefficients in this setting depends of the redundancy but also on the depth of the circuit. For both of these results, one can wonder if the vanishing phenomena do not arise from the effective number of qubits in the light cone and if an ansatz made of local 2-design is not already a very expressive ansatz in the associated subspace.

Finally, we would like to point out that our results could be extended to the case of subspace preserving quantum circuits. In this type of PQCs, one can restrict the computation to a particular subspace by using input states which lie in the subspace, reducing the dimension of the effective Hilbert space. These methods allow to avoid Barren Plateaus while considering subspaces of polynomial size [4, 27, 28, 29, 30] but question the quantum advantage of such models [31]. Considering a subspace preserving ansatz, our results can easily be adapted. The dependency over the frequency distribution will still hold, but the value of d (the dimension of the Hilbert space) will be substituted by the dimension of the subspace. Therefore, models generated by subspace preserving circuits could exhibit similar *inductive bias* arising from the redundancy constraint on the variance of its Fourier coefficients.

5 Numerical Results

In this section, we simulate the distribution of the Fourier coefficients for several types of circuits and encoding strategies allowing us to compare the numerical simulations with our theoretical results presented in Section 3.

5.1 Methodology

A description of the different types of parameterized circuit architectures used can be found in Appendix D. Each circuit consists of a choice of encoding layers (encoding Hamiltonians), alternated with trainable layers, L times. Each trainable layer is a repetition of the same ansatz block (See Appendix D). Finally, these blocks can act globally on all qubits, or locally on m qubits, with m being constant.

The statistical properties of the PQC are obtained with the following method: for each ansatz (parameterized circuit's architecture), we pick at random a large number of parameter vectors θ s. For each vector, we evaluate the model $f(x, \theta)$ as many points $x \in \mathbb{R}$ as the Shannon criterion establishes. We obtain the model's Fourier coefficients $\{c_\omega(\theta)\}_{\omega \in \Omega}$ by applying the discrete Fourier transform to the measurement output. We then aggregate the results for all θ s and compute the variance $\text{Var}(c_\omega)$ for each $\omega \in \Omega$.

As we are performing simulations, we are computing the wave function analytically and hence have access to the direct probabilities of each state. Therefore, the shot noise from measurement is not taken into account.

We use three distinct approaches for Hamiltonian encoding. The first is *Pauli encoding*, which is implemented here by applying the same single-qubit Pauli rotation gate with $H = \sigma_x$ applied on each available qubit, as seen in the inset within Fig.8a. Secondly, we use *exponential* encoding which, as described in Appendix A.2, generates an exponentially large spectrum Ω by also using single qubit rotations but with scaling factors introduced in [14] (see Fig.8b). Finally, we also consider the *Golomb* encoding in the single circuit layer setting ($L = 1$) which is obtained by using a global Hamiltonian encoding whose diagonal elements are those of a perfect Golomb ruler [13].

Furthermore, two types of observables are considered. A global observable where the measurement is acting non-trivially and simultaneously on all of the qubits: $O_G = |\mathbf{0}\rangle\langle\mathbf{0}|$ as seen in Fig.7a and a local observable where an average is taken over single qubit measurements $O_L = \frac{1}{n} \sum_j |0\rangle\langle 0|_j \otimes \mathbb{1}_j$ as seen in Fig.7b.

We note that the locality of the observable will determine the scaling of some terms in our theoretical results. Thus, we give here the observable dependent quantities that we will be further used in the numerical simulations.

The global observable O_G is a rank $r = 1$ projector on the whole Hilbert space. Hence, we have:

$$\text{Tr}(O_G) = \|O_G\|_2^2 = \sum_{i,j} |O_{G,(i,j)}^{\otimes 2}| = 1. \quad (24)$$

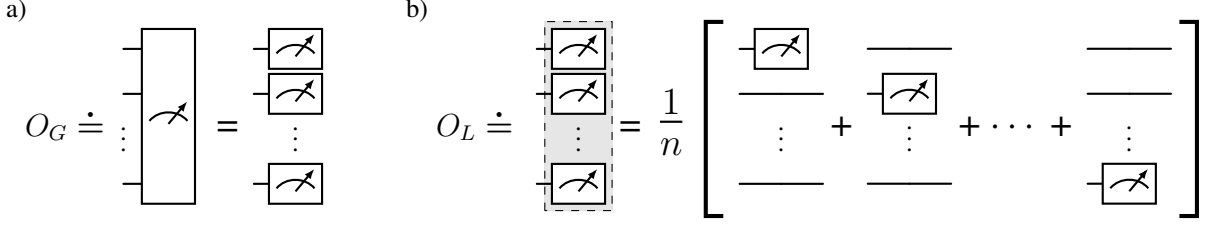


Figure 7: a) Global and b) Local Measurements.

For the local observable O_L , it is a rank $r = d/2$ ($d = 2^n$) projector on the whole Hilbert space and we get:

$$\text{Tr}(O_L) = d/2, \quad \|O_L\|_2^2 = \frac{d/2 + (n-1)d/4}{n}, \quad \sum_{i,j} |O_{L,(i,j)}^{\otimes 2}| = d^2/4. \quad (25)$$

5.2 Trainable layers as global 2-design

We consider trainable layers that form an exact 2-design, by using five repetitions of the *Strongly Entangling* elementary ansatz described in Fig.18.

For a single-layer circuit ($L = 1$), Theorem 1 establishes a linear relationship between the variance of c_ω and the redundancy of the corresponding frequency. For $L > 1$, the relationship in Theorem 2 also involves the partial redundancies (See Definition 6).

In Fig.8, we show that the numerics match Theorem 1 for the Pauli and the exponential encodings respectively. Precisely, we see that the values of $\text{Var}[c_\omega]$ and $|R(\omega)|$ coincide, after a linear rescaling. Fig.8b shows that the exponential encoding strategy has a broader spectrum Ω than the Pauli encoding strategy in Fig.8a. In addition, both encoding methods display their predicted frequency distributions defined by $|R(\omega)|$ (See appendix A.2 for details).

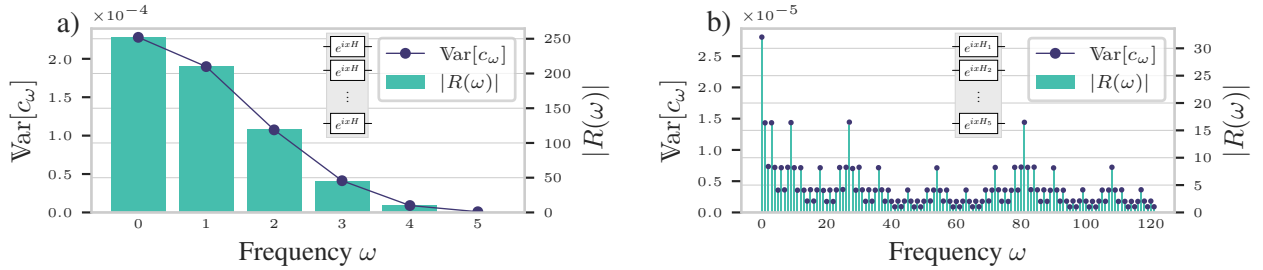


Figure 8: For $n = 5$ qubits, one circuit layer $L = 1$, five repetitions of the strongly entangling ansatz per trainable layer (see Appendix D) and global observable O_G ; relation between the variance of each Fourier coefficient $\text{Var}[c_\omega]$ and its redundancy $|R(\omega)|$. Values plotted for two different encoding strategies, a) Pauli encoding and b) exponential encoding.

In Fig.9, we simulate the same circuit, focusing on the Pauli encoding strategy, and observe the scaling of the Fourier coefficients variance with the number of qubits. In addition, we distinguish two cases: local observable in Fig.9a and global observable in Fig.9b.

In both cases, we observe that the simulated variance and the one predicted by Theorem 1 match. While it is less obvious why we have this behavior for the local observable in Fig.9a, it is actually due to the fact that with the strongly entangling circuit, the local observable backward light cone covers all of the circuit. However, the difference between considering a local observable and a global one can be seen through the steepness of the slopes of each frequency variance as the number of qubits increases and through the number of qubits from which we start observing a strictly decreasing variance. This is due to the different scalings of the observable dependent terms in the number of qubits present in Theorem 1 (See Eq.(24) and Eq.(25)).

Indeed, as predicted by Theorem 1, we observe that the Fourier coefficients variance vanish exponentially. Nonetheless, the vanishing phenomena for the high frequencies is not captured by the plots since we stop the simulations at $n = 12$ qubits.

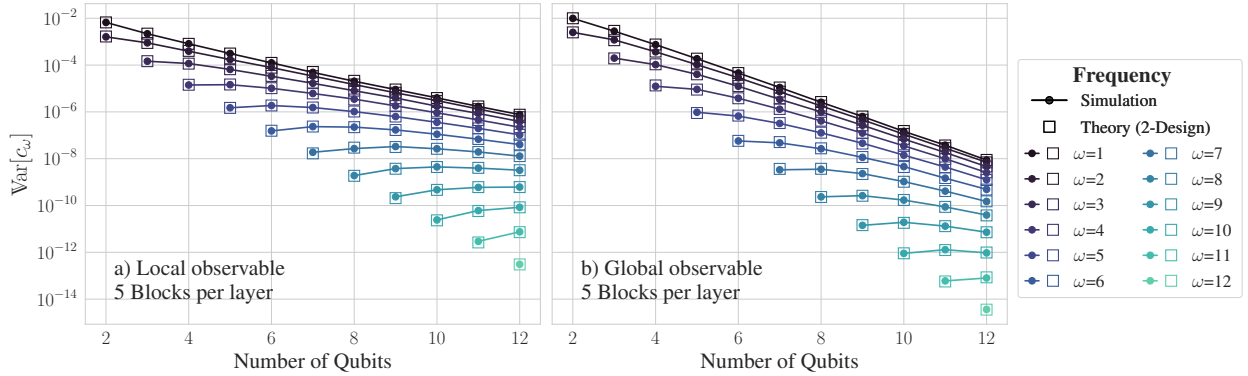


Figure 9: Variance of the Fourier coefficients against the number of qubits for a single circuit layer ($L = 1$). Five repetitions of the strongly entangling ansatz per trainable layer are used ensuring full connectivity. a) Case of local observable. b) Case of global observable. Each color corresponds to a certain frequency ω , squares of the same color correspond to the variance theory for 2-design from Theorem 1 and the dots correspond to the simulated variance.

For the case of a reuploading circuit, we provide in Appendix C similar plots showing again that simulation and theory in Theorem 2 coincide. Precisely, we reproduce in Fig.16 similar plots as in Fig.8 for a reuploading model with $L = 2$ circuit layers.

5.3 Trainable layers as ε -approximate 2-design

In this section, we simulate parameterized circuits which gradually move away from being an exact 2-design. To do so, we decrease the number of qubits on which the trainable blocks, within a trainable layer, are acting on (or *connectivity*). We consider that each local trainable block (noted V in the figures) forms a 2-design on the subset of qubits on which it acts non-trivially by using five repetitions of the strongly entangling ansatz applied to the corresponding m -qubit subsystem. We note that the smaller m (low connectivity), the entanglement between qubits decreases. We also observe numerically that the lower the connectivity, the higher the value of ε , which corresponds to the monomial distance from being a 2-design (see Definition 4). The numerical computation of this distance is expensive and hence we only compute it for $n = 4$ qubits. Specifically, we calculate the 2^{4n} -dimensional matrix $\mathcal{A}_{U(\Theta)}^{(2)}$ as given in Definition 4 and keep its biggest coefficient in absolute value. To do so, we obtain the Haar second-moment operator with the Weingarten Calculus [32] and the second-moment operator generated by the trainable unitary by computing the empirical average over different instances of $W(\theta)$ using randomly picked parameter vectors θ s. We ensured that the sample size used to compute the empirical average is large enough to have a low variance on the computed average values.

In Fig.10, the block V acts non trivially on $m = 1, m = 2$ and $m = 4$ qubits in Fig.10a, Fig.10b and Fig.10c respectively. For each case, we compare the simulated values of the variance of c_ω with two theoretical values: the upper bound from Theorem 3 (approximate 2-design), and the result from Theorem 1 (exact 2-design) using the global observable O_G . We notice that as ε decreases, the simulated variance gets closer to the local 2-design result from Theorem 1. Moreover, the bound from Theorem 3 is satisfied and seems to be highly correlated with the simulated variance. In addition, it gets tighter as we approach the 2-design setting, exactly coinciding with the result from Theorem 1 when the trainable unitaries form an exact 2-design (See Fig.10c).

We also consider the exponential and Golomb encoding strategies with the same circuit architecture as the one used in Fig.10b ($m = 2$ and global observable O_G) to further assess the quality of the bound given in Theorem 3. In Fig.11, we see again that the bound and the simulated variances are highly correlated, showing both a clear dependence on the redundancies.

In addition, if we consider the same setting but using the local observable O_L , we get the results plotted in Fig.12. First, we notice that the simulated spectrum does not cover all of the theoretical spectrum. This observation can be explained by the fact that the casual light cone of the local observable does not cover the encoding gates all at once,

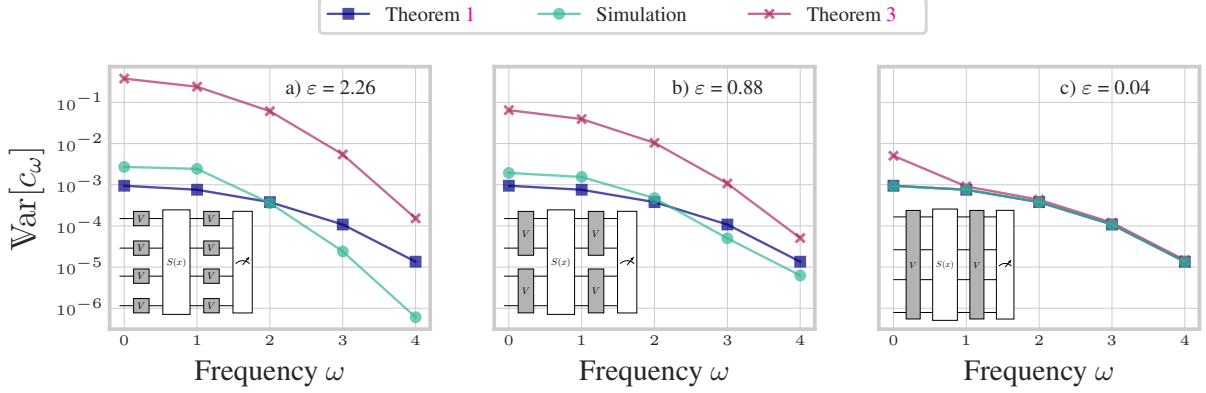


Figure 10: Comparison between simulated (in green) and two theoretical values for the variance of c_ω : global 2-design setting (in blue) and ε -approximate 2 design setting (in pink). Parameterized layers are made of local blocks V made of 5 repetitions of the *Strongly Entangling* ansatz acting each on a) $m = 1$ qubits b) $m = 2$ qubits c) $m = 4$ qubits, with a Pauli encoding layer, and the global observable O_G .

generating a sub-spectrum of the one observed in Fig.11 where the global observable O_G is used. Secondly, we see that the upper bound is still satisfied but is more loose compared to the global observable case.

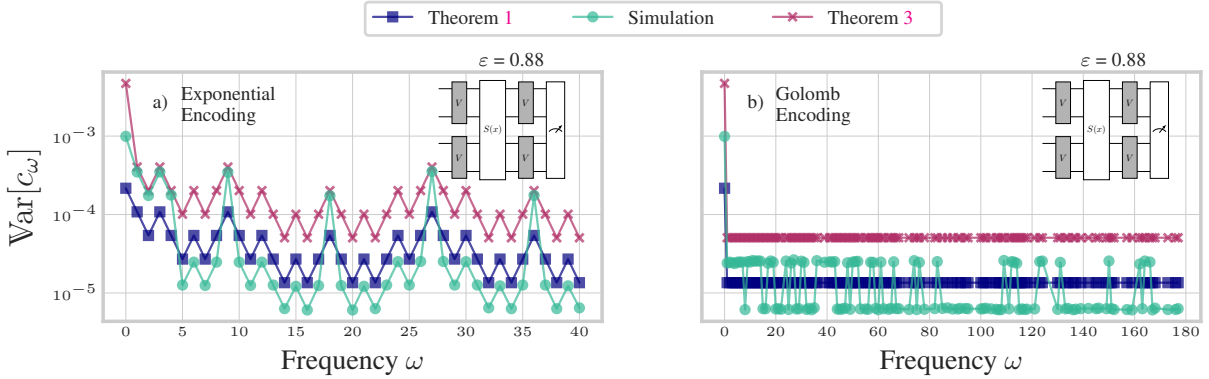


Figure 11: Same setting as in Fig.10b but with a) Exponential Encoding b) Golomb encoding.

5.4 Trainable layers made of Local 2-design blocks

In the following, we will be using a brickwise circuit made of $m = 2$ local trainable blocks forming an exact 2-design on the corresponding 2-qubit subsystem. We also consider a single layer circuit ($L = 1$) as depicted in Fig.4. To do so, we take trainable layers made of repetitions of the *Simplified Two Design Ansatz* described in Fig.19 and we refer to the repetition number by the depth of the trainable layer. In Fig.13, we gradually increase the depth of the trainable layers, each from 1 to 20, which should reach a global 2-design eventually for the number of qubits we are considering [25]. We also distinguish in this setting the case of local and global observables.

First, we observe that as the depth increases, the simulated variance gets closer to the 2 design theory with the global observable case converging more quickly, matching it exactly in Fig.13f and Fig.13h (depth 10 and 20 respectively for the global observable) and in Fig.13g (depth 20 for the local observable).

For the local observable with trainable layers of depth 1 (See Fig.13a), we observe the absence of some frequencies. This can be explained by the locality of the observable, the low connectivity of the trainable layers and the fact that the depth is smaller than $\log(n) \forall n > 2$. Indeed, for larger depths (bigger than $\log(n)$), we see that we do cover all of the theoretical spectrum because the light cone covers all of the encoding gates.

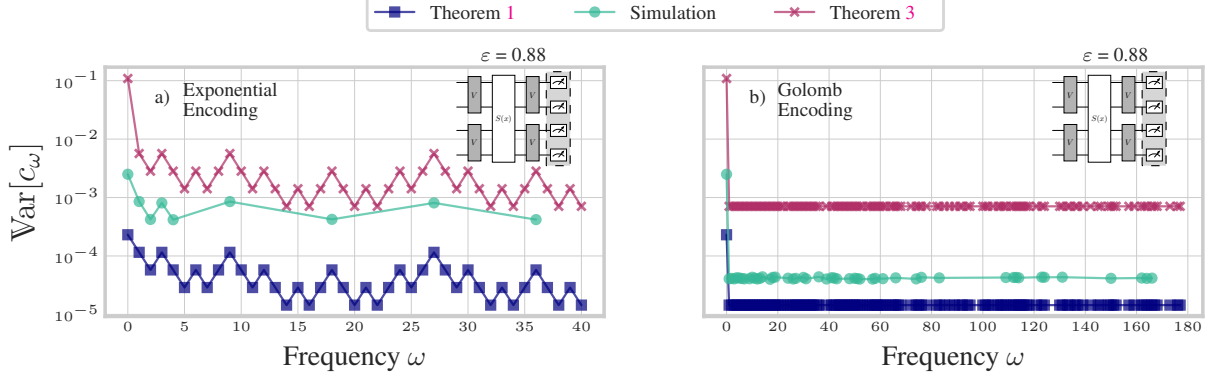


Figure 12: Comparison between simulated (in green) and two theoretical values for the variance of c_ω : global 2-design setting (in blue) and ε -approximate 2 design setting (in pink). Parameterized layers are made of 2-local blocks V made of 5 repetitions of the *Strongly Entangling* ansatz with the local observable O_L and a) Exponential encoding strategy b) Golomb encoding strategy.

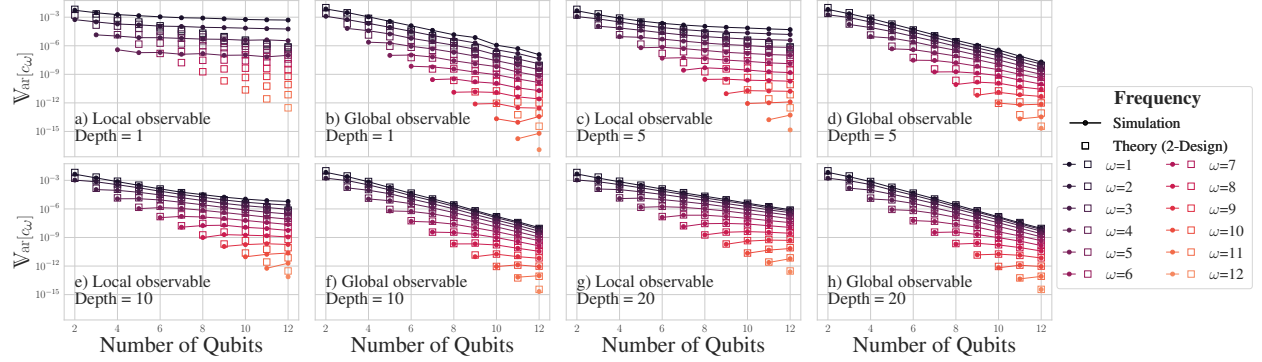


Figure 13: Variance of the Fourier coefficients against the number of qubits for a single circuit layer ($L = 1$) made with the brickwise structure (Fig.4) by using repetitions of the Simplified Two Design ansatz (See Fig.19), Pauli encoding and $n = 2, 3, \dots, 12$ qubits. We gradually increase the depth of the trainable layers a)-f), alternating global and local observables. Each color corresponds to a certain frequency ω , squares of the same color correspond to the variance theory for 2-design of c_ω and the dots correspond to the simulated variance.

Secondly, the vanishing phenomenon is observed in all cases for the majority of the frequencies but with different slopes except for the case of local observable and depth 1 in Fig.13a (consistent with [24]). For the same trainable layers depth, The steepness of the slope is smaller when considering the local observable and it increases with a depth for a fixed locality of the observable.

Besides, under this Brick-wise setting, we confirm the validity of the bound derived in Theorem 4 illustrated in Fig.14. Here we extract the lightcone for different depths (L_2) of the second trainable layer $W^{(2)}$ and plot the simulated variance of each Fourier coefficient generated by the light cone, the bound from Theorem 4 as well as the variance under the 2-design assumption on the light cone trainable layers from Eq.(B46). We perform the simulations in Fig.14 for the Pauli encoding strategy and replicate it for the exponential and Golomb encoding strategies in the fixed setting of $L_2 = 2$ in Fig.15.

As seen before, we observe that the bound from Theorem 4 is satisfied and seems highly correlated with the simulated variance for all the encoding strategies considered.

Finally, when we assume that the restriction of each of the trainable layers to the light cone forms a 2-design (on the subsystems on which it acts non trivially), we observe that the Fourier coefficients variance in this setting is below the simulated variance. This observation supports the fact that the variance in the 2-design lightcone setting may provide a lower bound for the variance over the light cone. Thus, we leave this question for a future work.

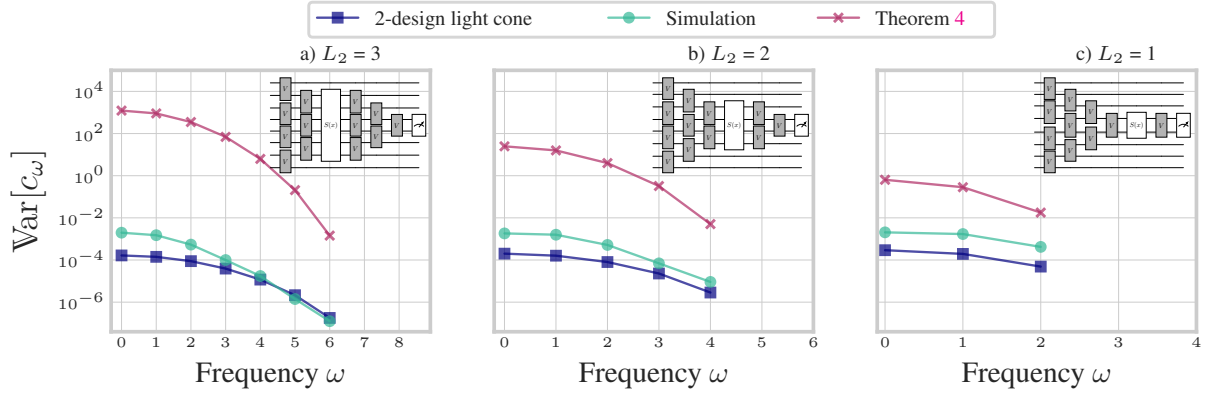


Figure 14: Variance of the Fourier coefficients in the local observable backward lightcone with Pauli encoding generated by three different methods: simulated variance in green, variance bound from Theorem 4 in pink and variance under the 2-design assumption on each of the lightcone trainable layers in blue. We gradually decrease the depth L_2 of the second trainable layer, from a)-c).

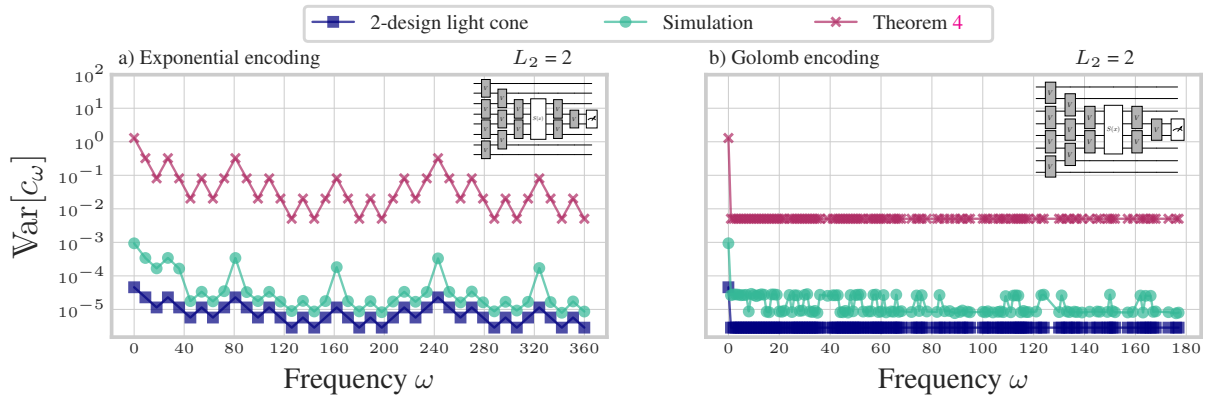


Figure 15: Variance of the Fourier coefficients in the local observable backward lightcone with $L_2 = 2$ generated by three different methods: simulated variance in green, variance bound from Theorem 4 in pink and variance under the 2-design assumption on each of the lightcone trainable layers in blue. a) Exponential encoding b) Golomb encoding.

6 Conclusion

In this work, we have studied the expressivity of parameterized quantum circuits (PQCs) used for learning purposes, through Fourier lens. Our results imply that the choice of the encoding Hamiltonians defines two important properties of the quantum model expressivity: the encoding *inductive bias* and the *vanishing expressivity* phenomena. The former captures the dependence of each Fourier coefficient’s variance, and therefore its degree of freedom, on the corresponding frequency redundancy. The latter is a statement about the scaling of the Fourier coefficients variance as the number of qubits grows. Specifically, we showed that models containing frequencies with relatively low redundancies suffer from a vanishing variance of those frequencies, reducing their expected expressivity.

The learning models obtained with PQCs are therefore more constrained than expected. Even though this reduces their expressivity, it also indicates an inductive bias which might be specific to quantum models. It is left as an open question to study potential benefits of such bias as a source of quantum advantage. On the other hand, could one try to classically reproduce this bias, using the fact that this bias can be determined a priori by looking at the circuit? Overall, one can use these guidelines to design more expressive PQCs, and to further study what differentiate the quantum Fourier model from its classical equivalent.

7 Code availability

Code based on PennyLane [33] to reproduce the figures and analysis is available at the following repository: <https://github.com/Marioherreroglez/quantum-fourier-expressivity/>. Circuit diagrams have been obtained with Qantikz [34].

Acknowledgments

This work is supported by the H2020-FETOPEN Grant PHOQUSING (GA no.: 899544), the Engineering and Physical Sciences Research Council (grants EP/T001062/1), and the Naval Group Centre of Excellence for Information Human factors and Signature Management (CEMIS).

References

- [1] Nathan Wiebe, Ashish Kapoor, and Krysta M. Svore. *Quantum Deep Learning*. May 2015. DOI: [10.48550/arXiv.1412.3489](https://doi.org/10.48550/arXiv.1412.3489).
- [2] M. Cerezo et al. “Variational quantum algorithms”. en. In: *Nature Reviews Physics* 3.9 (Sept. 2021), pp. 625–644. ISSN: 2522-5820. DOI: [10.1038/s42254-021-00348-9](https://doi.org/10.1038/s42254-021-00348-9).
- [3] Andrew Arrasmith et al. “Equivalence of quantum barren plateaus to cost concentration and narrow gorges”. en. In: *Quantum Science and Technology* 7.4 (Oct. 2022), p. 045015. ISSN: 2058-9565. DOI: [10.1088/2058-9565/ac7d06](https://doi.org/10.1088/2058-9565/ac7d06).
- [4] Martin Larocca et al. “Diagnosing Barren Plateaus with Tools from Quantum Optimal Control”. en. In: *Quantum* 6 (Sept. 2022), p. 824. ISSN: 2521-327X. DOI: [10.22331/q-2022-09-29-824](https://doi.org/10.22331/q-2022-09-29-824).
- [5] Jarrod R. McClean et al. “Barren plateaus in quantum neural network training landscapes”. en. In: *Nature Communications* 9.1 (Nov. 2018), p. 4812. ISSN: 2041-1723. DOI: [10.1038/s41467-018-07090-4](https://doi.org/10.1038/s41467-018-07090-4).
- [6] Christa Zoufal. *Generative Quantum Machine Learning*. Nov. 2021. DOI: [10.48550/arXiv.2111.12738](https://doi.org/10.48550/arXiv.2111.12738).
- [7] Maria Schuld, Ryan Sweke, and Johannes Jakob Meyer. “The effect of data encoding on the expressive power of variational quantum machine learning models”. In: *Physical Review A* 103.3 (Mar. 2021), p. 032430. ISSN: 2469-9926, 2469-9934. DOI: [10.1103/PhysRevA.103.032430](https://doi.org/10.1103/PhysRevA.103.032430).
- [8] Jonas Landman et al. *Classically Approximating Variational Quantum Machine Learning with Random Fourier Features*. en. Oct. 2022.
- [9] Franz J. Schreiber, Jens Eisert, and Johannes Jakob Meyer. “Classical surrogates for quantum learning models”. In: *Physical Review Letters* 131.10 (Sept. 2023), p. 100803. ISSN: 0031-9007, 1079-7114. DOI: [10.1103/PhysRevLett.131.100803](https://doi.org/10.1103/PhysRevLett.131.100803).
- [10] Sofiene Jerbi et al. “Quantum machine learning beyond kernel methods”. en. In: *Nature Communications* 14.1 (Jan. 2023), p. 517. ISSN: 2041-1723. DOI: [10.1038/s41467-023-36159-y](https://doi.org/10.1038/s41467-023-36159-y).
- [11] Ryan Sweke et al. *Potential and limitations of random Fourier features for dequantizing quantum machine learning*. Sept. 2023. DOI: [10.48550/arXiv.2309.11647](https://doi.org/10.48550/arXiv.2309.11647).
- [12] Adrián Pérez-Salinas et al. “Data re-uploading for a universal quantum classifier”. In: *Quantum* 4 (Feb. 2020), p. 226. ISSN: 2521-327X. DOI: [10.22331/q-2020-02-06-226](https://doi.org/10.22331/q-2020-02-06-226).
- [13] Evan Peters and Maria Schuld. “Generalization despite overfitting in quantum machine learning models”. In: *Quantum* 7 (Dec. 2023), p. 1210. ISSN: 2521-327X. DOI: [10.22331/q-2023-12-20-1210](https://doi.org/10.22331/q-2023-12-20-1210).
- [14] S. Shin, Y. S. Teo, and H. Jeong. *Exponential data encoding for quantum supervised learning*. en. June 2022. DOI: [10.1103/PhysRevA.107.012422](https://doi.org/10.1103/PhysRevA.107.012422).
- [15] Ben Jaderberg et al. *Let Quantum Neural Networks Choose Their Own Frequencies*. Sept. 2023. DOI: [10.48550/arXiv.2309.03279](https://doi.org/10.48550/arXiv.2309.03279).
- [16] Sofiene Jerbi et al. *Shadows of quantum machine learning*. May 2023. DOI: [10.48550/arXiv.2306.00061](https://doi.org/10.48550/arXiv.2306.00061).
- [17] Matthias C. Caro et al. “Encoding-dependent generalization bounds for parametrized quantum circuits”. en-GB. In: *Quantum* 5 (Nov. 2021), p. 582. DOI: [10.22331/q-2021-11-17-582](https://doi.org/10.22331/q-2021-11-17-582).
- [18] Alice Barthe and Adrián Pérez-Salinas. *Gradients and frequency profiles of quantum re-uploading models*. Nov. 2023. DOI: [10.48550/arXiv.2311.10822](https://doi.org/10.48550/arXiv.2311.10822).
- [19] Weijie Xiong et al. *On fundamental aspects of quantum extreme learning machines*. Dec. 2023. DOI: [10.48550/arXiv.2312.15124](https://doi.org/10.48550/arXiv.2312.15124).
- [20] Zoë Holmes et al. “Connecting ansatz expressibility to gradient magnitudes and barren plateaus”. In: *PRX Quantum* 3.1 (Jan. 2022), p. 010313. ISSN: 2691-3399. DOI: [10.1103/PRXQuantum.3.010313](https://doi.org/10.1103/PRXQuantum.3.010313).

- [21] Sukin Sim, Peter D. Johnson, and Alan Aspuru-Guzik. “Expressibility and entangling capability of parameterized quantum circuits for hybrid quantum-classical algorithms”. In: *Advanced Quantum Technologies* 2.12 (Dec. 2019), p. 1900070. ISSN: 2511-9044, 2511-9044. DOI: [10.1002/qute.201900070](https://doi.org/10.1002/qute.201900070).
- [22] Zbigniew Puchała and Jarosław Adam Miszczyk. “Symbolic integration with respect to the Haar measure on the unitary group”. In: *Bulletin of the Polish Academy of Sciences Technical Sciences* 65.1 (Feb. 2017), pp. 21–27. ISSN: 2300-1917. DOI: [10.1515/bpasts-2017-0003](https://doi.org/10.1515/bpasts-2017-0003).
- [23] Richard A. Low. *Pseudo-randomness and Learning in Quantum Computation*. June 2010. DOI: [10.48550/arXiv.1006.5227](https://doi.org/10.48550/arXiv.1006.5227).
- [24] M. Cerezo et al. “Cost Function Dependent Barren Plateaus in Shallow Parametrized Quantum Circuits”. In: *Nature Communications* 12.1 (Mar. 2021), p. 1791. ISSN: 2041-1723. DOI: [10.1038/s41467-021-21728-w](https://doi.org/10.1038/s41467-021-21728-w).
- [25] Aram W. Harrow and Saeed Mehraban. “Approximate Unitary t-Designs by Short Random Quantum Circuits Using Nearest-Neighbor and Long-Range Gates”. en. In: *Communications in Mathematical Physics* 401.2 (July 2023), pp. 1531–1626. ISSN: 1432-0916. DOI: [10.1007/s00220-023-04675-z](https://doi.org/10.1007/s00220-023-04675-z).
- [26] Martin Larocca et al. “Theory of overparametrization in quantum neural networks”. In: *Nature Computational Science* 3.6 (June 2023), pp. 542–551. ISSN: 2662-8457. DOI: [10.1038/s43588-023-00467-6](https://doi.org/10.1038/s43588-023-00467-6).
- [27] N. L. Diaz et al. *Showcasing a Barren Plateau Theory Beyond the Dynamical Lie Algebra*. Oct. 2023.
- [28] Enrico Fontana et al. *The Adjoint Is All You Need: Characterizing Barren Plateaus in Quantum Ans*”atze. Sept. 2023. DOI: [10.48550/arXiv.2309.07902](https://doi.org/10.48550/arXiv.2309.07902).
- [29] Léo Monbroussou et al. *Trainability and Expressivity of Hamming-Weight Preserving Quantum Circuits for Machine Learning*. Sept. 2023. DOI: [10.48550/arXiv.2309.15547](https://doi.org/10.48550/arXiv.2309.15547).
- [30] Michael Ragone et al. *A Unified Theory of Barren Plateaus for Deep Parametrized Quantum Circuits*. Sept. 2023.
- [31] Eric R. Anschuetz et al. “Efficient classical algorithms for simulating symmetric quantum systems”. In: *Quantum* 7 (Nov. 2023), p. 1189. ISSN: 2521-327X. DOI: [10.22331/q-2023-11-28-1189](https://doi.org/10.22331/q-2023-11-28-1189).
- [32] Antonio Anna Mele. *Introduction to Haar Measure Tools in Quantum Information: A Beginner’s Tutorial*. Aug. 2023. DOI: [10.48550/arXiv.2307.08956](https://doi.org/10.48550/arXiv.2307.08956).
- [33] Ville Bergholm et al. *PennyLane: Automatic differentiation of hybrid quantum-classical computations*. July 2022. DOI: [10.48550/arXiv.1811.04968](https://doi.org/10.48550/arXiv.1811.04968).
- [34] Alastair Kay. *Tutorial on the Quantikz Package*. June 2023. DOI: [10.48550/arXiv.1809.03842](https://doi.org/10.48550/arXiv.1809.03842).
- [35] Motohisa Fukuda, Robert Koenig, and Ion Nechita. “RTNI - A symbolic integrator for Haar-random tensor networks”. In: *Journal of Physics A: Mathematical and Theoretical* 52.42 (Oct. 2019), p. 425303. ISSN: 1751-8113, 1751-8121. DOI: [10.1088/1751-8121/ab434b](https://doi.org/10.1088/1751-8121/ab434b).
- [36] Maria Schuld et al. “Circuit-centric quantum classifiers”. In: *Physical Review A* 101.3 (Mar. 2020), p. 032308. ISSN: 2469-9926, 2469-9934. DOI: [10.1103/PhysRevA.101.032308](https://doi.org/10.1103/PhysRevA.101.032308).

A Appendix: Preliminaries

A.1 Quantum Models with Hamiltonian encoding as Large Fourier series

For completeness, we revisit the proof in [7], showing that a Quantum model with Hamiltonian encoding can be expressed as a truncated Fourier series of the form in Eq.(1), with a spectrum constructed from the encoding Hamiltonians eigenvalues defined in Eq.(5).

We start by detailing the proof for the one-dimensional input case ($x \in \mathbb{R}$) and generalize it afterwards to the D -dimensional input case ($x \in \mathbb{R}^D$).

To do so, we consider an L layered ansatz of the following form $U(x; \theta) = W^{(L+1)}(\theta)S^{(L)}(x) \dots S^{(1)}(x)W^{(1)}(\theta)$ as described in Eq.(2). In what follows, we drop the explicit dependence of the trainable layers $W^{(l)}(\theta)$ on the parameter vector θ for simplicity and recall that the trainable and encoding unitaries are d -dimensional matrices acting on n qubits ($d = 2^n$).

We consider the Hamiltonian encoding scheme where the classical input $x \in \mathbb{R}$ is encoded as the time evolution of some Hamiltonian. Thus, the encoding unitary in each layer l is of the form $S^l(x) = e^{-ixH_l} \quad \forall l \in \{1, \dots, L\}$. If one considers $H_l = P_l D_l P_l^\dagger$ and injects P_l and P_l^\dagger in the parameterized unitaries W^{l+1} and W^l respectively, then $S^l(x)$ can be rewritten in the following form $S^l(x) = \text{diag}(e^{-ix\lambda_1^l}, \dots, e^{-ix\lambda_d^l})$ where λ_i^l s are eigenvalues of the underlying d -dimensional encoding Hamiltonian H_l .

We start by applying the first layer $S^{(1)}(x)W^{(1)}$ on the $|0\rangle$ computational basis state and we iterate through the remaining layers to obtain $|\psi(x; \theta)\rangle = U(x; \theta)|0\rangle$.

$$\begin{aligned} S^{(1)}(x)W^{(1)}|0\rangle &= \sum_{j_1=1}^d W_{j_1 1}^{(1)} e^{-ix\lambda_{j_1}^1} |j_1\rangle \\ S^{(2)}(x)W^{(2)}S^{(1)}(x)W^{(1)}|0\rangle &= \sum_{j_2=1}^d \sum_{j_1=1}^d W_{j_2 j_1}^{(2)} W_{j_1 1}^{(1)} e^{-ix(\lambda_{j_1}^1 + \lambda_{j_2}^2)} |j_2\rangle \\ &\vdots \\ W^{(L+1)} \prod_{l=1}^L S^{(l)}(x)W^{(l)}|0\rangle &= \sum_{k=1}^d \sum_{\mathbf{J} \in [d]^L} W_{k j_L}^{(L+1)} \dots W_{j_1 1}^{(1)} e^{-ix\Lambda_{\mathbf{J}}} |k\rangle \end{aligned}$$

where $\Lambda_{\mathbf{J}} = \sum_{j_l \in \mathbf{J}} \lambda_{j_l}$ and $\mathbf{J} = (j_1, \dots, j_L) \in \llbracket 1, d \rrbracket^L$.

The full quantum model can be written as a truncated Fourier series:

$$\begin{aligned} f(x; \theta) &= \langle 0|U(x; \theta)^\dagger O U(x; \theta)|0\rangle = \sum_{k, k'=1}^d \sum_{\mathbf{J}, \mathbf{J}' \in [d]^L} (W_{k' j'_L}^{(L+1)} \dots W_{j'_1 1}^{(1)})^* \langle k'|O|k\rangle (W_{k j_L}^{(L+1)} \dots W_{j_1 1}^{(1)}) e^{-ix(\Lambda_{\mathbf{J}} - \Lambda_{\mathbf{J}'})} \\ &= \sum_{\omega \in \Omega} \sum_{\mathbf{J}, \mathbf{J}' \in R(\omega)} c_\omega e^{-ix\omega} \end{aligned}$$

Hence, the expression of the Fourier coefficient is obtained by grouping multi-indices $(\mathbf{J}, \mathbf{J}')$ that lead to the same frequency ω (i.e. $\Lambda_{\mathbf{J}} - \Lambda_{\mathbf{J}'} = \omega$), i.e. in the frequency generator $R(\omega)$:

$$c_\omega = \sum_{\mathbf{J}, \mathbf{J}' \in R(\omega)} \sum_{k, k'} W_{j'_1 0}^{(1)*} W_{j'_2 j'_1}^{(2)*} \dots W_{k' j'_L}^{(L+1)*} O_{k' k} W_{k j_L}^{(L+1)} \dots W_{j_2 j_1}^{(2)} W_{j_1 0}^{(1)} \quad (\text{A1})$$

with

$$\begin{aligned} \Omega &= \left\{ \sum_{l \in [L]} (\lambda_{j_l}^l - \lambda_{j'_l}^l) \mid (j_1, \dots, j_L), (j'_1, \dots, j'_L) \in \llbracket 1, d \rrbracket^L \right\} \\ R(\omega) &= \left\{ (\mathbf{J}, \mathbf{J}') \in \llbracket 1, d \rrbracket^L \times \llbracket 1, d \rrbracket^L \mid \sum_{l \in [L]} (\lambda_{j_l}^l - \lambda_{j'_l}^l) = \omega \right\} \end{aligned} \quad (\text{A2})$$

We note here that using encoding Hamiltonians that act non trivially only on a subset of the n qubits will increase the eigenvalues degeneracy. Hence the redundancies $|R(\omega)|$ of all the frequencies $\omega \in \Omega$ according to Definition 1 will be multiplied by the same factor.

We further introduce the *partial* frequency generator as it will serve to derive Theorem 2 and to make comments on the spectrum distribution in general.

Definition 6 (Partial Frequency Generator). *Considering an L -layered quantum Fourier model as described in Eq.(1-5), we denote by $R_h^l(\omega)$ the ensemble of eigenvalue indices giving rise to the frequency ω by considering only encoding layers from h to l . The partial redundancy $|R_h^l(\omega)|$ is the size of this set:*

$$R_h^l(\omega) = \left\{ ((j_h, \dots, j_l), (j'_h, \dots, j'_l)) \in \llbracket 1, d \rrbracket^{l-h+1} \times \llbracket 1, d \rrbracket^{l-h+1} \left| \sum_{k=h}^l (\lambda_{j_k}^k - \lambda_{j'_k}^k) = \omega \right. \right\} \quad (\text{A3})$$

For simplicity, we denote the frequency generator $R_1^L(\omega)$ by $R(\omega)$ as defined in Definition 1 and the frequency generator from a single layer $R_l^l(\omega)$ by $R_l(\omega)$.

We can now generalize the Quantum model Fourier Series representation to the D -dimensional input setting. Assume that for $x = (x_1, \dots, x_D) \subset \mathbb{R}^D$, each component x_k is encoded as the time evolution of some Hamiltonians $H_l^{(k)} \forall l \in [L]$, such that $S^l(x) = \prod_{k=1}^D e^{-ix_k H_l^{(k)}}$. The Quantum Fourier model takes the form $f(x, \theta) = \sum_{\omega \in \Omega} c_\omega(\theta) e^{-i\omega^T x}$ and the spectrum Ω becomes the following D -dimensional Cartesian product $\Omega = \Omega_1 \times \Omega_2 \times \dots \times \Omega_D$, where each Ω_k is defined as in Eq.(A2) on its own set of Hamiltonians.

In this context, note that the frequencies ω are now vectors in \mathbb{R}^D and there are D different trees to build Ω (see Fig 2). Note that for notation simplicity, we assumed that L encoding layers were applied on each input's component, but it can be generalized to any number of layers per dimension.

We therefore see that the size of the spectrum $|\Omega|$ can potentially grow exponentially with the number of encoding layers and the dimension of the input data. For instance, consider a D -dimensional vector x and L Pauli-encoding layers for each dimension in such a way that there are LD encoding layers in the PQC. The size of the spectrum Ω would scale as $O(L^d)$, which becomes quickly intractable as d increases.

A.2 Spectrum distribution

From the above spectrum construction, one can make several observations regarding the spectrum structure and its size by considering different Hamiltonian encoding schemes. We further comment on how the spectrum distribution interacts with the Fourier coefficient expression in Eq.(A1).

In what follows, we will focus on the one-dimensional setting ($x \in \mathbb{R}$) but all the results can be easily applied to the higher dimensional setting ($x \in \mathbb{R}^D$).

Lemma 1. *(Sequential and parallel encoding) Consider the spectrum Ω_{parallel} obtained from a re-uploading circuit with L layers and encoding Hamiltonians H_1, \dots, H_L acting each on n -qubits, such that $H_l = P_l D_l P_l^\dagger, \forall l \in [L]$. The spectrum Ω_{parallel} is the same as the spectrum $\Omega_{\text{sequential}}$ obtained by considering a single layered circuit acting on nL -qubits with an encoding Hamiltonian of the form $H = P \sum_{l=1}^L D_l^{(nl, n(l+1))} P^\dagger$ where $D_l^{(nl, n(l+1))}$ acts non trivially on the subset of the total nL qubits indexed from nl to $n(l+1)$ and $P = P_1 \otimes P_2 \otimes \dots \otimes P_L$.*

Proof. We consider a single layer reuploading circuit of the form in Eq.(2) ($L = 1$) with the following encoding layer unitary acting on nL qubits:

$$\begin{aligned} S(x) &:= e^{-ixH_1} \otimes e^{-ixH_2} \otimes \dots \otimes e^{-ixH_L} \\ &= P_1 e^{-ixD_1} P_1^\dagger \otimes P_2 e^{-ixD_2} P_2^\dagger \otimes P_L \dots e^{-ixD_L} P_L^\dagger \\ &= P e^{-ix \sum_{l=1}^L D_l^{(nl, n(l+1))}} P^\dagger \end{aligned}$$

where $H_l = P_l D_l P_l^\dagger, D_l = \text{diag}(\lambda_1^l, \dots, \lambda_d^l)$ contains the eigenvalues of the Hamiltonian H_l and $P = P_1 \otimes P_2 \otimes \dots \otimes P_L$.

□

This result was already proven in [7] to convey that we can use the encoding gates in sequence or in parallel (reuploading model) to get the same spectrum. In practice, we will have a combination of the *sequential* and the *parallel* encodings

since each encoding layer in the reuploading model is usually made of one-qubit or two-qubit gates. Hence a more general form of the spectrum is the following:

$$\Omega = \left\{ \sum_{l \in [L]} \sum_{k \in [K_l]} (\lambda_{j_l, k}^{l, k} - \lambda_{j'_l, k}^{l, k}) \mid (j_{1,1}, \dots, j_{1,K}, \dots, j_{L,1}, \dots, j_{L,K}), (j'_{1,1}, \dots, j'_{1,K}, \dots, j'_{L,1}, \dots, j'_{L,K}) \in \llbracket 1, 2^{n/K} \rrbracket^{KL} \right\} \quad (\text{A4})$$

where K_l is the number of blocks of the l^{th} encoding layer and $\lambda_{j_l, k}^{l, k}$ is the eigenvalue of the local Hamiltonian $H_{l, k}$ acting non trivially on the k^{th} subsystem in layer l .

From the above construction, one can easily see that the spectrum Ω is conserved under permutation of the encoding layers and even under permutation of tensor product unitaries within the layers. However, the permutation invariance of the spectrum does not imply that we get the same quantum model under encoding blocks permutation since the expression of the Fourier coefficients in Eq.(A1) is not invariant under permutation of the indices in $(J, J') \in R(\omega)$.

Lemma 2. (Recursive spectrum construction)

We recall that $R_h^L(\omega) = \{(J := (j_h, \dots, j_L), J' := (j'_h, \dots, j'_L)) \in [d]^{L-h+1} \times [d]^{L-h+1} ; \Lambda_J - \Lambda_{J'} = \omega\}$. We denote by Ω^l the spectrum obtained from the l^{th} encoding layer and its corresponding frequency generator $R_l(\omega)$ as defined in Definition 6. Consider a Quantum Fourier model on n -qubits with L layers and a spectrum Ω . For a fixed frequency $\omega \in \Omega$, we have the following recursive relation between $R_h^L(\omega)$ and $R_{h+1}^L(\omega)$:

$$R_h^L(\omega) = \bigcup_{\substack{j_h, j'_h=1 \\ k_h=\lambda_{j_h} - \lambda_{j'_h}}}^d \{R_{h+1}^L(\omega - k_h) \times \{(j_h, j'_h)\}\}$$

Consequently, $|R_1^L(\omega)| = \sum_{k_L, \dots, k_2, k_1} \beta_{k_L} \dots \beta_{k_1} \delta_{\sum_{l=1}^L k_l}^\omega$ with $k_l \in \Omega_{distinct}^l, \forall l \in [L]$, Ω^l is the spectrum generated by the l^{th} encoding layer and $\beta_{k_l} := |R_l(k_l)|$ is the redundancy of the frequency k_l in Ω^l .

Proof. Let $(J, J') \in R_h^L(\omega)$,

$$\omega = \Lambda_J - \Lambda_{J'} = \sum_{l=h}^L (\lambda_{j_l} - \lambda_{j'_l}) = \sum_{l=h+1}^L (\lambda_{j_l} - \lambda_{j'_l}) + (\lambda_{j_h} - \lambda_{j'_h})$$

$$R_h^L(\omega) = \bigcup_{\substack{j_h, j'_h=1 \\ k_h=\lambda_{j_h} - \lambda_{j'_h}}}^d \{R_{h+1}^L(\omega - k_h) \times \{(j_h, j'_h)\}\}$$

$$|R_h^L(\omega)| = \sum_{\substack{j_h, j'_h=1 \\ k_h=\lambda_{j_h} - \lambda_{j'_h}}}^d |R_{h+1}^L(\omega - k_h)| = \sum_{k_h \in \Omega_{distinct}^h} |R_h(k_h)| |R_{h+1}^L(\omega - k_h)| = \sum_{k_h \in \Omega_{distinct}^h} \beta_{k_h} |R_{h+1}^L(\omega - k_h)|$$

Therefore we obtain : $|R_1^L(\omega)| = \sum_{k_L, \dots, k_2} \beta_{k_L} \dots \beta_{k_2} |R_1(\omega - \sum_{l=2}^L k_l)| = \sum_{k_L, \dots, k_2, k_1} \beta_{k_L} \dots \beta_{k_1} \delta_{\sum_{l=1}^L k_l}^\omega$ with each $k_l \in \Omega_{distinct}^l$, Ω^l is the spectrum generated by the l^{th} encoding layer and β_{k_l} is the redundancy of the frequency k_l in Ω^l . \square

Whether we are considering sequential encoding, parallel encoding or both, the result of Lemma 2 enables us to track the evolution of the paths in the quantum tree (See Fig.2) leading to a certain frequency and mainly to characterize the size of the spectrum $|\Omega|$ and the frequency redundancies $|R(\omega)|$.

First, one can easily see that $\forall l \in [L], |R_l(0)| \geq 2^n$. Hence the recursive construction of the spectrum implies that all frequencies that can be generated from a subset of $\kappa < L$ layers have an exponential redundancy in the number of qubits and in the number of the remaining $(L - \kappa)$ layers. Specifically, for these frequencies we have $|R(\omega)| \geq 2^{n(L-\kappa)}$.

Consequently, adopting the reuploading scheme leads inevitably to exponential redundancies in n as mentioned in [18]. Moreover, if one considers tensor product encoding unitaries within a single encoding layer (i.e. Pauli rotations), then the frequencies already generated by few blocks will have exponential redundancies in n .

We give some examples of encoding Hamiltonians and explicit the obtained spectrum, its size and the redundancies scaling in each case. For more details, we refer the reader to a discussion of the degeneracy of a Quantum Fourier model spectrum in [13] (See Appendix C).

A.2.1 Pauli encoding

The Pauli encoding scheme consists in using Pauli matrices $\{\sigma_x, \sigma_y, \sigma_z\}$ as encoding Hamiltonians, such that a single encoding layer is a tensor product of Pauli rotations parameterized by x : $S^l(x) := \otimes_{i=1}^n e^{-ix\sigma/2}$, $\sigma \in \{\sigma_x, \sigma_y, \sigma_z\}$. In this case, all eigenvalues are $\lambda = \pm 1/2$. Hence by using Eq. A4, the set of frequencies we obtain by applying Pauli rotations on all n -qubits in each of the L layers are consecutive integer frequencies from $-nL$ to nL . Hence the size of the spectrum $|\Omega| = 2nL$ and $|R(k)| = \binom{2nL}{nL-|k|} \forall k \in \llbracket -nL, nL \rrbracket$. The redundancy value can be obtained by using Lemma 2.

A.2.2 Exponential encoding

If we consider single qubit Pauli rotations for encoding with a scaling coefficient, the largest spectrum we can get is of size $|\Omega| = 3^{nL}$ since the spectrum of a scaled Pauli matrix is of the form $\{-\lambda, \lambda\}$. One spectrum that reaches this limit is the set of consecutive integer frequencies from $-\frac{3^{nL}}{2}$ to $\frac{3^{nL}}{2}$ with $|\Omega| = 3^{nL}$. This spectrum is obtained by using the scaling coefficient 3^{jl} in the Pauli rotation gate acting on qubit j in layer l . This scheme was introduced in [14] under the name of *exponential encoding*, which refers to the exponential size of the spectrum in the number of qubits/layers. We note that $|R(\omega = k)| = 2^{nL-T(|k|)}$ where $T(|k|)$ takes values in $\llbracket 0, nL \rrbracket$. More details about the proof are provided in [13, 14].

A.2.3 Non degenerate encoding (Golomb encoding)

As mentioned in Lemma 2, with the reuploading scheme we will certainly have frequencies with redundancies exponential in the number of layers. However to surpass the limit $|\Omega^l| = 3^n$ per layer l , one needs to consider non separable encoding unitaries in a single layer. A perfectly non degenerate spectrum for a single encoding layer ($|R(\omega)| = 1 \forall \omega \in \Omega \setminus \{0\}$) was proposed in [13] by setting the diagonal of the data-encoding Hamiltonian to the elements of a Golomb ruler. However, we stress again that using this scheme in the reuploading model will give rise to redundancies that are still exponential in nL for frequencies generated from few layers since the null frequency in a single layer has redundancy $|R(0)| = 2^n$.

B Appendix: Proofs

B.1 Proof of theorem 2

We recall the Theorem 2:

Theorem 2. Consider an L -layered Quantum Fourier model with Fourier coefficients $c_\omega(\theta)$ in Eq. (3) with spectrum Ω and redundancies $|R(\omega)|$. We assume that each of the parameterized layers form independently a 2-design (under the uniform distribution over their parameters). The expectation and variance of each Fourier coefficient in the spectrum Ω is given by:

$$\begin{aligned} \mathbb{E}_\theta[c_\omega(\theta)] &= \frac{\text{Tr}(O)}{d} \delta_\omega^0 \\ \text{Var}_\theta[c_\omega(\theta)] &\simeq \frac{d\|O\|_2^2 - \text{Tr}(O)^2}{d(d^2 - 1)} \left[\frac{|R_1^L(\omega)| - |R_2^L(\omega)|}{d(d+1)(d^2-1)^{L-1}} + \sum_{j=3}^L \frac{|R_j^L(\omega)|}{d(d^2-1)^{L-j+2}} \right] + \frac{\text{Tr}(O)^2 - d\|O\|_2^2}{d^2(d^2-1)} \delta_\omega^0 \end{aligned} \quad (13)$$

Here $R_j^L(\omega)$ denotes the partial spectrum formed from the j^{th} up to the L^{th} encoding layers as defined in Definition (6).

Proof. We start by proving the expression of the expectation value of a Fourier coefficient and note that it is sufficient to establish this result under the 1-design hypothesis. To do so, we apply the Weingarten formula of the first moment [32] on Eq.(A1). We get:

$$\begin{aligned} \mathbb{E}_{W^{(1)}, \dots, W^{(L+1)} \sim U(N)} [c_\omega] &= \sum_{\substack{k, k' \\ J, J' \in R(\omega)}} \frac{\delta_{j_1}^{j'_1} \delta_{j_2}^{j'_2} \dots \delta_{j_L}^{j'_L} \delta_k^{k'} O_{k'k}}{d^{L+1}} = \sum_{\substack{k \\ J, J' \in R(\omega)}} \frac{\delta_{j_1}^{j'_1} \delta_{j_2}^{j'_2} \dots \delta_{j_L}^{j'_L} O_{kk}}{d^{L+1}} = \sum_{J, J' \in R(\omega)} \delta_J^{J'} \frac{\text{Tr}(O)}{d^{L+1}} \\ &= \frac{\text{Tr}(O)}{d} \delta_\omega^0 \end{aligned} \quad (B1)$$

The variance of a Fourier coefficient for a reuploading VQC (i.e $L > 1$) is obtained recursively starting from the variance of a single-layered circuit and using the recursive relation between the partial redundancies $R_h^L(\omega)$ established in Lemma 2.

From Eq.(A1), we give the expression of $\mathbb{E}_{W^{(1)}, \dots, W^{(L+1)} \sim U(N)} [|c_\omega|^2]$:

$$\begin{aligned} \mathbb{E}_{W^{(1)}, \dots, W^{(L+1)} \sim U(N)} [|c_\omega|^2] &= \sum_{\substack{I, I' \in R(\omega) \\ J, J' \in R(\omega)}} \mathbb{E} \left[W_{j_1 i_1}^{(1)} W_{i_1' j_1'}^{(1)} W_{j_1' i_1}^{(1)*} W_{i_1 j_1}^{(1)*} \right] \\ &\quad \mathbb{E} \left[W_{j_2 j_1}^{(2)} W_{i_2' i_1'}^{(2)} W_{j_2' j_1'}^{(2)*} W_{i_2 i_1}^{(2)*} \right] \\ &\quad \vdots \\ &\quad \mathbb{E} \left[W_{j_L j_{L-1}}^{(L)} W_{i_L' i_{L-1}'}^{(L)} W_{j_L' j_{L-1}'}^{(L)*} W_{i_L i_{L-1}}^{(L)*} \right] \\ &\quad \sum_{\substack{k, k' \\ h, h'}} \mathbb{E} \left[W_{k j_L}^{(L+1)} W_{h' i_L'}^{(L+1)} W_{k' j_L'}^{(L+1)*} W_{h i_L}^{(L+1)*} \right] O_{k' k} O_{h h'} \end{aligned} \tag{B2}$$

Using the Weingarten calculus for first and second moment monomials [32], we compute independently the terms in the sum of Eq.(B2):

- The first term depends on the parameterized part of the first layer $W^{(1)}$: $\mathbb{E}_{W^{(1)}} \left[W_{j_1 i_1}^{(1)} W_{i_1' j_1'}^{(1)} W_{j_1' i_1}^{(1)*} W_{i_1 j_1}^{(1)*} \right] = \frac{1}{d(d+1)} \left(\delta_{j_1 i_1}^{j_1' i_1'} + \delta_{i_1 i_1'}^{j_1 j_1'} \right)$

- The last term depends on the parameterized part $W^{(L+1)}$ and the observable O :

$$\begin{aligned} \mathbb{E}_{W^{(L+1)}} \sum_{\substack{k, k' \\ h, h'}} \left[W_{k j_L}^{(L+1)} W_{h' i_L'}^{(L+1)} W_{k' j_L'}^{(L+1)*} W_{h i_L}^{(L+1)*} \right] O_{k' k} O_{h h'} \\ = \delta_{j_L i_L}^{j_L' i_L'} \left(\frac{d \text{Tr}(O)^2 - \|O\|^2}{d(d^2 - 1)} \right) + \delta_{i_L i_L'}^{j_L j_L'} \left(\frac{d \|O\|^2 - \text{Tr}(O)^2}{d(d^2 - 1)} \right) = C_1 \delta_{j_L i_L}^{j_L' i_L'} + C_2 \delta_{i_L i_L'}^{j_L j_L'} \end{aligned}$$

where $C_1 = \frac{d \text{Tr}(O)^2 - \|O\|^2}{d(d^2 - 1)}$ and $C_2 = \frac{d \|O\|^2 - \text{Tr}(O)^2}{d(d^2 - 1)}$.

- For the remaining layers, we get $\forall l \notin \{1, L+1\}$

$$\begin{aligned} \mathbb{E}_{W^{(l)}} \left[W_{j_l i_{l-1}}^{(l)} W_{i_{l-1}' j_{l-1}'}^{(l)} W_{j_l' i_{l-1}}^{(l)*} W_{i_{l-1} j_l}^{(l)*} \right] \\ = \frac{\delta_{j_l i_{l-1}}^{j_l' i_{l-1}'} \delta_{j_{l-1} i_{l-1}'}^{j_{l-1}' i_{l-1}'} + \delta_{i_{l-1} i_{l-1}'}^{j_l j_{l-1}'} \delta_{j_{l-1} i_{l-1}'}^{j_l' i_{l-1}'} - \delta_{j_l i_{l-1}}^{j_l' i_{l-1}'} \delta_{i_{l-1} i_{l-1}'}^{j_{l-1}' j_{l-1}'} + \delta_{i_{l-1} i_{l-1}'}^{j_l j_{l-1}'} \delta_{j_{l-1} i_{l-1}'}^{j_l' i_{l-1}'} }{d^2 - 1} \end{aligned}$$

We denote by c_ω^L the Fourier coefficient if we consider the full circuit up to the L layer and we establish in what follows a recursion relation between $\mathbb{E}[|c_\omega^L|^2]$ and $\mathbb{E}[|c_\omega^{L-1}|^2]$ where c_ω^{L-1} is a Fourier coefficient of the quantum model generated by the first $L - 1$ layers.

$$\begin{aligned}
\mathbb{E}_{W^{(1)}, \dots, W^{(L+1)} \sim U(N)} [|c_\omega^L|^2] &= \sum_{\substack{J, J' \in R_1^L(\omega) \\ I, I' \in R_1^L(\omega)}} \mathbb{E} \left[W_{j_1 1}^{(1)} W_{i'_1 1}^{(1)} W_{j'_1 1}^{(1)*} W_{i_1 1}^{(1)*} \right] \\
&\quad \mathbb{E} \left[W_{j_2 j_1}^{(2)} W_{i'_2 i'_1}^{(2)} W_{j'_2 j'_1}^{(2)*} W_{i_2 i_1}^{(2)*} \right] \\
&\quad \vdots \\
&\quad \mathbb{E} \left[W_{j_{L-1} j_{L-2}}^{(L-1)} W_{i'_{L-1} i'_{L-2}}^{(L-1)} W_{j'_{L-1} j'_{L-2}}^{(L-1)*} W_{i_{L-1} i_{L-2}}^{(L-1)*} \right] \\
&\quad \mathbb{E} \left[W_{j_L j_{L-1}}^{(L)} W_{i'_L i'_{L-1}}^{(L)} W_{j'_L j'_{L-1}}^{(L)*} W_{i_L i_{L-1}}^{(L)*} \right] \\
&\quad (C_1 \delta_{j_L}^{j'_L} \delta_{i_L}^{i'_{L-1}} + C_2 \delta_{i_L}^{j'_L} \delta_{i'_L}^{j'_L})
\end{aligned} \tag{B3}$$

$$\begin{aligned}
\mathbb{E}_{W^{(1)}, \dots, W^{(L)} \sim U(N)} [|c_\omega^{L-1}|^2] &= \sum_{\substack{J, J' \in R_1^{L-1}(\omega) \\ I, I' \in R_1^{L-1}(\omega)}} \mathbb{E} \left[W_{j_1 1}^{(1)} W_{i'_1 1}^{(1)} W_{j'_1 1}^{(1)*} W_{i_1 1}^{(1)*} \right] \\
&\quad \mathbb{E} \left[W_{j_2 j_1}^{(2)} W_{i'_2 i'_1}^{(2)} W_{j'_2 j'_1}^{(2)*} W_{i_2 i_1}^{(2)*} \right] \\
&\quad \vdots \\
&\quad \mathbb{E} \left[W_{j_{L-1} j_{L-2}}^{(L-1)} W_{i'_{L-1} i'_{L-2}}^{(L-1)} W_{j'_{L-1} j'_{L-2}}^{(L-1)*} W_{i_{L-1} i_{L-2}}^{(L-1)*} \right] \\
&\quad (C_1 \delta_{j_{L-1}}^{j'_{L-1}} \delta_{i_{L-1}}^{i'_{L-1}} + C_2 \delta_{i_{L-1}}^{j'_{L-1}} \delta_{i'_{L-1}}^{j'_{L-1}})
\end{aligned} \tag{B4}$$

In what follows, we use the color code [...] to refer to the product of expectation values over the parameterized blocks from layers 1 to $L - 1$ as done in Eq.(B3). To make appear $\mathbb{E}_{W^{(1)}, \dots, W^{(L)} \sim U(N)} |c_\omega^{L-1}|^2$, we expand $\mathbb{E} \left[W_{j_L j_{L-1}}^{(L)} W_{i'_L i'_{L-1}}^{(L)} W_{j'_L j'_{L-1}}^{(L)*} W_{i_L i_{L-1}}^{(L)*} \right] (C_1 \delta_{j_L}^{j'_L} \delta_{i_L}^{i'_{L-1}} + C_2 \delta_{i_L}^{j'_L} \delta_{i'_L}^{j'_L})$ in the expression of $\mathbb{E}_{W^{(1)}, \dots, W^{(L+1)} \sim U(N)} |c_\omega^L|^2$. This expansion is done by means of the recursive decomposition of $R_1^L(\omega)$. To do so, we first decompose the expression of $\mathbb{E} [|c_\omega^L|^2]$ into $A_1^L(\omega)$ and $A_2^L(\omega)$ and explicit afterwards the recursive relation for each of the terms.

$$\begin{aligned}
\mathbb{E} [|c_\omega^L|^2] &= \sum_{\substack{J, J' \in R_1^L(\omega) \\ I, I' \in R_1^L(\omega)}} [\dots] \mathbb{E} \left[W_{j_L j_{L-1}}^{(L)} W_{i'_L i'_{L-1}}^{(L)} W_{j'_L j'_{L-1}}^{(L)*} W_{i_L i_{L-1}}^{(L)*} \right] (C_1 \delta_{j_L}^{j'_L} \delta_{i_L}^{i'_{L-1}} + C_2 \delta_{i_L}^{j'_L} \delta_{i'_L}^{j'_L}) \\
&= C_1 A_1^L(\omega) + C_2 A_2^L(\omega) \\
A_1^L(\omega) &= \sum_{\substack{J, J' \in R_1^L(\omega) \\ I, I' \in R_1^L(\omega)}} \delta_{j_L}^{j'_L} \delta_{i_L}^{i'_{L-1}} \mathbb{E} \left[W_{j_L j_{L-1}}^{(L)} W_{i'_L i'_{L-1}}^{(L)} W_{j'_L j'_{L-1}}^{(L)*} W_{i_L i_{L-1}}^{(L)*} \right] \\
A_2^L(\omega) &= \sum_{\substack{J, J' \in R_1^L(\omega) \\ I, I' \in R_1^L(\omega)}} \delta_{i_L}^{j'_L} \delta_{i'_L}^{j'_L} \mathbb{E} \left[W_{j_L j_{L-1}}^{(L)} W_{i'_L i'_{L-1}}^{(L)} W_{j'_L j'_{L-1}}^{(L)*} W_{i_L i_{L-1}}^{(L)*} \right]
\end{aligned} \tag{B5}$$

we start with the first step of the recursion ($L = 1$):

$$\begin{aligned}
A_1^1(\omega) &= \sum_{\substack{j_1, j'_1 \in R_1(\omega) \\ i_1, i'_1 \in R_1(\omega)}} \mathbb{E} \left[W_{j_1 1}^{(1)} W_{i'_1 1}^{(1)} W_{j'_1 1}^{(1)*} W_{i_1 1}^{(1)*} \right] \delta_{j_1}^{j'_1} \delta_{i_1}^{i'_1} = \sum_{\substack{j_1, j'_1 \in R_1(\omega) \\ i_1, i'_1 \in R_1(\omega)}} \left(\frac{\delta_{j_1}^{j'_1} \delta_{i_1}^{i'_1} + \delta_{i_1}^{j_1} \delta_{i'_1}^{j'_1}}{d(d+1)} \right) \delta_{j_1}^{j'_1} \delta_{i_1}^{i'_1} \\
&= \sum_{\substack{j_1, j'_1 \in R_1(\omega) \\ i_1, i'_1 \in R_1(\omega)}} \frac{\delta_{j_1}^{j'_1} \delta_{i_1}^{i'_1}}{d(d+1)} + \sum_{\substack{j_1, j'_1 \in R_1(\omega) \\ i_1, i'_1 \in R_1(\omega)}} \frac{\delta_{i_1}^{j_1} \delta_{i'_1}^{j'_1}}{d(d+1)} = \sum_{\substack{j_1, j'_1 \in R_1(\omega) \\ i_1, i_1 \in R_1(\omega)}} \frac{1}{d(d+1)} + \sum_{\substack{j_1, j_1 \in R_1(\omega)}} \frac{1}{d(d+1)} \\
&= \frac{d^2}{d(d+1)} \delta_\omega^0 + \frac{d}{d(d+1)} \delta_\omega^0 = \delta_\omega^0
\end{aligned} \tag{B6}$$

$$\begin{aligned}
A_2^1(\omega) &= \sum_{\substack{j_1, j'_1 \in R_1(\omega) \\ i_1, i'_1 \in R_1(\omega)}} \mathbb{E} \left[W_{j_1 1}^{(1)} W_{i'_1 1}^{(1)} W_{j'_1 1}^{(1)*} W_{i_1 1}^{(1)*} \right] \delta_{i_1}^{j_1} \delta_{i'_1}^{j'_1} = \sum_{\substack{j_1, j'_1 \in R_1(\omega) \\ i_1, i'_1 \in R_1(\omega)}} \left(\frac{\delta_{j_1}^{j'_1} \delta_{i_1}^{i'_1} + \delta_{i_1}^{j_1} \delta_{i'_1}^{j'_1}}{d(d+1)} \right) \delta_{i_1}^{j_1} \delta_{i'_1}^{j'_1} \\
&= \sum_{\substack{j_1, j'_1 \in R_1(\omega) \\ i_1, i'_1 \in R_1(\omega)}} \frac{\delta_{j_1}^{j'_1} \delta_{i_1}^{i'_1} \delta_{i_1}^{j_1} \delta_{i'_1}^{j'_1}}{d(d+1)} + \sum_{\substack{j_1, j'_1 \in R_1(\omega) \\ i_1, i'_1 \in R_1(\omega)}} \frac{\delta_{i_1}^{j_1} \delta_{i'_1}^{j'_1}}{d(d+1)} = \frac{d}{d(d+1)} \delta_\omega^0 + \sum_{\substack{j_1, j'_1 \in R_1(\omega)}} \frac{1}{d(d+1)} \\
&= \frac{1}{d+1} \delta_\omega^0 + \frac{|R_1(\omega)|}{d(d+1)}
\end{aligned}$$

The recursive relation between $A_1^L(\omega)$ and $A_1^{L-1}(\omega)$ is then given by:

$$\begin{aligned}
A_1^L(\omega) &= \sum_{\substack{J, J' \in R_1^L(\omega) \\ I, I' \in R_1^L(\omega)}} [\dots] \delta_{j_L}^{j'_L} \delta_{i_L}^{i'_L} \mathbb{E} \left[W_{j_L j_{L-1}}^{(L)} W_{i'_L i'_{L-1}}^{(L)} W_{j'_L j'_{L-1}}^{(L)*} W_{i_L i_{L-1}}^{(L)*} \right] \\
&= \sum_{\substack{j_L, j'_L=1 \\ i_L, i'_L=1}}^d [\dots] \delta_{j_L}^{j'_L} \delta_{i_L}^{i'_L} \left(\frac{\delta_{j_L}^{j'_L} \delta_{i_L}^{i'_L} \delta_{j_{L-1}}^{j'_{L-1}} \delta_{i_{L-1}}^{i'_{L-1}} + \delta_{i_L}^{j'_L} \delta_{i'_L}^{j'_L} \delta_{i_{L-1}}^{j'_{L-1}} \delta_{i'_{L-1}}^{j'_{L-1}}}{d^2 - 1} - \frac{\delta_{j'_L}^{j'_L} \delta_{i'_L}^{i'_L} \delta_{j_{L-1}}^{j'_{L-1}} \delta_{i'_{L-1}}^{j'_{L-1}} + \delta_{i_L}^{j'_L} \delta_{i'_L}^{j'_L} \delta_{j_{L-1}}^{j'_{L-1}} \delta_{i'_{L-1}}^{j'_{L-1}}}{d(d^2 - 1)} \right) \\
&\quad J, J' \in R_1^{L-1}(\omega - k_L) \times (j_L, j'_L) \\
&\quad I, I' \in R_1^{L-1}(\omega - k_L) \times (i_L, i'_L) \\
&= \sum_{\substack{j_L=1 \\ i_L=1}}^d [\dots] \left(\frac{\delta_{j_{L-1}}^{j'_{L-1}} \delta_{i_{L-1}}^{i'_{L-1}} + \delta_{i_L}^{j'_L} \delta_{i'_L}^{j'_L} \delta_{i_{L-1}}^{j'_{L-1}} \delta_{i'_{L-1}}^{j'_{L-1}}}{d^2 - 1} - \frac{\delta_{j_{L-1}}^{j'_{L-1}} \delta_{i_{L-1}}^{j'_{L-1}} + \delta_{i_L}^{j'_L} \delta_{i'_L}^{j'_L} \delta_{j_{L-1}}^{j'_{L-1}} \delta_{i'_{L-1}}^{j'_{L-1}}}{d(d^2 - 1)} \right) \\
&= \sum_{j_L=1}^d \sum_{i_L=j_L} \sum_{\substack{J, J' \in R_1^{L-1}(\omega-0) \times (j_L, j_L) \\ I, I' \in R_1^{L-1}(\omega-0) \times (j_L, j_L)}} [\dots] \left(\frac{\delta_{j_{L-1}}^{j'_{L-1}} \delta_{i_{L-1}}^{i'_{L-1}} + \delta_{i_{L-1}}^{j'_{L-1}} \delta_{i'_{L-1}}^{j'_{L-1}}}{d^2 - 1} - \frac{\delta_{j_{L-1}}^{j'_{L-1}} \delta_{i_{L-1}}^{j'_{L-1}} + \delta_{i_{L-1}}^{j'_{L-1}} \delta_{i'_{L-1}}^{j'_{L-1}}}{d(d^2 - 1)} \right) \\
&\quad + \sum_{j_L=1}^d \sum_{i_L \neq j_L} \sum_{\substack{J, J' \in R_1^{L-1}(\omega-0) \times (j_L, j_L) \\ I, I' \in R_1^{L-1}(\omega-0) \times (i_L, i_L)}} [\dots] \left(\frac{\delta_{j_{L-1}}^{j'_{L-1}} \delta_{i_{L-1}}^{i'_{L-1}}}{d^2 - 1} - \frac{\delta_{i_{L-1}}^{j'_{L-1}} \delta_{i'_{L-1}}^{j'_{L-1}}}{d(d^2 - 1)} \right) \\
&= \sum_{j_L=1}^d \sum_{\substack{J, J' \in R_1^{L-1}(\omega-0) \times (j_L, j_L) \\ I, I' \in R_1^{L-1}(\omega-0) \times (j_L, j_L)}} [\dots] \left(\frac{\delta_{j_{L-1}}^{j'_{L-1}} \delta_{i_{L-1}}^{i'_{L-1}} + \delta_{i_{L-1}}^{j'_{L-1}} \delta_{i'_{L-1}}^{j'_{L-1}}}{d(d+1)} \right) \\
&\quad + \sum_{j_L=1}^d \sum_{i_L \neq j_L} \sum_{\substack{J, J' \in R_1^{L-1}(\omega-0) \times (j_L, j_L) \\ I, I' \in R_1^{L-1}(\omega-0) \times (i_L, i_L)}} [\dots] \left(\frac{\delta_{j_{L-1}}^{j'_{L-1}} \delta_{i_{L-1}}^{i'_{L-1}}}{d^2 - 1} - \frac{\delta_{i_{L-1}}^{j'_{L-1}} \delta_{i'_{L-1}}^{j'_{L-1}}}{d(d^2 - 1)} \right) \\
&= d \sum_{\substack{J, J' \in R_1^{L-1}(\omega-0) \\ I, I' \in R_1^{L-1}(\omega-0)}} [\dots] \left(\frac{\delta_{j_{L-1}}^{j'_{L-1}} \delta_{i_{L-1}}^{i'_{L-1}} + \delta_{i_{L-1}}^{j'_{L-1}} \delta_{i'_{L-1}}^{j'_{L-1}}}{d(d+1)} \right) + d(d-1) \sum_{\substack{J, J' \in R_1^{L-1}(\omega-0) \\ I, I' \in R_1^{L-1}(\omega-0)}} [\dots] \left(\frac{\delta_{j_{L-1}}^{j'_{L-1}} \delta_{i_{L-1}}^{i'_{L-1}}}{d^2 - 1} - \frac{\delta_{i_{L-1}}^{j'_{L-1}} \delta_{i'_{L-1}}^{j'_{L-1}}}{d(d^2 - 1)} \right) \\
&= \frac{1}{d+1} [A_1^{L-1}(\omega) + A_2^{L-1}(\omega)] + \frac{d}{d+1} A_1^{L-1}(\omega) - \frac{1}{d+1} A_2^{L-1}(\omega) \\
&= A_1^{L-1}(\omega)
\end{aligned} \tag{B7}$$

We showed that $\forall \omega \in \Omega, \forall L \geq 2, A_1^L(\omega) = A_1^{L-1}(\omega)$. Hence,

$$\forall \omega \in \Omega, \forall L \geq 1, A_1^L(\omega) = A_1^1(\omega) \tag{B8}$$

For the recursive relation between $A_2^L(\omega)$ and $A_2^{L-1}(\omega)$, we get the following:

$$\begin{aligned}
A_2^L(\omega) &= \sum_{\substack{J, J' \in R_1^L(\omega) \\ I, I' \in R_1^L(\omega)}} [\dots] \delta_{i_L}^{j_L} \delta_{i'_L}^{j'_L} \mathbb{E} \left[W_{j_L j_{L-1}}^{(L)} W_{i'_L i'_{L-1}}^{(L)} W_{j'_L j'_{L-1}}^{(L)*} W_{i_L i_{L-1}}^{(L)*} \right] \\
&= \sum_{\substack{i_L, i'_L=1 \\ j_L, j'_L=1 \\ I, I' \in R_1^{L-1}(\omega - k_L) \times (i_L, i'_L) \\ J, J' \in R_1^{L-1}(\omega - k_L) \times (j_L, j'_L)}} [\dots] \delta_{i_L}^{j_L} \delta_{i'_L}^{j'_L} \left(\frac{\delta_{j_L}^{i_L} \delta_{i_L}^{i'_L} \delta_{j_{L-1}}^{i_{L-1}} \delta_{i_{L-1}}^{i'_{L-1}} + \delta_{i_L}^{j_L} \delta_{i'_L}^{j'_L} \delta_{i_{L-1}}^{j_{L-1}} \delta_{i'_{L-1}}^{j'_{L-1}}}{d^2 - 1} - \frac{\delta_{j_L}^{i'_L} \delta_{i'_L}^{i_{L-1}} \delta_{j_{L-1}}^{i_{L-1}} + \delta_{i_L}^{j_L} \delta_{i'_L}^{j'_L} \delta_{j_{L-1}}^{i_{L-1}} \delta_{i'_{L-1}}^{j'_{L-1}}}{d(d^2 - 1)} \right) \\
&= \sum_{j_L, j'_L=1}^d \sum_{J, J' \in R_1^{L-1}(\omega - k_L) \times (j_L, j'_L)} [\dots] \left(\frac{\delta_{j_L}^{i_L} \delta_{j_{L-1}}^{i_{L-1}} \delta_{i_{L-1}}^{i'_{L-1}} + \delta_{i_{L-1}}^{j_L} \delta_{i'_{L-1}}^{j_L}}{d^2 - 1} - \frac{\delta_{j_L}^{i'_L} \delta_{i_{L-1}}^{i'_{L-1}} \delta_{i'_{L-1}}^{j_{L-1}} + \delta_{i_{L-1}}^{j_L} \delta_{i'_{L-1}}^{j_{L-1}}}{d(d^2 - 1)} \right) \\
&= \sum_{j_L=1}^d \sum_{j'_L=j_L} \sum_{J, J' \in R_1^{L-1}(\omega - k_L) \times (j_L, j_L)} [\dots] \left(\frac{\delta_{j_{L-1}}^{i_{L-1}} \delta_{i_{L-1}}^{i'_{L-1}} + \delta_{i_{L-1}}^{j_{L-1}} \delta_{i'_{L-1}}^{j_{L-1}}}{d^2 - 1} - \frac{\delta_{j_{L-1}}^{i_{L-1}} \delta_{i'_{L-1}}^{j_{L-1}} + \delta_{i_{L-1}}^{j_{L-1}} \delta_{i'_{L-1}}^{j_{L-1}}}{d(d^2 - 1)} \right) \\
&\quad + \sum_{j_L=1}^d \sum_{j'_L \neq j_L} \sum_{J, J' \in R_1^{L-1}(\omega - k_L) \times (j_L, j'_L)} [\dots] \left(\frac{\delta_{i_{L-1}}^{j_{L-1}} \delta_{i'_{L-1}}^{j_{L-1}}}{d^2 - 1} - \frac{\delta_{j_{L-1}}^{i_{L-1}} \delta_{i'_{L-1}}^{j_{L-1}}}{d(d^2 - 1)} \right) \\
&= \sum_{j_L=1}^d \sum_{j'_L=j_L} \sum_{J, J' \in R_1^{L-1}(\omega - 0) \times (j_L, j_L)} [\dots] \left(\frac{\delta_{j_{L-1}}^{i_{L-1}} \delta_{i_{L-1}}^{i'_{L-1}} + \delta_{i_{L-1}}^{j_{L-1}} \delta_{i'_{L-1}}^{j_{L-1}}}{d(d+1)} \right) \\
&\quad + \sum_{j_L=1}^d \sum_{j'_L \neq j_L} \sum_{J, J' \in R_1^{L-1}(\omega - k_L) \times (j_L, j'_L)} [\dots] \left(\frac{\delta_{i_{L-1}}^{j_{L-1}} \delta_{i'_{L-1}}^{j_{L-1}}}{d^2 - 1} - \frac{\delta_{j_{L-1}}^{i_{L-1}} \delta_{i'_{L-1}}^{j_{L-1}}}{d(d^2 - 1)} \right) \\
&= d \sum_{J, J' \in R_1^{L-1}(\omega - 0)} [\dots] \left(\frac{\delta_{j_{L-1}}^{i_{L-1}} \delta_{i_{L-1}}^{i'_{L-1}} + \delta_{i_{L-1}}^{j_{L-1}} \delta_{i'_{L-1}}^{j_{L-1}}}{d(d+1)} \right) + \sum_{\substack{j_L, j'_L \\ j'_L \neq j_L}} \sum_{J, J' \in R_1^{L-1}(\omega - k_L)} [\dots] \left(\frac{\delta_{i_{L-1}}^{j_{L-1}} \delta_{i'_{L-1}}^{j_{L-1}}}{d^2 - 1} - \frac{\delta_{j_{L-1}}^{i_{L-1}} \delta_{i'_{L-1}}^{j_{L-1}}}{d(d^2 - 1)} \right) \\
&= \frac{1}{d+1} [A_1^{L-1}(\omega) + A_2^{L-1}(\omega)] + \sum_{\substack{j_L, j'_L \\ j'_L \neq j_L}} \left[\frac{1}{d^2 - 1} A_2^{L-1}(\omega - k_L) - \frac{1}{d(d^2 - 1)} A_1^{L-1}(\omega - k_L) \right] \\
&= \frac{1}{d+1} [\delta_\omega^0 + A_2^{L-1}(\omega)] + \sum_{\substack{j_L, j'_L \\ j'_L \neq j_L}} \left[\frac{1}{d^2 - 1} A_2^{L-1}(\omega - k_L) - \frac{1}{d(d^2 - 1)} \delta_\omega^{k_L} \right] \\
&= \frac{1}{d+1} [\delta_\omega^0 + A_2^{L-1}(\omega)] + \sum_{\substack{j_L, j'_L \\ j'_L \neq j_L}} \frac{A_2^{L-1}(\omega - k_L)}{d^2 - 1} - \frac{|R_L(\omega)| - d\delta_\omega^0}{d(d^2 - 1)} \\
&= \frac{d-1}{d^2 - 1} A_2^{L-1}(\omega) + \sum_{\substack{j_L, j'_L \\ j'_L \neq j_L}} \frac{A_2^{L-1}(\omega - k_L)}{d^2 - 1} + \frac{d\delta_\omega^0}{d^2 - 1} - \frac{|R_L(\omega)|}{d(d^2 - 1)} \\
&= \sum_{j_L, j'_L} \frac{A_2^{L-1}(\omega - k_L)}{d^2 - 1} - \frac{A_2^{L-1}(\omega)}{d^2 - 1} + \frac{d\delta_\omega^0}{d^2 - 1} - \frac{|R_L(\omega)|}{d(d^2 - 1)} \\
&= \sum_{k_L \in \Omega_{distinct}^L} \frac{|R_L(k_L)| - \delta_{k_L}^0}{d^2 - 1} A_2^{L-1}(\omega - k_L) + \frac{d\delta_\omega^0}{d^2 - 1} - \frac{|R_L(\omega)|}{d(d^2 - 1)}
\end{aligned}$$

(B9)

Thus, the final recursion formula for $A_2^L(\omega)$ is the following:

$$\begin{aligned} \forall \omega, \forall L \geq 2, A_2^L(\omega) &= \sum_{k_L \in \Omega_{distinct}^L} \frac{|R_L(k_L)| - \delta_{k_L}^0}{d^2 - 1} A_2^{L-1}(\omega - k_L) + \frac{d\delta_\omega^0}{d^2 - 1} - \frac{|R_L(\omega)|}{d(d^2 - 1)} \\ &= \sum_{k_L \in \Omega_{distinct}^L} \alpha_{k_L} A_2^{L-1}(\omega - k_L) + \frac{d\delta_\omega^0}{d^2 - 1} - \frac{|R_L(\omega)|}{d(d^2 - 1)} \end{aligned}$$

We iterate through L to find the expression of $A_2^L(\omega)$:

$$\begin{aligned} A_2^L(\omega) &= \sum_{k_L, \dots, k_2} \alpha_{k_L} \dots \alpha_{k_2} \left[\frac{\delta_{\omega - \sum_{l=2}^L k_l}^0}{d+1} + \frac{|R_1(\omega - \sum_{l=2}^L k_l)|}{d(d+1)} \right] \\ &+ \sum_{k_L, \dots, k_3} \alpha_{k_L} \dots \alpha_{k_3} \left[\frac{d\delta_{\omega - \sum_{l=3}^L k_l}^0}{d^2 - 1} - \frac{|R_2(\omega - \sum_{l=3}^L k_l)|}{d(d^2 - 1)} \right] \\ &+ \dots + \sum_{k_L, \dots, k_h} \alpha_{k_L} \dots \alpha_{k_h} \left[\frac{d\delta_{\omega - \sum_{l=h}^L k_l}^0}{d^2 - 1} - \frac{|R_{h-1}(\omega - \sum_{l=h}^L k_l)|}{d(d^2 - 1)} \right] + \dots \\ &+ \sum_{k_L} \alpha_{k_L} \left[\frac{d\delta_{\omega - k_L}^0}{d^2 - 1} - \frac{|R_{L-1}(\omega - k_L)|}{d(d^2 - 1)} \right] + \frac{d\delta_\omega^0}{d^2 - 1} - \frac{|R_L(\omega)|}{d(d^2 - 1)} \end{aligned} \quad (\text{B10})$$

We have $\alpha_{k_l} = \frac{(|R_l(k_l)| - \delta_{k_l}^0)}{d^2 - 1} = \frac{(\beta_{k_l} - \delta_{k_l}^0)}{d^2 - 1} \simeq \frac{\beta_{k_l}}{d^2 - 1}$ so we can replace α_{k_l} with $\frac{\beta_{k_l}}{d^2 - 1}$ in the above expression since $\beta_0 \geq d$.

In this step, we use the expression of the recursive redundancy relation in Lemma 2 to simplify the generic term in the summation of Eq.(B10):

$$\begin{aligned} \frac{1}{(d^2 - 1)^{L-h+1}} \sum_{k_L, \dots, k_h} \beta_{k_L} \dots \beta_{k_h} \left[\frac{d\delta_{\omega - \sum_{l=h}^L k_l}^0}{d^2 - 1} - \frac{|R_{h-1}(\omega - \sum_{l=h}^L k_l)|}{d(d^2 - 1)} \right] \\ = \frac{d}{(d^2 - 1)^{L-h+2}} |R_h^L(\omega)| - \frac{1}{d(d^2 - 1)^{L-h+2}} |R_{h-1}^L(\omega)| \end{aligned} \quad (\text{B11})$$

Finally, we inject Eq.(B11) in Eq.(B10) and get:

$$\begin{aligned} A_2^L(\omega) &= \frac{1}{(d^2 - 1)^{L-1}} \sum_{k_L, \dots, k_2} \beta_{k_L} \dots \beta_{k_2} \left[\frac{\delta_{\omega - \sum_{l=2}^L k_l}^0}{d+1} + \frac{|R_1(\omega - \sum_{l=2}^L k_l)|}{d(d+1)} \right] \\ &+ \sum_{h=3}^L \left[\frac{d}{(d^2 - 1)^{L-h+2}} |R_h^L(\omega)| - \frac{1}{d(d^2 - 1)^{L-h+2}} |R_{h-1}^L(\omega)| \right] \\ &+ \frac{d\delta_\omega^0}{d^2 - 1} - \frac{|R_L(\omega)|}{d(d^2 - 1)} \\ &= \frac{1}{d(d+1)(d^2 - 1)^{L-1}} |R_1^L(\omega)| + \left(\frac{1}{(d+1)(d^2 - 1)^{L-1}} - \frac{1}{d(d^2 - 1)^{L-1}} \right) |R_2^L(\omega)| \\ &+ \sum_{h=3}^{L-1} \left(\frac{d}{(d^2 - 1)^{L-h+2}} - \frac{1}{d(d^2 - 1)^{L-h+1}} \right) |R_h^L(\omega)| + \left(\frac{d}{(d^2 - 1)^2} - \frac{1}{d(d^2 - 1)} \right) |R_L(\omega)| + \frac{d\delta_\omega^0}{d^2 - 1} \\ &= \frac{1}{d(d+1)(d^2 - 1)^{L-1}} |R_1^L(\omega)| - \frac{1}{d(d+1)(d^2 - 1)^{L-1}} |R_2^L(\omega)| + \sum_{h=3}^L \frac{1}{d(d^2 - 1)^{L-h+2}} |R_h^L(\omega)| + \frac{d\delta_\omega^0}{d^2 - 1} \end{aligned} \quad (\text{B12})$$

By combining Eq.(B8) and Eq.(B12), we retrieve the result from Theorem 2:

$$\mathbb{E}[|c_\omega^L|^2] = C_1 A_1^L(\omega) + C_2 A_2^L(\omega) = C_1 \delta_\omega^0 + C_2 A_2^L(\omega)$$

□

B.2 Proof of theorem 3

We recall Theorem 3:

Theorem 3. Consider a single layered Quantum Fourier model with spectrum Ω , Fourier coefficients $c_\omega(\theta)$ and redundancies $|R(\omega)|$. We assume that each of the two parameterized layers forms an ε -approximate 2-design according to the monomial definition introduced in Definition (4). The variance of the model's Fourier coefficients obeys the following bound:

$$\text{Var}_\theta[c_\omega(\theta)] \leq \text{Var}_{\text{Haar}}[c_\omega(\theta)] + \left(\frac{C_1 \varepsilon}{d^2} + \frac{C_2 \varepsilon}{d(d+1)} \right) |R(\omega)| + C_2 \frac{\varepsilon^2}{d^2} |R(\omega)|^2 \quad (14)$$

where $C_1 = \frac{d\|O\|^2 - \text{Tr}(O)^2}{d(d^2-1)}$, $C_2 = \sum_{l,k} \frac{|O_{l,k}^{\otimes 2}|}{d^2}$ and $\text{Var}_{\text{Haar}}[c_\omega]$ is the variance of a Fourier coefficient under the 2-design assumption given in Theorem 1.

Here we provide an upper bound on the variance of each Fourier coefficient in the setting of a single layered QFM when each of the two parameterized layers form an ε -approximate 2 design according to the monomial definition introduced in Definition 4. In the proof, it will be more clear why we adopted this definition.

We note that if we assume that the parameterized layers form each a 1-design, then the expectation value of each Fourier coefficient is zero except for the null frequency as mentioned in B.1.

The main takeaway from this result is that the bound is polynomial in the frequency redundancy. This shows that the degree to which a Fourier coefficient concentrates around its mean (which is 0 under the 1-design hypothesis for non null frequencies) is restricted by its appearance frequency in the spectrum construction, thus introducing an encoding dependent *inductive bias*. The proof of this Theorem follows a similar proof to the one given in [20] where they used the same techniques to compute a bound on the variance of the quantum model's gradient.

Proof. Let us first recall the Fourier coefficient expression for a single encoding layer ($L = 1$ in Eq.(A1)):

$$c_\omega = \sum_{j_1, j'_1 \in R(\omega)} \sum_{k, k'} W_{j'_1 0}^{(1)*} W_{j_2 j'_1}^{(2)*} O_{k'k} W_{j_2 j_1}^{(2)} W_{j_1 0}^{(1)} \quad (B13)$$

Then, the expectation of the modulus squared of the coefficient c_ω is given by:

$$\begin{aligned} \mathbb{E}[|c_\omega|^2] &= \sum_{\substack{i_1, i'_1 \in R(\omega) \\ j_1, j'_1 \in R(\omega)}} \mathbb{E}_{W^{(1)}} \left[W_{j_1 0}^{(1)} W_{i'_1 0} W_{j'_1 0}^{(1)*} W_{i_1 0}^{(1)*} \right] \mathbb{E}_{W^{(2)}} \left[\left(W^{(2)\dagger} O W^{(2)} \right)_{j'_1, j_1} \left(W^{(2)\dagger} O W^{(2)} \right)_{i'_1, i_1} \right] \\ &= \sum_{\substack{i_1, i'_1 \in R(\omega) \\ j_1, j'_1 \in R(\omega)}} \text{Tr} \left[\mathbb{E}_{W^{(1)}} \left[W^{(1)\otimes 2} |00\rangle \langle 00| W^{(1)\dagger \otimes 2} |j'_1 i_1\rangle \langle j_1 i'_1| \right] \right] \text{Tr} \left[\mathbb{E}_{W^{(2)}} \left[W^{(2)\otimes 2} |j_1 i'_1\rangle \langle j'_1 i_1| W^{(2)\dagger \otimes 2} O^{\otimes 2} \right] \right] \end{aligned} \quad (B14)$$

where we use in the second equality the property $\text{Tr}[A] \times \text{Tr}[B] = \text{Tr}[A \otimes B]$.

We recall here that in Theorem 3 we consider that both parameterized unitaries have the same ε -distance to a 2-design. However the following proof works if each of the parameterized unitaries have different distributions with different distances to a 2-design. Hence, both expectation terms in Eq.(B14) can be written using the superoperator

$$\begin{aligned}
\mathcal{A}_W^{(2)}(\cdot) &:= \int_{\text{Haar}} d\mu(W) W^{\otimes 2}(\cdot) (W^\dagger)^{\otimes 2} - \int_W dW W^{\otimes 2}(\cdot) (W^\dagger)^{\otimes 2}: \\
\text{Tr} \left[\mathbb{E}_{W^{(1)}} \left[W^{(1)\otimes 2} |00\rangle \langle 00| W^{(1)\dagger\otimes 2} |j'_1 i_1\rangle \langle j_1 i'_1| \right] \right] &= \mathbb{E}_{\text{Haar}} \left[\text{Tr} \left[W^{(1)\otimes 2} |00\rangle \langle 00| W^{(1)\dagger\otimes 2} |j'_1 i_1\rangle \langle j_1 i'_1| \right] \right] \\
&\quad - \text{Tr} \left[\mathcal{A}_W^{(2)}(|00\rangle \langle 00|) |j'_1 i_1\rangle \langle j_1 i'_1| \right] \\
&= \frac{\delta_{j_1, j'_1} \delta_{i_1, i'_1} (\delta_{\omega, 0}) + \delta_{i_1, j_1} \delta_{i'_1, j'_1}}{d(d+1)} - \text{Tr} \left[\mathcal{A}_W^{(2)}(|00\rangle \langle 00|) |j'_1 i_1\rangle \langle j_1 i'_1| \right] \\
\text{Tr} \left[\mathbb{E}_{W^{(2)}} \left[W^{(2)\otimes 2} |j_1 i'_1\rangle \langle j'_1 i_1| W^{(2)\dagger\otimes 2} O^{\otimes 2} \right] \right] &= \mathbb{E}_{\text{Haar}} \left[\text{Tr} \left[W^{(2)\otimes 2} |j_1 i'_1\rangle \langle j'_1 i_1| W^{(2)\dagger\otimes 2} O^{\otimes 2} \right] \right] \\
&\quad - \text{Tr} \left[\mathcal{A}_W^{(2)}(|j_1, i'_1\rangle \langle j'_1, i_1|) O^{\otimes 2} \right] \\
&= K_1 \delta_{j_1, j'_1} \delta_{i_1, i'_1} (\delta_{\omega, 0}) + K_2 \delta_{i_1, j_1} \delta_{i'_1, j'_1} - \text{Tr} \left[\mathcal{A}_W^{(2)}(|j_1, i'_1\rangle \langle j'_1, i_1|) O^{\otimes 2} \right]
\end{aligned} \tag{B15}$$

The expectation with respect to the Haar measure in both terms is simply computed using the Weingarten calculus formula for the second moment monomials [32] where

$$K_1 = \frac{d \text{Tr}(O)^2 - \|O\|_2^2}{d(d^2 - 1)} \quad \text{and} \quad K_2 = \frac{d \|O\|_2^2 - \text{Tr}(O)^2}{d(d^2 - 1)} \tag{B16}$$

By substituting the terms of Eq.(B15) in Eq.(B14), we get the following expression:

$$\begin{aligned}
\mathbb{E} [|c_\omega|^2] &= \mathbb{E}_{\text{Haar}} [|c_\omega|^2] - \sum_{\substack{i_1, i'_1 \in R(\omega) \\ j_1, j'_1 \in R(\omega)}} \left(\frac{\delta_{j_1, j'_1} \delta_{i_1, i'_1} (\delta_{\omega, 0}) + \delta_{i_1, j_1} \delta_{i'_1, j'_1}}{d(d+1)} \right) \text{Tr} \left[\mathcal{A}^{\otimes 2}(|j_1, i'_1\rangle \langle j'_1, i_1|) O^{\otimes 2} \right] \\
&\quad - \sum_{\substack{i_1, i'_1 \in R(\omega) \\ j_1, j'_1 \in R(\omega)}} \left(K_1 \delta_{j_1, j'_1} \delta_{i_1, i'_1} (\delta_{\omega, 0}) + K_2 \delta_{i_1, j_1} \delta_{i'_1, j'_1} \right) \text{Tr} \left[\mathcal{A}_W^{(2)}(|00\rangle \langle 00|) |j'_1, i_1\rangle \langle j_1, i'_1| \right] \\
&\quad + \sum_{\substack{i_1, i'_1 \in R(\omega) \\ j_1, j'_1 \in R(\omega)}} \text{Tr} \left[\mathcal{A}_W^{(2)}(|00\rangle \langle 00|) |j'_1, i_1\rangle \langle j_1, i'_1| \right] \text{Tr} \left[\mathcal{A}^{\otimes 2}(|j_1, i'_1\rangle \langle j'_1, i_1|) O^{\otimes 2} \right]
\end{aligned} \tag{B17}$$

$\forall \omega \in \Omega \setminus \{0\}$, we can further simplify the expression in Eq.(B17),

$$\begin{aligned}
\mathbb{E} [|c_\omega|^2] &= \mathbb{E}_{\text{Haar}} [|c_\omega|^2] - \sum_{j_1, j'_1 \in R(\omega)} \frac{1}{d(d+1)} \text{Tr} \left[\mathcal{A}^{\otimes 2}(|j_1, i'_1\rangle \langle j_1, i'_1|) O^{\otimes 2} \right] \\
&\quad - \sum_{j_1, j'_1 \in R(\omega)} K_2 \text{Tr} \left[\mathcal{A}_W^{(2)}(|00\rangle \langle 00|) |j'_1, j_1\rangle \langle j_1, j'_1| \right] \\
&\quad + \sum_{\substack{i_1, i'_1 \in R(\omega) \\ j_1, j'_1 \in R(\omega)}} \text{Tr} \left[\mathcal{A}_W^{(2)}(|00\rangle \langle 00|) |j'_1, i_1\rangle \langle j_1, i'_1| \right] \text{Tr} \left[\mathcal{A}^{\otimes 2}(|j_1, i'_1\rangle \langle j_1, i'_1|) O^{\otimes 2} \right]
\end{aligned} \tag{B18}$$

For $\omega = 0$, we obtain:

$$\begin{aligned}
\mathbb{E} [|c_0|^2] &= \mathbb{E}_{\text{Haar}} [|c_0|^2] - \sum_{\substack{i_1, i'_1 \in R(\omega) \\ j_1, j'_1 \in R(\omega)}} \left(\frac{\delta_{j_1, j'_1} \delta_{i_1, i'_1} (\delta_{\omega, 0}) + \delta_{i_1, j_1} \delta_{i'_1, j'_1}}{d(d+1)} \right) \text{Tr} \left[\mathcal{A}^{\otimes 2}(|j_1, i'_1\rangle \langle j_1, i'_1|) O^{\otimes 2} \right] \\
&\quad - \sum_{\substack{i_1, i'_1 \in R(\omega) \\ j_1, j'_1 \in R(\omega)}} \left(K_1 \delta_{j_1, j'_1} \delta_{i_1, i'_1} (\delta_{\omega, 0}) + K_2 \delta_{i_1, j_1} \delta_{i'_1, j'_1} \right) \text{Tr} \left[\mathcal{A}_W^{(2)}(|00\rangle \langle 00|) |j'_1, i_1\rangle \langle j_1, i'_1| \right] \\
&\quad + \sum_{\substack{i_1, i'_1 \in R(\omega) \\ j_1, j'_1 \in R(\omega)}} \text{Tr} \left[\mathcal{A}_W^{(2)}(|00\rangle \langle 00|) |j'_1, i_1\rangle \langle j_1, i'_1| \right] \text{Tr} \left[\mathcal{A}^{\otimes 2}(|j_1, i'_1\rangle \langle j_1, i'_1|) O^{\otimes 2} \right]
\end{aligned} \tag{B19}$$

From Eq.(B17), we see that a Fourier coefficient's variance is the sum over coefficients of the superoperator \mathcal{A}_W^2 selected by the frequency generator $R(\omega)$. In order to keep the dependence on the redundancies $|R(\omega)|$, we use the monomial definition 4 of approximate 2-design which gives an upper bound on the superoperator coefficients in the computational basis. Hence, we take

$$\varepsilon = \max_{\substack{i_1, i'_1, j_1, j'_1 \in [d] \\ k, k' \in [d^4]}} d^2 |\mathcal{A}_W^{\otimes 2}(|j_1, i'_1\rangle \langle j'_1, i_1|)_{k, k'}|$$

Consequently, we get

$$|\text{Tr} [\mathcal{A}_W^{\otimes 2}(|00\rangle \langle 00|) |j'_1, i_1\rangle \langle j_1, i'_1|]| \leq \frac{\varepsilon}{d^2}$$

and

$$\text{Tr} [\mathcal{A}_W(|j'_1, i_1\rangle \langle j_1, i'_1|)O^{\otimes 2}] = \sum_{k, k' \in [d]} |(\mathcal{A}_W^{\otimes 2} |j_1, i'_1\rangle \langle j'_1, i_1|)_{k, k'}| |O_{kk'}^{\otimes 2}| \leq \frac{\varepsilon}{d^2} \sum_{k, k' \in [d]} |O_{kk'}^{\otimes 2}|$$

By applying the triangular inequality in Eq.(B17), one arrives to the upper bound obtained in Theorem 3:

$$\mathbb{E} [|c_\omega|^2] \leq \mathbb{E}_{\text{Haar}} [|c_\omega|^2] + \frac{|R(\omega)|}{d(d+1)} \varepsilon \sum_{kk'} \frac{|O_{kk'}^{\otimes 2}|}{d^2} + K_2 \frac{|R(\omega)|}{d^2} \varepsilon + \frac{|R(\omega)|^2 \varepsilon^2}{d^2} \sum_{kk'} \frac{|O_{kk'}^{\otimes 2}|}{d^2} \quad (\text{B20})$$

□

B.3 Proof of Corollary 2

We recall Corollary 2:

Corollary 2. *Consider a single layered Quantum Fourier model $f(x, \theta)$. We assume that each of the two parameterized layers forms an ε -approximate 2-design according to the monomial definition introduced in Definition 4. For a fixed $x \in \mathcal{X}$, the variance of the model $f(x, \theta)$ obeys the following bound:*

$$\text{Var}_\theta [f(x, \theta)] \leq \text{Var}_{\text{Haar}} [f(x, \theta)] + \left(\frac{C_1 \varepsilon}{d^2} + \frac{C_2 \varepsilon}{d(d+1)} \right) d^2 + C_2 \varepsilon^2 d^2 \quad (15)$$

where $\text{Var}_{\text{Haar}} [f(x, \theta)]$ is the variance under the 2-design assumption detailed in Appendix B.3 and the constants C_1 and C_2 have the same definition as in Theorem 3.

Proof. We recall that $f(x, \theta)$ for a fixed data point $x \in \mathbb{R}$ is a real valued function. Hence, $\forall x \in \mathbb{R}$, its variance is given by $\text{Var}_\theta [f(x, \theta)] = \mathbb{E}_\theta [f(x, \theta)]^2 - \mathbb{E}_\theta [f(x, \theta)]^2$.

By using the same steps in the previous theorem proof and the same definition of the constants K_1 and K_2 , the model function f can be rewritten in the following form:

$$\begin{aligned} \mathbb{E}_\theta [f(x, \theta)^2] &= \mathbb{E}_{\text{Haar}} [f(x, \theta)^2] - \sum_{j_1, j'_1, i_1, i'_1} \left(\frac{\delta_{j_1, j'_1} \delta_{i_1, i'_1} + \delta_{i_1, j_1} \delta_{i'_1, j'_1}}{d(d+1)} \right) \text{Tr} [\mathcal{A}^{\otimes 2}(|j_1, i'_1\rangle \langle j'_1, i_1|)O^{\otimes 2}] \\ &\quad - \sum_{j_1, j'_1, i_1, i'_1} (K_1 \delta_{j_1, j'_1} \delta_{i_1, i'_1} + K_2 \delta_{i_1, j_1} \delta_{i'_1, j'_1}) \text{Tr} [\mathcal{A}_W^{(2)}(|00\rangle \langle 00|) |j'_1, i_1\rangle \langle j_1, i'_1|] \\ &\quad + \sum_{j_1, j'_1, i_1, i'_1} \text{Tr} [\mathcal{A}_W^{(2)}(|00\rangle \langle 00|) |j'_1, i_1\rangle \langle j_1, i'_1|] \text{Tr} [\mathcal{A}^{\otimes 2}(|j_1, i'_1\rangle \langle j'_1, i_1|)O^{\otimes 2}] e^{-ix(\lambda_{j_1} - \lambda_{j'_1} - \lambda_{i_1} + \lambda_{i'_1})} \end{aligned} \quad (\text{B21})$$

with $\forall x \in \mathbb{R}$,

$$\begin{aligned}
\mathbb{E}_{\text{Haar}} [f(x, \theta)^2] &= \sum_{j_1, j'_1, i_1, i'_1} \left(\frac{\delta_{j_1, j'_1} \delta_{i_1, i'_1} + \delta_{i_1, j_1} \delta_{i'_1, j'_1}}{d(d+1)} \right) (K_1 \delta_{j_1, j'_1} \delta_{i_1, i'_1} + K_2 \delta_{i_1, j_1} \delta_{i'_1, j'_1}) e^{-ix(\lambda_{j_1} - \lambda_{j'_1} - \lambda_{i_1} + \lambda_{i'_1})} \\
&= \sum_{j_1, j'_1, i_1, i'_1} \left[\frac{K_1}{d(d+1)} \delta_{j_1, j'_1} \delta_{i_1, i'_1} + \frac{K_2}{d(d+1)} \delta_{i_1, j_1} \delta_{i'_1, j'_1} + \frac{K_1 + K_2}{d(d+1)} \delta_{j_1, j'_1} \delta_{i_1, i'_1} \delta_{i_1, j_1} \delta_{i'_1, j'_1} \right] e^{-ix(\lambda_{j_1} - \lambda_{j'_1} - \lambda_{i_1} + \lambda_{i'_1})} \\
&= \frac{d^2 + d}{d(d+1)} (K_1 + K_2) \\
&= \frac{\text{Tr}[O]^2 + \text{Tr}[O^2]}{d(d+1)} \\
\text{Var}_{\text{Haar}} [f(x, \theta)] &= \mathbb{E}_{\text{Haar}} [f(x, \theta)^2] - \mathbb{E}_{\text{Haar}} [f(x, \theta)]^2 = \frac{\text{Tr}[O^2] + \text{Tr}[O^2]}{d(d+1)} - \frac{\text{Tr}[O]^2}{d^2}
\end{aligned} \tag{B22}$$

If we assume that each of the parameterized layers form a 1-design, then $\mathbb{E}_\theta[f(x, \theta)] = \mathbb{E}_{\text{Haar}}[f(x, \theta)]$ and the variance of f becomes:

$$\begin{aligned}
\text{Var}_\theta[f(x, \theta)] &= \text{Var}_{\text{Haar}} [f(x, \theta)^2] - \sum_{j_1, j'_1, i_1, i'_1} \left(\frac{\delta_{j_1, j'_1} \delta_{i_1, i'_1} + \delta_{i_1, j_1} \delta_{i'_1, j'_1}}{d(d+1)} \right) \text{Tr} [\mathcal{A}^{\otimes 2}(|j_1, i_1\rangle \langle j'_1, i_1|) O^{\otimes 2}] \\
&\quad - \sum_{j_1, j'_1, i_1, i'_1} (K_1 \delta_{j_1, j'_1} \delta_{i_1, i'_1} + K_2 \delta_{i_1, j_1} \delta_{i'_1, j'_1}) \text{Tr} [\mathcal{A}_w^{(2)}(|00\rangle \langle 00|) |j'_1, i_1\rangle \langle j_1, i'_1|] \\
&\quad + \sum_{j_1, j'_1, i_1, i'_1} \text{Tr} [\mathcal{A}_w^{(2)}(|00\rangle \langle 00|) |j'_1, i_1\rangle \langle j_1, i'_1|] \text{Tr} [\mathcal{A}^{\otimes 2}(|j_1, i_1\rangle \langle j'_1, i_1|) O^{\otimes 2}] e^{-ix(\lambda_{j_1} - \lambda_{j'_1} - \lambda_{i_1} + \lambda_{i'_1})}
\end{aligned} \tag{B23}$$

By performing the triangular inequality, we get the bound in Corollary 2:

$$\text{Var}_\theta[f(x, \theta)] \leq \frac{\text{Tr}[O^2]}{d(d+1)} + \left(\frac{K_1}{d^2} + \frac{K_2}{d(d+1)} \right) \epsilon d^2 + K_2 \epsilon^2 d^2 \tag{B24}$$

□

B.4 Variance under the local 2-design setting

B.4.1 Preliminaries

In this section, we present properties of Haar integration over Haar random unitaries that we will use in the main proof of Theorem 4.

Lemma 1. *Let $\mathcal{H} = \mathcal{H}_w \otimes \mathcal{H}_{\bar{w}}$ be a bipartite Hilbert space and let $\{W(\theta)\}_{\theta \in \Theta}$ be a parameterized unitary acting on \mathcal{H}_w and forming a 2-design when considering a uniform distribution over the variational parameters Θ . Then, for any arbitrary linear operators $A, B, C, D : \mathcal{H} \rightarrow \mathcal{H}$ such that $A = A_w \otimes A_{\bar{w}}$ and $C = C_w \otimes C_{\bar{w}}$, we have:*

$$\begin{aligned}
&\int_{\Theta} \text{Tr}_w [A(W \otimes \mathbb{1}_{\bar{w}}) B(W^\dagger \otimes \mathbb{1}_{\bar{w}})] \text{Tr}_w [C(W \otimes \mathbb{1}_{\bar{w}}) D(W^\dagger \otimes \mathbb{1}_{\bar{w}})] dW(\Theta) \\
&= \int_W \text{Tr}_w [A(W \otimes \mathbb{1}_{\bar{w}}) B(W^\dagger \otimes \mathbb{1}_{\bar{w}})] \text{Tr}_w [C(W \otimes \mathbb{1}_{\bar{w}}) D(W^\dagger \otimes \mathbb{1}_{\bar{w}})] dW \\
&= \frac{\text{Tr}_w [B] \text{Tr}_w [D]}{2^{2m} - 1} A_{\bar{w}} C_{\bar{w}} \left(\text{Tr} [A_w] \text{Tr} [C_w] - \frac{\text{Tr} [A_w C_w]}{2^m} \right) + \frac{\text{Tr}_w [B(C_{\bar{w}} \otimes \mathbb{1}_w) D]}{2^{2m} - 1} \left(\text{Tr} [A_w C_w] - \frac{\text{Tr} [A_w] \text{Tr} [C_w]}{2^m} \right)
\end{aligned} \tag{B25}$$

Lemma 2. *Let $\mathcal{H} = \mathcal{H}_w \otimes \mathcal{H}_{\bar{w}}$ be a bipartite Hilbert space. Then, for any arbitrary linear operators $A_w, B_w : \mathcal{H}_w \rightarrow \mathcal{H}_w, S : \mathcal{H} \rightarrow \mathcal{H}$, we have:*

$$\text{Tr}_{\bar{w}} [|p\rangle \langle q| (A_w \otimes \mathbb{1}_{\bar{w}}) S (B_w \otimes \mathbb{1}_{\bar{w}})] = |p\rangle \langle q|_w A_w \text{Tr}_{\bar{w}} [(\mathbb{1}_w \otimes |p\rangle \langle q|_{\bar{w}}) S] B_w$$

Lemma 3. Let \mathcal{H} be a composite Hilbert space such that $\mathcal{H} = \mathcal{H}_{\tau_a} \otimes \mathcal{H}_{\tau_b} \otimes \mathcal{H}_z \otimes \mathcal{H}_y$ and \mathcal{H}_x a subspace of $\mathcal{H}_{\tau_a} \otimes \mathcal{H}_{\tau_b} \otimes \mathcal{H}_z$. Then, for any unitary X acting on \mathcal{H} , W_τ acting non trivially on subspace $\mathcal{H}_\tau = \mathcal{H}_{\tau_a} \otimes \mathcal{H}_{\tau_b}$ and $Y_i = (W_\tau^\dagger \otimes \mathbb{1}_{\bar{\tau}})X_i(W_\tau \otimes \mathbb{1}_{\bar{\tau}})\forall i \in \{1, 2\}$, we get:

$$E_\tau[Tr[Tr_x[Y_1]Tr_x[Y_2]]] = \begin{cases} \frac{2^{m/2}}{2^m+1}Tr[Tr_{x,\tau}[X_1]Tr_{x,\tau}[X_2] + Tr_{x\setminus\tau}[X_1]Tr_{x\setminus\tau}[X_2]], & \text{if } x \cap \tau \in \{\tau_a, \tau_b\} \\ Tr[Tr_x[X_1]Tr_x[X_2]], & \text{otherwise} \end{cases} \quad (\text{B26})$$

Proof. For ease of notation, we denote the Hilbert space by its associated subsystem index.

$$Tr_x[Y] = \begin{cases} Tr_\tau[(W_\tau^\dagger \otimes \mathbb{1}_y)X(W_\tau \otimes \mathbb{1}_y)], & \text{if } x = \tau \\ (W_\tau^\dagger \otimes \mathbb{1}_y)Tr_x[X](W_\tau \otimes \mathbb{1}_y), & \text{if } x \cap \tau = \emptyset \\ Tr_\tau[(W_\tau^\dagger \otimes \mathbb{1}_y)Tr_{x\setminus\tau}[X](W_\tau \otimes \mathbb{1}_y)], & \text{if } \tau \subset x \\ Tr_{\tau_a}[(W_\tau^\dagger \otimes \mathbb{1}_y)Tr_{x\setminus\tau}[X](W_\tau \otimes \mathbb{1}_y)], & \text{if } x \cap \tau = \tau_a \\ Tr_{\tau_b}[(W_\tau^\dagger \otimes \mathbb{1}_y)Tr_{x\setminus\tau}[X](W_\tau \otimes \mathbb{1}_y)], & \text{if } x \cap \tau = \tau_b \end{cases}$$

For the case where $x \cap \tau = \emptyset$,

$$\begin{aligned} E_\tau[Tr[Tr_x[Y_1]Tr_x[Y_2]]] &= E_\tau[Tr[(W_\tau^\dagger \otimes \mathbb{1}_y)Tr_x[X_1]Tr_x[X_2](W_\tau \otimes \mathbb{1}_y)]] \\ &= E_\tau[Tr[Tr_x[X_1]Tr_x[X_2]]] \\ &= Tr[Tr_x[X_1]Tr_x[X_2]] \end{aligned}$$

In both cases $x = \tau$ and $\tau \subset x$, we get $Tr_x[Y] = Tr_\tau[(W_\tau^\dagger \otimes \mathbb{1}_y)Tr_z[X](W_\tau \otimes \mathbb{1}_y)]$ where $z = \emptyset, x \setminus \tau$ respectively. Hence, to compute $E_\tau[Tr[Tr_x[Y_1]Tr_x[Y_2]]]$, we apply 2 for $\omega = \tau, A = C = \mathbb{1}, B = Tr_z[X_1]$ and $D = Tr_z[X_2]$:

$$\begin{aligned} E_\tau[Tr[Tr_x[Y_1]Tr_x[Y_2]]] &= Tr[Tr_{\tau,z}[X_1]Tr_{\tau,z}[X_2]] \\ &= Tr[Tr_x[X_1]Tr_x[X_2]] \end{aligned}$$

For the last 2 cases where the intersection between x and τ is a singleton (i.e. $x \cap \tau \in \{\tau_a, \tau_b\}$), we use the *Random Tensor Network Integrator* (RTNI) package [35] and get the following:

$$E_\tau[Tr[Tr_x[Y_1]Tr_x[Y_2]]] = \frac{2^{m/2}}{2^m+1} [Tr[Tr_{x,\tau}[X_1]Tr_{x,\tau}[X_2]] + Tr[Tr_{x\setminus\tau}[X_1]Tr_{x\setminus\tau}[X_2]]]$$

□

B.4.2 Integrate over a brickwise circuit of local 2-design blocks

In this section, we provide a general method to compute the second moment superoperator of a brickwise circuit made of parameterized local 2-design blocks (no encoding part is evolved). The methods used and the expression of the second moment superoperator will be useful to prove Theorem 4 and to give a better intuition about the monomial ε -distance to a 2-design as defined in Definition 4, for this type of circuits.

We therefore consider a circuit with a brickwise structure as described in Fig.4 acting on $n = m \times A$ qubits with depth L , A blocks per layer and circular connectivity. Each block acts on m qubits and forms a 2-design on the corresponding m -qubit subsystem. We denote by $U(\theta)$ the parameterized unitary generated by this circuit and by $U_{j,l}(\theta)$ the unitary corresponding to the j^{th} block in the l^{th} layer.

For layers with an odd index l , we denote the set of subsystems on which its blocks act non-trivially by $\{s_h\}_{h=1}^A$ and for even layers, we use the notation $\{\tau_h\}_{h=1}^A$ for the corresponding subsystems. Using this notation, we can decompose each subsystem s_h into $s_h = (s_h)_1 \cup (s_h)_2$ and similarly each subsystem τ_h into $\tau_h = (\tau_h)_1 \cup (\tau_h)_2$ where each subsystem $(s_h)_i, (\tau_h)_i$ acts on $m/2$ qubits.

We note that in the following proof, we will consider that each layer l contains A_l blocks in order to account for brickwise circuits with slightly different configurations (mainly the brickwise light cone). However, to compute the second moment superoperator, we simply consider that $A_l = A \forall l \in [L]$.

We recall here the expression of a single coefficient of the second moment superoperator corresponding to the circuit unitary $U(\theta)$ indexed by multi-indices $\mathbf{qp} := (q_1, q_2, p_1, p_2) \in [2^{4n}]$ and $\mathbf{rs} := (r_1, r_2, s_1, s_2) \in [2^{4n}]$:

$$\begin{aligned} (M_{U(\theta)}^{(2)})_{\mathbf{qp}, \mathbf{rs}} &= \int_{\theta} dU(\theta) (U(\theta)^{\otimes 2} \otimes (U(\theta)^*)^{\otimes 2})_{\mathbf{qp}, \mathbf{rs}} \\ &:= \int_{\theta} U_{q_1, r_1} U_{q_2, r_2} U_{p_1, s_1}^* U_{p_2, s_2}^* dU(\theta) \end{aligned} \quad (\text{B27})$$

For convenience, we rewrite the second moment superoperator as follows:

$$\begin{aligned} (M_{U(\theta)}^{(2)})_{\mathbf{p}, \mathbf{q}, \mathbf{r}, \mathbf{s}} &= \int_{\theta} U_{q_1, r_1} U_{q_2, r_2} U_{p_1, s_1}^* U_{p_2, s_2}^* dU(\theta) \\ &= \int_{\mathcal{U}} \text{Tr} [|p_1\rangle\langle q_1| U Y_1 U^\dagger] \text{Tr} [|p_2\rangle\langle q_2| U Y_2 U^\dagger] dU \\ &:= E_{\mathcal{U}} [\text{Tr} [|p_1\rangle\langle q_1| U Y_1 U^\dagger] \text{Tr} [|p_2\rangle\langle q_2| U Y_2 U^\dagger]] \end{aligned} \quad (\text{B28})$$

where $Y_1 = |r_1\rangle\langle s_1|$ and $Y_2 = |r_2\rangle\langle s_2|$.

In order to compute the above expectation value, one needs to integrate over all the local 2-design blocks forming the circuit unitary $U(\theta)$. Under the assumption that the blocks are independent, we can perform the integration iteratively. To do so, we first start by integrating over the blocks of the first layer and then we integrate over the remaining blocks (blocks from the 2^{nd} up to the L^{th} layer).

Considering that the h^{th} block of the first layer acts non trivially on subsystem s_h (with the corresponding unitary matrix $U_{h,1}(\theta)$), we introduce the following notations where we drop θ for simplicity:

$$X_h^{pq} := \text{Tr}_{h^+} [(\mathbb{1}_{h^-} \otimes |p\rangle\langle q|_{h^+}) \tilde{U}^{(h,1)}] \quad \forall h \in \{1, \dots, A_1\} \quad (\text{B29})$$

$$f_h(x) := \text{Tr} [\text{Tr}_x [X_h^{p_1 q_1}] \text{Tr}_x [X_h^{p_2 q_2}]] \quad \forall h < A_1, \forall x \subseteq h^- \quad (\text{B30})$$

where $h^+ := \{s_{h+1} \cup s_{h+2} \cup \dots, s_{A_1}\}$, $h^- := \{s_1 \cup s_2 \cup \dots, s_{h-1} \cup s_h\}$, $\tilde{U}^{(h,1)} := U^{(h,1)} Y U^{(h,1)\dagger}$ and $U^{(h,1)}$ is the circuit unitary U after removing the first h blocks from the first layer. We notice here that X_h^{pq} acts on subsystem h^- and that it does no longer depend on the first h blocks of the first layer. We note that $X_0^{pq} := \text{Tr} [|p\rangle\langle q| U Y U^\dagger]$ and $X_{A_1}^{pq} := \tilde{U}^{(A_1,1)}$.

We give the following recursive relation between X_h^{pq} and X_{h+1}^{pq} using Lemma 2 and for ease of notation, we shortly use $h+1$ to denote subsystem s_{h+1} :

$$\begin{aligned} X_h^{pq} &= \text{Tr}_{h+1} [\text{Tr}_{(h+1)^+} [(\mathbb{1}_{h^-} \otimes |p\rangle\langle q|_{h^+}) (\mathbb{1}_{h^-} \otimes U_{h+1,1} \otimes \mathbb{1}_{(h+1)^+}) \tilde{U}^{(h+1)} (\mathbb{1}_{h^-} \otimes U_{h+1,1}^\dagger \otimes \mathbb{1}_{(h+1)^+})]] \\ &= \text{Tr}_{h+1} [(\mathbb{1}_{h^-} \otimes |p\rangle\langle q|_{h+1}) (\mathbb{1}_{h^-} \otimes U_{h+1,1}) X_{h+1}^{pq} (\mathbb{1}_{h^-} \otimes U_{h+1,1}^\dagger)] \end{aligned}$$

We then apply Lemma 1 and get the following $\forall h < A_1, \forall x \subseteq h^-$,

$$\begin{aligned} E_{U_{h+1,1}} [f_h(x)] &= E_{U_{h+1,1}} [\text{Tr} [\text{Tr}_x [X_h^{p_1 q_1}] \text{Tr}_x [X_h^{p_2 q_2}]]] \\ &= \alpha_{h+1} \text{Tr} [\text{Tr}_{h+1} [\text{Tr}_x [X_{h+1}^{p_1 q_1}] \text{Tr}_{h+1} [\text{Tr}_x [X_{h+1}^{p_2 q_2}]]]] + \beta_{h+1} \text{Tr} [\text{Tr}_x [X_{h+1}^{p_1 q_1}] \text{Tr}_x [X_{h+1}^{p_2 q_2}]] \\ &= \alpha_{h+1} f_{h+1}(x \cup (h+1)) + \beta_{h+1} f_{h+1}(x) \end{aligned} \quad (\text{B31})$$

with the coefficients α_{h+1} and β_{h+1} defined as follows and explicitly dependent on indices (p_1, q_1, p_2, q_2) :

$$\begin{aligned} \alpha_{h+1}(p_1, q_1, p_2, q_2) &:= \frac{1}{2^{2m} - 1} (\delta_{(p_1, q_1)_{h+1}} \delta_{(p_2, q_2)_{h+1}} - \frac{\delta_{(q_1, p_2)_{h+1}} \delta_{(p_1, q_2)_{h+1}}}{2^m}) \\ &= \frac{1}{2^{2m} - 1} \left(C_{h+1}(p_1, q_1, p_2, q_2) - \frac{D_{h+1}(p_1, q_1, p_2, q_2)}{2^m} \right) \\ \beta_{h+1}(p_1, q_1, p_2, q_2) &:= \frac{1}{2^{2m} - 1} (\delta_{(q_1, p_2)_{h+1}} \delta_{(p_1, q_2)_{h+1}} - \frac{\delta_{(p_1, q_1)_{h+1}} \delta_{(p_2, q_2)_{h+1}}}{2^m}) \\ &= \frac{1}{2^{2m} - 1} \left(D_{h+1}(p_1, q_1, p_2, q_2) - \frac{C_{h+1}(p_1, q_1, p_2, q_2)}{2^m} \right) \end{aligned}$$

Using Eq.(B31), we integrate iteratively over the A_1 blocks of the first layer as follows:

$$\begin{aligned}
& \prod_{j=1}^{A_1} E_{U_{j1}} [Tr[[p_1]\langle q_1|WY_1U^\dagger]Tr[[p_2]\langle q_2|WY_2U^\dagger]] \\
&= \prod_{j=1}^{A_1} E_{U_{j1}} [f_0(\emptyset)] \\
&= \prod_{j=2}^{A_1} E_{U_{j1}} [\alpha_1 f_1(1) + \beta_1 f_1(\emptyset)] \\
&= \prod_{j=3}^{A_1} E_{U_{j1}} [\alpha_1 (\alpha_2 f_2(12) + \beta_2 f_2(1)) + \beta_1 (\alpha_2 f_2(2) + \beta_2 f_2(\emptyset))] \\
&\vdots \\
&= \sum_{x_1 \in P_1} a_{x_1}(p_1, q_1, p_2, q_2) f_{A_1}(x_1), \quad a_{x_1}(p_1, q_1, p_2, q_2) := \prod_{h \in x_1} \alpha_h(p_1, q_1, p_2, q_2) \prod_{h \in \bar{x}_1} \beta_h(p_1, q_1, p_2, q_2)
\end{aligned} \tag{B32}$$

Here P_1 is the power set of the ensemble $\{1, 2, \dots, A_1\}$, hence containing 2^{A_1} subsystems. We also recall from Eq.(B30) that:

$$f_{A_1}(x_1) := Tr[Tr_{x_1}[U^{(A_1,1)}Y_1U^{(A_1,1)\dagger}]Tr_{x_1}[U^{(A_1,1)}Y_2U^{(A_1,1)\dagger}]]$$

where $U^{(A_1,1)}$ is the unitary representing the circuit from the 2^{nd} up to the L^{th} layer (i.e. the A_1 blocks of the first layer are removed).

We notice that in the expression of $f_{A_1}(x_1)$, we no longer have the dependence on the indices \mathbf{qp} , which contribution is now contained in the coefficients a_{x_1} .

To integrate over the remaining blocks, we introduce the following notations $\forall t \in \{1, 2\}, \forall l \in \{2, \dots, L\}$ and $\forall h \in \{1, \dots, A_l\}$

$$\begin{aligned}
Z_{h,l}^t &:= U^{(h,l)}Y_tU^{(h,l)\dagger} \\
g_{h,l}(x) &:= Tr[Tr_x[Z_{h,l}^1]Tr_x[Z_{h,l}^2]]
\end{aligned}$$

where $U^{(h,l)}$ is the circuit unitary after removing the layers $i \in \{1, \dots, l-1\}$ and the first h blocks of the l^{th} layer. We also note that $g_{0,l}(x) = g_{A_{l-1},l-1}(x) \forall l \in \{3, \dots, L\}$, $g_{0,2}(x) := f_{A_1}(x)$ and $g_{A_L,L}(x) := Tr[Tr_x[Y_1]Tr_x[Y_2]]$.

By applying Lemma 3, we obtain the following formula allowing to integrate recursively over the remaining blocks. We note that depending on the parity of the layer index l , we use s_h or τ_h (here we use τ_h but we get the same formula for s_h) to denote the subsystem on which the block h is acting non trivially:

$$E_{U_{h+1,l}}[g_{h,l}(x)] = \begin{cases} g_{h+1,l}(x), & \text{if } \tau_{h+1} \cap x \in \{\emptyset, \tau_{h+1}\} \\ \frac{2^{m/2}}{2^m+1} (g_{h+1,l}(x \cup \tau_{h+1}) + g_{h+1,l}(x \setminus \tau_{h+1})), & \text{otherwise} \end{cases} \tag{B33}$$

According to the recursive formula above, one can easily notice that for a fixed layer l , integrating $g_{0,l}(x)$ over its A_l blocks amounts to determining all the *non trivial* intersections between the current subsystem x and the layer blocks subsystems $\{\tau_h\}_{h=1}^{A_l}$ (if l is even otherwise $\{s_h\}_{h=1}^{A_l}$). In other terms, the set $I_l(x) := \{h|x \cap \tau_h \in \{(\tau_h)_1, (\tau_{h+1})_2\} \forall h \in [A_l]\}$ will contain the blocks over which we are going to effectively integrate by adding the multiplicative factor $\frac{2^{m/2}}{2^m+1}$ and *branching* subsystem x into the two new subsystems $x \cup \tau_{h+1}$ and $x \setminus \tau_{h+1}$.

Formally, we get $\forall 2 \leq l \leq L$:

$$\prod_{j=1}^{A_l} E_{U_{jl}}[g_{0,l}(x_{l-1})] = \sum_{x_l \in P_l(x_{l-1})} \left(\frac{2^{m/2}}{2^m+1}\right)^{d_l(x_{l-1})} g_{A_l,l}(x_l) \tag{B34}$$

where $d_l(x_{l-1}) := |I_l(x_{l-1})|$ and $P_l(x_{l-1})$ is the set of subsystems generated after each *branching* of x_{l-1} obtained by following the rule in Eq.(B33).

For ease of notation we drop the explicit dependence of a_{x_1} on (p_1, q_1, p_2, q_2) . By combining Eq.(B32) and Eq.(B34), we get the final expression of the second moment coefficient:

$$\begin{aligned}
(M_{U(\theta)}^{(2)})_{\mathbf{p},\mathbf{q},\mathbf{r},\mathbf{s}} &= \prod_{i=1}^L \prod_{j=1}^{A_i} E_{U_{j_i}} [f_0(\emptyset)] \\
&= \prod_{i=3}^L \prod_{j=1}^{A_i} E_{U_{j_i}} \left[\sum_{x_1 \in P_1} a_{x_1} \prod_{j=1}^{A_2} E_{U_{j_2}} [f_{A_1}(x_1)] \right] \\
&= \prod_{i=3}^L \prod_{j=1}^{A_i} E_{U_{j_i}} \left[\sum_{x_1 \in P_1} a_{x_1} \prod_{j=1}^{A_2} E_{U_{j_2}} [g_{0,2}(x_1)] \right] \\
&= \prod_{i=3}^L \prod_{j=1}^{A_i} E_{U_{j_i}} \left[\sum_{x_1 \in P_1} a_{x_1} \sum_{x_2 \in P_2(x_1)} \left(\frac{2^{m/2}}{2^m + 1} \right)^{d_2(x_1)} g_{0,3}(x_2) \right] \\
&= \sum_{x_1 \in P_1} a_{x_1} \sum_{x_2 \in P_2(x_1)} \sum_{x_3 \in P_3(x_2)} \cdots \sum_{x_L \in P_L(x_{L-1})} \left(\frac{2^{m/2}}{2^m + 1} \right)^{\sum_{i=2}^L d_i(x_{i-1})} g_{A_L, L}(x_L) \\
&= \sum_{x_1 \in P_1} a_{x_1} \sum_{x_2 \in P_2(x_1)} \sum_{x_3 \in P_3(x_2)} \cdots \sum_{x_L \in P_L(x_{L-1})} \left(\frac{2^{m/2}}{2^m + 1} \right)^{\sum_{i=2}^L d_i(x_{i-1})} \text{Tr}[\text{Tr}_{x_L}[Y_1] \text{Tr}_{x_L}[Y_2]] \\
&= \sum_{x_1 \in P_1} a_{x_1} \sum_{x_L \in P_f(x_1)} \left(\frac{2^{m/2}}{2^m + 1} \right)^{d(x_L)} \text{Tr}[\text{Tr}_{x_L}[Y_1] \text{Tr}_{x_L}[Y_2]] \\
&= \sum_{x_1 \in P_1} a_{x_1} \sum_{x_L \in P_f(x_1)} \left(\frac{2^{m/2}}{2^m + 1} \right)^{d(x_L)} \delta(r_1, s_1)_{x_L} \delta(r_1, s_2)_{\overline{x_L}} \delta(r_2, s_2)_{x_L} \delta(r_2, s_1)_{\overline{x_L}}
\end{aligned} \tag{B35}$$

Where $P_f(x_1)$ is the set of all subsystems obtained by applying the branching rule in Eq.(B33) starting from x_1 and iterating through all the blocks in the circuits. We note as well that $d(x_L) := \sum_{i=2}^L d_i(x_{i-1})$ is the total number of branchings of x_1 leading to the final subsystem $x_L \in P_f(x_1)$.

One can remark from the above expression of the second moment superoperator coefficient that the coefficient a_{x_1} may scale in the number of blocks of the first layer $A_1 := A$ and that the sum $\sum_{x_L \in P_f(x_1)} \left(\frac{2^{m/2}}{2^m + 1} \right)^{d(x_L)}$ will eventually scale in L , the circuit depth.

Moreover, we note that the expression holds for a light cone made of local 2-design blocks and acting on $n = m \times A_1$ qubits where $A_l = L - l + 1, \forall l \in [L]$. In this setting, we have exactly the same expression as in Eq.(B35), with $P_f(x_1)$ the set of subsystems obtained by applying the branching rule from Eq.B33 on the light cone blocks. Therefore, what differs between considering a full circuit made of local 2-design blocks and a light cone of the same circuit is the set of final subsystems $P_f(x_1)$ and its corresponding branching count $d(x_L) \forall x_L \in P_f(x_1)$.

However, in both cases, the construction of $P_f(x_1) \forall x_1 \in P_1$ and hence the calculation of $d(x_L)$ is quite cumbersome. Therefore, we derive the following upper bound on this sum.

To do so, we know that

$$f_A(x_1) = \text{Tr}[\text{Tr}_{x_1}[U^{(A)} Y_1 U^{(A)\dagger}] \text{Tr}_{x_1}[U^{(A)} Y_2 U^{(A)\dagger}]] = \sum_{x_L \in P_f(x_1)} \left(\frac{2^{m/2}}{2^m + 1} \right)^{d(x_L)} \text{Tr}[\text{Tr}_{x_L}[Y_1] \text{Tr}_{x_L}[Y_2]] \tag{B36}$$

If Y_1, Y_2 are projectors (i.e. $r_i = s_i, i \in \{1, 2\}$), then using the sub multiplicative property of positive semi definite matrices, we get $f_A(x_1) \leq \text{Tr}[Y_1] \text{Tr}[Y_2] = 1$

For $Y_1 = Y_2 = |0\rangle\langle 0|$, we get $f_A(x_1) = \sum_{x \in P_f(x_1)} \left(\frac{2^{m/2}}{2^m + 1} \right)^{d(x)} \leq 1$. Therefore for arbitrary Y_1 and Y_2 , we get:

$$f_A(x_1) \leq \text{Tr}[\text{Tr}_{x_L}[Y_1] \text{Tr}_{x_L}[Y_2]] \tag{B37}$$

We note that this upper bound holds for a full brickwise circuit or a lightcone over the same circuit, which can be observed in Section 5 (See Fig.15).

Indeed, as will be detailed in the next section, Eq.(B35) and Eq.(B37) will be key in obtaining the expression of the Fourier coefficients variance over a light cone, leading to the upper bound in theorem 4.

B.4.3 Proof of Theorem 4

We consider the brick-wise circuit architecture made of m -local encoding blocks and m -local 2-design parameterized blocks as illustrated in Fig.4. We recall Theorem 4 in this setting:

Theorem 4. *Consider a single layered Quantum Fourier model with Fourier coefficients $c_\omega(\theta)$ in the form of Eq. (3) using a brick wise circuit architecture with spectrum Ω , redundancies $|R(\omega)|$ and observable $O = \hat{O}_{s_k} \otimes \mathbb{1}_{\bar{s}_k}$. Assume that each variational block forms a 2-design on the corresponding m -qubit subsystem.*

1. If $\|\hat{O}_{s_k}\|_2^2 \leq 2^m$, then:

$$\text{Var}[c_\omega] \leq \left(\frac{2^{m+1}}{2^{2m} - 1} \right)^{2L_2} |R_{E_k}(\omega)|^2 \quad (16)$$

2. If \hat{O}_{s_k} is a projector of rank r , then:

$$\text{Var}[c_\omega] \leq \left(\frac{2^{m+1}}{2^{2m} - 1} \right)^{2L_2} \left(\frac{r}{2^m} \right)^2 |R_{E_k}(\omega)|^2 \quad (17)$$

where $R_{E_k}(\omega)$ is the frequency generator obtained from the encoding blocks inside the observable backward light cone \mathcal{L}_k (acting non trivially on S_{E_k}) and L_2 is the depth of the post-encoding parameterized block $W^{(2)}$.

In the following proof, using similar techniques as presented in B.4.2, we give an expression of the variance of the Fourier coefficients under the local 2-design setting described in Section 3.3. However, as the obtained expression involves cumbersome calculations, we give in Theorem 4 an upper bound on the Fourier coefficients variance that depends on the circuit depth and the frequency redundancy.

In what follows, we use the same notations from the previous section B.4.2 and we consider a circuit with a first parameterized layer $W^{(1)}$ of depth L_1 , a layer of encoding blocks $S(x)$ and a final parameterized layer $W^{(2)}$ of depth L_2 as depicted in Fig.4 acting initially on $n = m \times A$ qubits. We recall here the expression of the expectation of the modulus squared of a Fourier coefficient c_ω (See Eq.(B14) for details):

$$\begin{aligned} \mathbb{E}[|c_\omega|^2] &= \sum_{\substack{I, I' \in R(\omega) \\ J, J' \in R(\omega)}} \mathbb{E}_{W^{(1)}} \left[\text{Tr} \left[|J'\rangle \langle J| W^{(1)} |0\rangle \langle 0| W^{(1)\dagger} \right] \text{Tr} \left[|I\rangle \langle I'| W^{(1)} |0\rangle \langle 0| W^{(1)\dagger} \right] \right] \\ &\quad \times \mathbb{E}_{W^{(2)}} \left[\text{Tr} \left[|J\rangle \langle J'| W^{(2)\dagger} O W^{(2)} \right] \text{Tr} \left[|I'\rangle \langle I| W^{(2)\dagger} O W^{(2)} \right] \right] \\ &= \sum_{\substack{I, I' \in R(\omega) \\ J, J' \in R(\omega)}} \Lambda(J, J', I, I') \Gamma(J, J', I, I') \end{aligned} \quad (B38)$$

Here $J, J' \in R(\omega)$ are multi indices of length A , the number of blocks in a single layer and each component (j_k, j'_k) corresponds to the indices of 2 eigenvalues of the 2^m -dimensional encoding unitary acting on subsystem $s_k, \forall k \in \{1, \dots, A\}$. For ease of notation, we introduce the shorthand $\Lambda(J, J', I, I')$ for the expectation over the pre-encoding unitary $W^{(1)}$ and $\Gamma(J, J', I, I')$ for the expectation over the post-encoding unitary $W^{(2)}$ in Eq.(B38).

We then consider an m -local observable of the form $O_k = \hat{O}_{s_k} \otimes \mathbb{1}_{\bar{s}_k}$ acting non trivially on subsystem s_k and we denote by \mathcal{L}_k the backward light cone associated to this observable. Precisely, \mathcal{L}_k is the subcircuit containing all blocks with at least one qubit causally connected to the input qubits of \hat{O}_{s_k} . We also denote the subsystem on which \mathcal{L}_k acts non trivially by $\mathcal{S}_{\mathcal{L}_k}$.

Due to the brick-wise circuit architecture and the locality of the observable, the quantum model is reduced to an effective model obtained by considering the restricted action of the circuit unitary on subsystem $\mathcal{S}_{\mathcal{L}_k}$:

$$f_{\mathcal{L}_k}(x) := \text{Tr} \left[|0\rangle \langle 0|_{\mathcal{L}_k} U(x, \theta)_{\mathcal{L}_k}^\dagger O_{\mathcal{L}_k} U(x, \theta)_{\mathcal{L}_k} \right] \quad (B39)$$

where $U(x, \theta)_{\mathcal{L}_k}^\dagger = W_{\mathcal{L}_k}^{(1)\dagger} S(x)_{\mathcal{L}_k}^\dagger W_{\mathcal{L}_k}^{(2)\dagger}$ is the adjoint circuit unitary restricted to the light cone acting on subsystem $\mathcal{S}_{\mathcal{L}_k}$.

Hence, Eq.(B38) can be rewritten using the following:

$$\begin{aligned}\Lambda(J, J', I, I') &= \mathbb{E}_{W_{\mathcal{L}_k}^{(1)}} \left[\text{Tr} \left[|J'\rangle \langle J|_{\mathcal{L}_k} W_{\mathcal{L}_k}^{(1)} |0\rangle \langle 0|_{\mathcal{L}_k} W_{\mathcal{L}_k}^{(1)\dagger} \right] \text{Tr} \left[|I\rangle \langle I'|_{\mathcal{L}_k} W_{\mathcal{L}_k}^{(1)} |0\rangle \langle 0|_{\mathcal{L}_k} W_{\mathcal{L}_k}^{(1)\dagger} \right] \right] \\ \Gamma(J, J', I, I') &= \mathbb{E}_{W_{\mathcal{L}_k}^{(2)}} \left[\text{Tr} \left[|J\rangle \langle J'|_{\mathcal{L}_k} W_{\mathcal{L}_k}^{(2)\dagger} O_{\mathcal{L}_k} W_{\mathcal{L}_k}^{(2)} \right] \text{Tr} \left[|I'\rangle \langle I|_{\mathcal{L}_k} W_{\mathcal{L}_k}^{(2)\dagger} O_{\mathcal{L}_k} W_{\mathcal{L}_k}^{(2)} \right] \right]\end{aligned}$$

Another consequence of restricting calculations to the light cone \mathcal{L}_k is spectrum reduction where only encoding blocks acting on subsystem $\mathcal{S}_{\mathcal{L}_k}$ are involved. Hence, in what follows $R(\omega)$ refers to the frequency generator made only of encoding blocks acting non trivially on subsystem $\mathcal{S}_{\mathcal{L}_k}$. Let us denote by \mathcal{S}_{E_k} the subsystem on which $W_{\mathcal{L}_k}^{(2)}$ (and similarly $S(x)$) acts non trivially and $\mathcal{S}_{\overline{E_k}} := \mathcal{S}_{E_k} \setminus \mathcal{S}_{E_k}$ as depicted in Fig.4. Consequently, we get

$$\begin{aligned}\Gamma(J, J', I, I') &= \delta_{(J, J')_{\overline{E_k}}} \delta_{(I, I')_{\overline{E_k}}} \mathbb{E}_{W_{E_k}^{(2)}} \left[\text{Tr} \left[|J\rangle \langle J'|_{E_k} W_{E_k}^{(2)\dagger} O_{E_k} W_{E_k}^{(2)} \right] \text{Tr} \left[|I'\rangle \langle I|_{E_k} W_{E_k}^{(2)\dagger} O_{E_k} W_{E_k}^{(2)} \right] \right] \\ &= \delta_{(J, J')_{\overline{E_k}}} \delta_{(I, I')_{\overline{E_k}}} \Gamma_2(J, J', I, I')\end{aligned}\quad (\text{B40})$$

In what follows whenever $\Gamma(J, J', I, I')$ is used, it actually refers to $\Gamma(J, J', I, I')_2$. Therefore, Eq.(B38) becomes:

$$\mathbb{E} [|c_\omega|^2] = \sum_{\substack{I, I' \in R(\omega) \\ J, J' \in R(\omega)}} \delta_{(J, J')_{\overline{E_k}}} \delta_{(I, I')_{\overline{E_k}}} \Lambda(J, J', I, I') \Gamma(J, J', I, I') \quad (\text{B41})$$

This implies that the above sum over $R(\omega)$ will effectively contain just the pairs $(J, J') \in R(\omega)$ such that $\forall s_l \in \mathcal{S}_{\overline{E_k}}, \lambda_{j_l} - \lambda_{j'_l} = 0$. Therefore the frequency generator becomes $R(\omega) := \{(J, J') \in [2^m]^{L_2} \times [2^m]^{L_2} \mid \sum_{l \in \mathcal{S}_{E_k}} (\lambda_{j_l} - \lambda_{j'_l}) = \omega\} \times \{(J, J) \in [2^m]^{L_1-1}\}$. In other terms, the effective spectrum is the one generated by encoding blocks acting non trivially on subsystems of \mathcal{S}_{E_k} and that is made redundant by adding null contributions from the encoding blocks outside the light cone.

In order to calculate $\Gamma(J, J', I, I')$ and $\Lambda(J, J', I, I')$, we use the same calculations from Eq.(B35) with a minor change of notations where A will take the values $L_1 + L_2 - 1$ and L_2 respectively. Therefore, we get:

$$\begin{aligned}\Lambda(J, J', I', I) &= \sum_{x_1 \in P_1^1} a_{x_1}(J, J', I', I) f^1(x_1, |0\rangle \langle 0|_{\mathcal{L}_k}) \\ &= \sum_{x_1 \in P_1^1} a_{x_1}(J, J', I', I) \sum_{x_L \in P_f^1(x_1)} \left(\frac{2^{m/2}}{2^m + 1} \right)^{d(x_L)} \text{Tr} [\text{Tr}_{x_L} [|0\rangle \langle 0|_{\mathcal{L}_k}]^2] \\ \Gamma(J, J', I', I) &= \sum_{x_1 \in P_1^2} a_{x_1}(J, J', I', I) f^2(x_1, O_{E_k}) \\ &= \sum_{x_1 \in P_1^2} a_{x_1}(J, J', I', I) \sum_{x_L \in P_f^2(x_1)} \left(\frac{2^{m/2}}{2^m + 1} \right)^{d(x_L)} \text{Tr} [\text{Tr}_{x_L} [O_{E_k}]^2]\end{aligned}\quad (\text{B42})$$

where P_1^1 and P_1^2 are the power sets of $\mathcal{S}_{\mathcal{L}_k}$ and \mathcal{S}_{E_k} respectively, P_f^1 and P_f^2 are the sets of final subsystems after branching over blocks of $W_{\mathcal{L}_k}^{(1)}$ and $W_{E_k}^{(2)}$ respectively, according to the construction detailed in Eq.(B35) and $f^i(x_1, H)$ is a shorthand for $\sum_{x_L \in P_f^i(x_1)} \left(\frac{2^{m/2}}{2^m + 1} \right)^{d(x_L)} \text{Tr} [\text{Tr}_{x_L} [H]^2]$, $\forall i \in \{1, 2\}$.

By substituting Eq.(B42) in Eq.(B41), we get the following expression of $\mathbb{E}[|c_\omega|^2]$:

$$\begin{aligned}
\mathbb{E}[|c_\omega|^2] &= \sum_{\substack{I, I' \in R(\omega) \\ J, J' \in R(\omega)}} \delta(J, J')_{\overline{E_k}} \delta(I, I')_{\overline{E_k}} \Lambda(J, J', I', I) \Gamma(J, J', I', I) \\
&= \sum_{\substack{I, I' \in R(\omega) \\ J, J' \in R(\omega)}} \delta(J, J')_{\overline{E_k}} \delta(I, I')_{\overline{E_k}} \left(\sum_{x_1 \in P_1^1} a_{x_1}(J, J', I', I) f^1(x_1, |0\rangle\langle 0|_{\mathcal{L}_k}) \right) \left(\sum_{y_1 \in P_1^2} a_{y_1}(J, J', I', I) f^2(y_1, O_{E_k}) \right) \\
&= \sum_{\substack{J, J' \in R_{E_k}(\omega) \\ J, J' \in R_{E_k}(\omega)}} \left(\sum_{y_1 \in P_1^2} a_{y_1} f^2(y_1, O_{E_k}) \right) \sum_{\substack{(J, J')_{\overline{E_k}} \\ (I, I')_{\overline{E_k}}}} \delta(J, J')_{\overline{E_k}} \delta(I, I')_{\overline{E_k}} \left(\sum_{x_1 \in P_1^1} a_{x_1} f^1(x_1, |0\rangle\langle 0|_{\mathcal{L}_k}) \right) \\
&= \left(\frac{1}{2^{2m} - 1} \right)^{L_1 + 2L_2 - 1} \sum_{\substack{J, J' \in R_{E_k}(\omega) \\ J, J' \in R_{E_k}(\omega)}} \left(\sum_{y_1 \in P_1^2} \tilde{a}_{y_1} f^2(y_1, O_{E_k}) \right) \sum_{x_1 \in P_1^1} f^1(x_1, |0\rangle\langle 0|_{\mathcal{L}_k}) \sum_{\substack{(J, J')_{\overline{E_k}} \\ (I, I')_{\overline{E_k}}}} \delta(J, J')_{\overline{E_k}} \delta(I, I')_{\overline{E_k}} \tilde{a}_{x_1}
\end{aligned} \tag{B43}$$

where $a_{x_1} := \left(\frac{1}{2^{2m} - 1} \right)^{L_1 + L_2 - 1} \tilde{a}_{x_1}$ and $a_{y_1} := \left(\frac{1}{2^{2m} - 1} \right)^{L_2} \tilde{a}_{y_1}$.

Summing over indices in $\overline{E_k}$ gives the following:

$$\begin{aligned}
\sum_{\substack{(J, J')_{\overline{E_k}} \\ (I, I')_{\overline{E_k}}}} \delta(J, J')_{\overline{E_k}} \delta(I, I')_{\overline{E_k}} \tilde{a}_{x_1} &= \sum_{J_{\overline{E_k}}, I_{\overline{E_k}}} \tilde{a}_{x_1} \delta(J, J')_{\overline{E_k}} \delta(I, I')_{\overline{E_k}} \\
&= \sum_{J_{\overline{E_k}}, I_{\overline{E_k}}} \prod_{l \in x_1} \left(C_l - \frac{D_l}{2^m} \right) \prod_{l \in \overline{x_1}} \left(D_l - \frac{C_l}{2^m} \right) (\delta(J, J')_{\overline{E_k}} \delta(I, I')_{\overline{E_k}}) \\
&= \prod_{l \in x_1 \cap E_k} \left(C_l - \frac{D_l}{2^m} \right) \prod_{l \in \overline{x_1} \cap E_k} \left(D_l - \frac{C_l}{2^m} \right) \sum_{J_{\overline{E_k}}, I_{\overline{E_k}}} \prod_{l \in x_1 \cap \overline{E_k}} \left(1 - \frac{\delta_{j_l, i_l}}{2^m} \right) \prod_{l \in \overline{x_1} \cap \overline{E_k}} \left(\delta_{j_l, i_l} - \frac{1}{2^m} \right) \\
&= \prod_{l \in x_1 \cap E_k} \left(C_l - \frac{D_l}{2^m} \right) \prod_{l \in \overline{x_1} \cap E_k} \left(D_l - \frac{C_l}{2^m} \right) \prod_{l \in x_1 \cap \overline{E_k}} \sum_{j_l, i_l} \left(1 - \frac{\delta_{j_l, i_l}}{2^m} \right) \prod_{l \in \overline{x_1} \cap \overline{E_k}} \sum_{j_l, i_l} \left(\delta_{j_l, i_l} - \frac{1}{2^m} \right) \\
&= \prod_{l \in x_1 \cap E_k} \left(C_l - \frac{D_l}{2^m} \right) \prod_{l \in \overline{x_1} \cap E_k} \left(D_l - \frac{C_l}{2^m} \right) \prod_{l \in x_1 \cap \overline{E_k}} (2^{2m} - 1) \prod_{l \in \overline{x_1} \cap \overline{E_k}} (2^m - 2^m) \\
&= \prod_{l \in x_1 \cap E_k} \left(C_l - \frac{D_l}{2^m} \right) \prod_{l \in \overline{x_1} \cap E_k} \left(D_l - \frac{C_l}{2^m} \right) (2^{2m} - 1)^{|x_1 \cap \overline{E_k}|} 0^{|\overline{x_1} \cap \overline{E_k}|} \\
&= \begin{cases} \prod_{l \in x_1 \cap E_k} \left(C_l - \frac{D_l}{2^m} \right) \prod_{l \in \overline{x_1} \cap E_k} \left(D_l - \frac{C_l}{2^m} \right) (2^{2m} - 1)^{|\overline{E_k}|}, & \text{if } \overline{E_k} \subset x_1 \\ 0, & \text{otherwise} \end{cases} \\
&= \begin{cases} \prod_{l \in x_1 \cap E_k} \left(C_l - \frac{D_l}{2^m} \right) \prod_{l \in \overline{x_1} \cap E_k} \left(D_l - \frac{C_l}{2^m} \right) (2^{2m} - 1)^{L_1 - 1}, & \text{if } \overline{E_k} \subset x_1 \\ 0, & \text{otherwise} \end{cases}
\end{aligned}$$

Thus, by substituting this above sum in Eq.(B43), we obtain:

$$\begin{aligned}
\mathbb{E}[|c_\omega|^2] &= \left(\frac{1}{2^{2m}-1}\right)^{2L_2} \sum_{\substack{J, J' \in R_{E_k}(\omega) \\ I, I' \in R_{E_k}(\omega)}} \sum_{y_1 \in P_1^2} \tilde{a}_{y_1} f^2(y_1, O_{E_k}) \sum_{x_1 \in P_1^1, \overline{E_k} \subset x_1} \prod_{l \in x_1 \cap E_k} \left(C_l - \frac{D_l}{2^m}\right) \prod_{l \in \overline{x_1} \cap E_k} \left(D_l - \frac{C_l}{2^m}\right) f^1(x_1, |0\rangle\langle 0|_{\mathcal{L}_k}) \\
&= \left(\frac{1}{2^{2m}-1}\right)^{2L_2} \sum_{\substack{J, J' \in R_{E_k}(\omega) \\ I, I' \in R_{E_k}(\omega)}} \sum_{y_1 \in P_1^2} \tilde{a}_{y_1} f^2(y_1, O_{E_k}) \sum_{x_1 \in P_1^2} \tilde{a}_{x_1} f^1(x_1 \cup \overline{E_k}, |0\rangle\langle 0|_{\mathcal{L}_k})
\end{aligned} \tag{B44}$$

In the above expression of $\mathbb{E}[|c_\omega|^2]$, we have $|\tilde{a}_x| \leq 1 \forall x \in P_1^2$ and from Eq.(B37) we have:

$$\begin{aligned}
f^1(x_1 \cup \overline{E_k}, |0\rangle\langle 0|_{\mathcal{L}_k}) &= \sum_{x \in P_f^1(x_1 \cup \overline{E_k})} \left(\frac{2^{m/2}}{2^m+1}\right)^{d(x)} Tr[Tr_{x_L}[|0\rangle\langle 0|_{\mathcal{L}_k}]^2] \\
&\leq Tr[Tr_{x_L}[|0\rangle\langle 0|_{\mathcal{L}_k}]^2] = 1 \\
f^2(y_1, O_{E_k}) &= \sum_{x \in P_f^2(y_1)} \left(\frac{2^{m/2}}{2^m+1}\right)^{d(x)} Tr[Tr_{x_L}[O_{E_k}]^2] \\
&\leq Tr[Tr_{x_L}[O_{E_k}]^2] \\
&\leq 2^{2mL_2}
\end{aligned}$$

where we use in the last inequality the hypothesis that $Tr[\hat{O}_{s_k}^2] \leq 2^m$.

Finally, by combining all the previous steps, we retrieve the upper bound in Theorem 4:

$$\mathbb{E}[|c_\omega|^2] \leq \left(\frac{2^{m+1}}{2^{2m}-1}\right)^{2L_2} |R_{E_k}(\omega)|^2$$

B.4.4 Fourier coefficients variance in a light cone forming a 2-design

In this section, we consider the same settings and notations from the previous section B.4.3 but we assume that $W_{\mathcal{L}_k}^{(1)}$ and $W_{E_k}^{(2)}$ form each a 2-design on subsystems $\mathcal{S}_{\mathcal{L}_k}$ and \mathcal{S}_{E_k} respectively. We follow the same steps as in the previous proof until we get to Eq.(B41). Then, we compute $\Gamma(J, J', I, I')$ and $\Lambda(J, J', I, I')$ under the 2-design assumption. Hence, by applying Weingarten calculus expression of the second moment [32], we obtain:

$$\begin{aligned}
\Lambda(J, J', I, I') &= \frac{1}{2^{2m(L_1+L_2-1)} - 1} \left(1 - \frac{1}{2^{m(L_1+L_2-1)}}\right) [\delta_{J, J'} \delta_{I, I'} + \delta_{J, I} \delta_{J', I'}] \\
\Gamma(J, J', I, I') &= \frac{1}{2^{2mL_2} - 1} \left[\delta_{(J, J')_{E_k}} \delta_{(I, I')_{E_k}} \left(Tr[O_{E_k}]^2 - \frac{Tr[O_{E_k}^2]}{2^{mL_2}}\right) + \delta_{(J, I)_{E_k}} \delta_{(J', I')_{E_k}} \left(Tr[O_{E_k}^2] - \frac{Tr[O_{E_k}]^2}{2^{mL_2}}\right) \right]
\end{aligned} \tag{B45}$$

Therefore, we substitute $\Gamma(J, J', I, I')$ and $\Lambda(J, J', I, I')$ in Eq.(B41) using the new expressions in Eq.(B45) and we get $\forall \omega \in \Omega \setminus \{0\}$:

$$\begin{aligned}
\mathbb{E}[|c_\omega|^2] &= \frac{1}{2^{m(L_1+L_2-1)}(2^{m(L_1+L_2-1)} + 1)(2^{2mL_2} - 1)} \sum_{\substack{I, I' \in R(\omega) \\ J, J' \in R(\omega)}} \delta_{(J, J')_{\overline{E_k}}} \delta_{(I, I')_{\overline{E_k}}} \delta_{J, I} \delta_{J', I'} \left(\text{Tr}[O_{E_k}^2] - \frac{\text{Tr}[O_{E_k}]^2}{2^{mL_2}} \right) \\
&= \frac{\left(\text{Tr}[O_{E_k}^2] - \frac{\text{Tr}[O_{E_k}]^2}{2^{mL_2}} \right)}{2^{m(L_1+L_2-1)}(2^{m(L_1+L_2-1)} + 1)(2^{2mL_2} - 1)} \sum_{\substack{(I, I')_{\overline{E_k}} \\ (J, J')_{\overline{E_k}}}} \delta_{(J, J')_{\overline{E_k}}} \delta_{(I, I')_{\overline{E_k}}} \delta_{(J, I)_{\overline{E_k}}} \delta_{(J', I')_{\overline{E_k}}} \sum_{\substack{I, I' \in R_{E_k}(\omega) \\ J, J' \in R_{E_k}(\omega)}} \delta_{(J, I)_{E_k}} \delta_{(J', I')_{E_k}} \\
&= \frac{2^{m(L_2-1)} \left(\text{Tr}[\hat{O}_k^2] - \frac{\text{Tr}[\hat{O}_k]^2}{2^m} \right)}{2^{m(L_1+L_2-1)}(2^{m(L_1+L_2-1)} + 1)(2^{2mL_2} - 1)} 2^{m(L_1-1)} |R_{E_k}(\omega)| \\
&= \frac{1}{2^m (2^{m(L_1+L_2-1)} + 1)(2^{2mL_2} - 1)} \left(\text{Tr}[\hat{O}_k^2] - \frac{\text{Tr}[\hat{O}_k]^2}{2^m} \right) |R_{E_k}(\omega)|
\end{aligned} \tag{B46}$$

B.5 Proof of theorem 5

We recall Theorem 5:

Theorem 5 (Fourier Norm Bound). *Consider an L -layered Quantum Fourier model $f(x, \theta)$ with spectrum Ω and observable O as defined in Eq.(3). Then,*

$$\forall x \in \mathbb{R}^d, \forall \theta \in \Theta, |f(x, \theta)|^2 \leq \|O\|_\infty^2 \tag{22}$$

$$\forall \theta \in \Theta, \sum_{\omega \in \Omega} |c_\omega(\theta)|^2 \leq \|O\|_\infty^2 \tag{23}$$

Proof. The first point can be proven by remarking that $\langle \psi | O | \psi \rangle$ can be maximized by taking $|\psi\rangle$ as the eigenvector associated to the largest eigenvalue of O .

For the second point, one can write by considering the half spectrum Ω_+

$$|f(x)|^2 = \left| \sum_{\omega \in \Omega_+} c_\omega e^{-i\omega^\top x} + c_\omega^* e^{i\omega^\top x} \right|^2 \tag{B47}$$

$$= \sum_{\omega \in \Omega_+} (c_\omega e^{-i\omega^\top x} + c_\omega^* e^{i\omega^\top x})(c_\omega^* e^{i\omega^\top x} + c_\omega e^{-i\omega^\top x}) \tag{B48}$$

$$+ 2 \sum_{\omega_1 \neq \omega_2} (c_{\omega_1} e^{-i\omega_1^\top x} + c_{\omega_1}^* e^{i\omega_1^\top x})(c_{\omega_2} e^{-i\omega_2^\top x} + c_{\omega_2}^* e^{i\omega_2^\top x}) \tag{B49}$$

$$= \sum_{\omega \in \Omega_+} 2|c_\omega|^2 + c_\omega^2 e^{-2i\omega^\top x} + c_\omega^{2*} e^{2i\omega^\top x} \tag{B50}$$

$$+ 2 \sum_{\omega_1 \neq \omega_2} c_{\omega_1} c_{\omega_2}^* e^{-i(\omega_1 - \omega_2)^\top x} + c_{\omega_1} c_{\omega_2} e^{-i(\omega_1 + \omega_2)^\top x} + c_{\omega_1}^* c_{\omega_2}^* e^{i(\omega_1 + \omega_2)^\top x} + c_{\omega_1}^* c_{\omega_2} e^{i(\omega_1 - \omega_2)^\top x} \tag{B51}$$

$$= 2 \sum_{\omega \in \Omega_+} |c_\omega|^2 + g(x) \tag{B52}$$

We finish the proof by finding x_0 such that $g(x_0) = 0$. This can be done with the lemma 3. We first reduce the problem to one variable and we introduce $h(t) = \sum_{\omega \in \Omega} a_\omega \cos(\omega_1 t + \omega_{2:d}^\top x'_0 + \phi_\omega)$ where x'_0 is an arbitrary vector of size $d-1$. \square

Lemma 3. *Let $h(t) = \sum_{\omega \in \Omega} a_\omega \cos(\omega t + \phi_\omega)$, with Ω being a discrete subset of \mathbb{R}^d , and $\phi_\omega \in \mathbb{R}$. Then it exists t_0 such that $g(t_0) = 0$.*

Proof. Let us suppose that $h(t)$ is of constant sign, we can assume it is positive on \mathbb{R} . If h is not of constant sign, by continuity it means that it exists t_0 such that $h(t_0) = 0$ and the proof is finished. We will show that $\forall \varepsilon > 0$ it exists T such that $|\int_0^T h(t)dt| < \varepsilon$. Then it means that h is equal to 0 over all the interval $[0, T]$, which proves the result.

We will now prove that $\forall \varepsilon > 0$, there exists a real T and integers q_ω s such that $\forall \omega \in \Omega, |2\pi T - q_\omega 2\pi/\omega| \leq \varepsilon$ which proves that $|\int_0^{2\pi T} h(t)dt| < \varepsilon$ since for each frequency we integrate over an integer number of periods.

We will show how to construct T and q_ω s for three values ω_1, ω_2 and ω_3 .

$$\text{Let } R_2 = \{k \frac{\omega_2}{\omega_1} - \lfloor k \frac{\omega_2}{\omega_1} \rfloor, k \in \mathbb{N}, k \in [0, N^2]\}$$

If one divides the interval $[0, 1]$ into N equal subintervals, then there are at least $N + 1$ elements of R_2 that are in the same subinterval. Let $\{k_1, \dots, k_{N+1}\}$ the integers corresponding to these elements.

Then let $R_3 = \{k \frac{\omega_3}{\omega_1} - \lfloor k \frac{\omega_3}{\omega_1} \rfloor, k \in \mathbb{N}, k \in \{k_1, \dots, k_{N+1}\}\}$. If one divides again the interval $[0, 1]$ into N equal subintervals, then there are at least 2 elements of R_3 that are in the same subinterval.

Then there exists k, k' such that

$$\begin{aligned} \left| k \frac{\omega_3}{\omega_1} - \lfloor k \frac{\omega_3}{\omega_1} \rfloor - (k' \frac{\omega_3}{\omega_1} - \lfloor k' \frac{\omega_3}{\omega_1} \rfloor) \right| &\leq \frac{1}{N} \\ \left| (k - k') \frac{\omega_3}{\omega_1} - (\lfloor k \frac{\omega_3}{\omega_1} \rfloor - \lfloor k' \frac{\omega_3}{\omega_1} \rfloor) \right| &\leq \frac{1}{N} \\ \left| (k - k') \frac{1}{\omega_1} - \frac{1}{\omega_3} (\lfloor k \frac{\omega_3}{\omega_1} \rfloor - \lfloor k' \frac{\omega_3}{\omega_1} \rfloor) \right| &\leq \frac{1}{N\omega_3} \end{aligned}$$

And since k and k' are in $\{k_1, \dots, k_{N+1}\}$, we also have

$$\left| (k - k') \frac{1}{\omega_1} - \frac{1}{\omega_2} (\lfloor k \frac{\omega_2}{\omega_1} \rfloor - \lfloor k' \frac{\omega_2}{\omega_1} \rfloor) \right| \leq \frac{1}{N\omega_2}$$

By taking $T = (k - k') \frac{1}{\omega_1}$ and $1/N = \varepsilon$, we proved the result for 3 numbers. One can apply the same construction for $|\Omega|$ number of frequencies by taking $N^{|\Omega|}$ integers at the beginning.

□

C Additional Numerics

C.1 Fourier coefficients variance in the 2-design setting for a reuploading model

We consider the same settings of Theorem 2 where we take a reuploading circuit with $L = 2$ circuit layers acting on $n = 4$ qubits. In Fig.16, we see that the simulated variance of the Fourier coefficients match the theoretical variance values predicted by Theorem 2 for the Pauli and exponential encoding strategies. The explicit dependence on the redundancies is harder to visualize as was done in Fig.8 because the variance expression from Theorem 2 include the partial redundancies. Nonetheless, we clearly observe in the case of pauli encoding that we have a gaussian distribution (negative frequencies are not plotted) with half of the frequencies suppressed. For the exponential encoding strategy, we see a gaussian distribution but with a higher variance than the Pauli case which is due to redundancies caused by the reuploading scheme and the fact that we are using the same encoding layer twice as explained in Appendix A.2.

C.2 Fourier coefficients variance in the approximate 2-design setting for a reuploading model

In Section 3.2, we showed in Theorem 3 an upper bound on $\text{Var}(c_\omega)$ in the case of a model with a single circuit layer ($L = 1$), being a second degree polynomial in $|R(\omega)|$. It was left as an open question to demonstrate a similar bound for $L > 1$. Fig.17 shows a simulation in the case of $L = 2$ circuit layers. We tried to fit a second degree polynomial in order to express the relation between $\text{Var}(c_\omega)$ and $|R(\omega)|$ directly. Even though one cannot simulate an upper bound but just a direct correlation, seeing this second-degree polynomial fitting well could indicate that the same kind of bound could be expected.

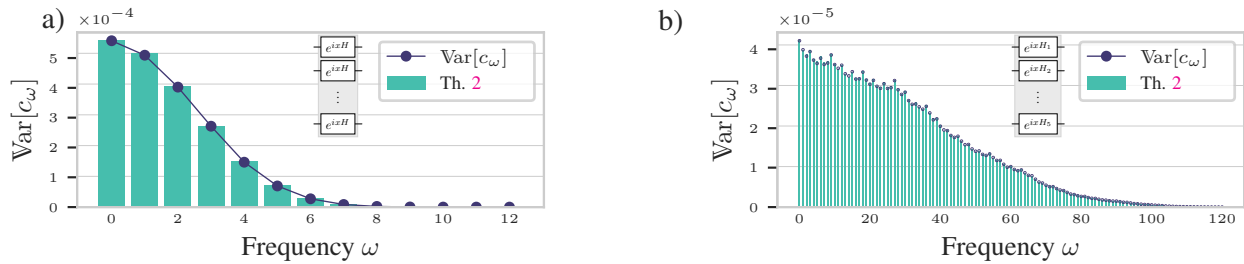


Figure 16: For $n = 4$ qubits, two circuit layers ($L = 2$) with the same encoding gates in each of the two encoding layers, five repetitions of the strongly entangling ansatz per trainable layer (see Appendix D); relation between the variance of each Fourier coefficient $\text{Var}[c_\omega]$ (blue dots) and its corresponding partial redundancies given by theorem 2 (green bars). Values are given for two different encoding strategies, a) Pauli encoding and b) exponential encoding.

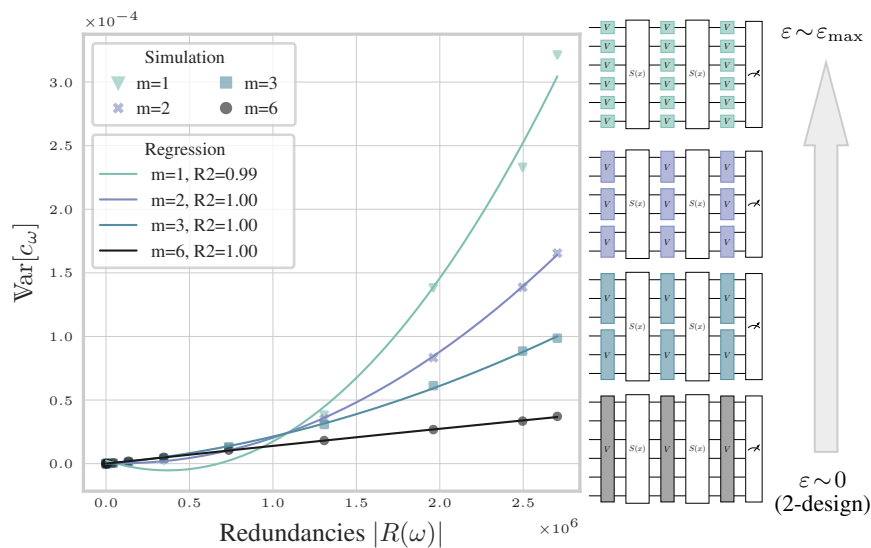


Figure 17: Fitting Fourier coefficients variance $\text{Var}[c_\omega]$ to a second degree polynomial in the redundancies $|R(\omega)|$ for four different circuit architecture (connectivity). As the locality of the trainable block decreases V , ϵ gets bigger and the trainable layers farther away from being a 2-design. R2 assesses the goodness of the fit, the closer to one the better.

D Ansätze for trainable layers

This section serves as a reference to the different circuit architectures that we considered in Section 5, explaining how a particular ansatz structure can be scaled in the number of qubits.

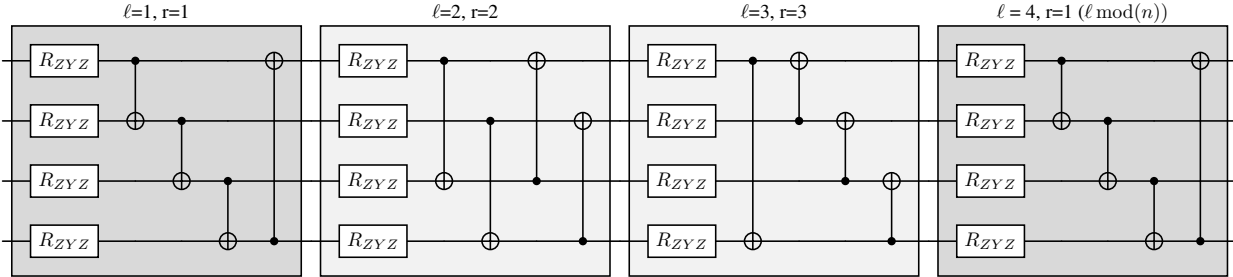


Figure 18: *Strongly Entangling Ansatz* [36]: The Ansatz depth varies with the number of qubits. To have all possible entanglers between qubits, one needs to have the number of blocks ℓ to be $\ell \geq n - 1$, with n the number of qubits and r is the range of the control gates given by $r = \ell \bmod(n)$.

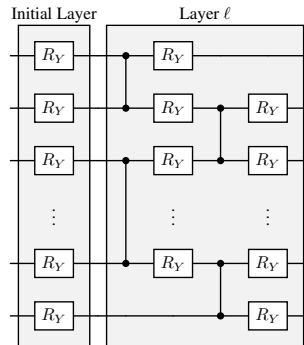


Figure 19: *Simplified Two Design Ansatz* [24]: An initial layer of Pauli-Y rotations and controlled-Z entanglers. Note that this ansatz has the same approximately the same amount of entangler gates as for the basic entangling ansatz layer, but double the number of parameters. It is composed of an initial layer and then the periodic layer is the one that will be repeated.